Magnetic Resonance Imaging in Paediatric Coronary Vasculopathy

Hussain, Mohammad

Awarding institution:
King's College London

Magnetic Resonance Imaging in Paediatric Coronary Vasculopathy

Dr. Mohammad Tarique Hussain

Thesis submitted to the University of London for the

Degree of Doctor of Philosophy (PhD)

Department of Imaging Sciences

King's College London

St Thomas' Hospital

London

SE1 7EH

ABSTRACT

Background

Coronary Allograft Vasculopathy (CAV) is the leading cause of late death for children after heart transplantation. It often presents late due to lack of ischaemic symptoms from the denervated allograft and it is difficult to detect using conventional angiography. A non-invasive diagnostic tool would be invaluable for the early detection and therefore, prevention of disease. MRI has the potential to achieve this by imaging coronary lumen, vessel wall and central vascular stiffness in a child-friendly free-breathing protocol lasting thirty minutes.

Methods

A three-dimensional steady-state-free-precession (3D SSFP) imaging sequence for coronary artery lumen imaging was optimised for its use in children. Patient based studies were performed to show the clinical potential for this approach. Furthermore, contrast-enhanced inversion-prepared coronary vessel wall imaging was investigated for its ability to detect intimal disease in CAV, using intravascular ultrasound to validate the findings. Finally, MRI was used to study the potential of aortic screening for rapid assessment of CAV.

ABSTRACT

Results

MRI coronary artery lumen imaging is feasible in children and reference values are provided. Contrast-enhanced vessel wall imaging has 91% accuracy in the detection of significant CAV. Further improvements in the technique can be achieved using high-field MRI (3.0 Tesla) or sublingual nitroglycerin. Central aortic stiffness is increased in children after heart transplantation and a relationship between this and CAV is demonstrated.

Conclusions

Coronary artery lumen and vessel wall MRI can be used to follow up children after heart transplantation. Non-invasive follow-up can be more frequent and has the potential to allow early prevention. From this research, there are wider implications for congenital heart disease, Kawasaki disease and cardiovascular atherosclerosis imaging

Table of Contents

List of Tables

List of Figures

Acknowledgements

The children and young adults that took part in this research were thoughtful, considerate and frankly, inspirational. It was a pleasure to have known you at this time and I hope that this research will pave the way for improving your care.

I would like to thank my supervisors Dr. Gerald Greil and Professor Rene Botnar for their invaluable help and advice throughout this research. I will always be grateful for your patience, support, guidance and time that you dedicated to supervising this thesis.

I cannot give enough thanks to Dr. Michael Burch who has supported me throughout my career and has given me his time, patience and trust. This is a debt that will be hard to repay. I would like to give a special thanks to the Heart Transplant team at Great Ormond Street Hospital and the Paediatric Cardiology team at Evelina Children's Hospital: In particular, Matthew Fenton for his encouragement and advice. I would also like to thank Professor Razavi and his entire team at the Division of Imaging Sciences, who have all helped to make this work possible.

Finally, I would like to dedicate this thesis to my parents, Mohammad Ali Sharafat Hussain and Ishrat-Un-Nisa Hussain; to my wife, Souad Messahel, and to my children Maysoon, Jenna and Hamza Hussain. Without your love and support, none of this would have been possible.

Publications arising from Thesis

Chapter 2.1.4

Hussain T, Lossnitzer D, Bellsham-Revell H, Valverde, I, Beerbaum P, Razavi R, Bell A, Schaeffter T, Botnar R, Uribe SA, Greil, G. 3D Dual-Phase Whole-Heart Magnetic Resonance Imaging: Clinical Implications for Congenital Heart Disease. Radiology. 2012 May;263(2):547-54

Chapter 4.1 & 4.2

Hussain T, Fenton M, Peel S, Wiethoff A, Taylor A, Muthurangu V, Razavi R, Botnar R, Burch M, Greil G. Detection and Grading of Coronary Allograft Vasculopathy in Children using Contrast-Enhanced Magnetic Resonance Imaging of the Coronary Vessel Wall. Circulation: Cardiovascular Imaging. 2013 Jan 1;6(1):91-8

Chapter 5.1

Hussain T, Burch M, Greil G; Cecelja M, Fenton M. Central Aortic Stiffness, Hypertension and Coronary Allograft Vasculopathy in Children. Journal of Heart and Lung Transplantation 2012 Dec;31(12):1318-20

Chapter 5.2

Hussain T, Clough RE, Cecelja M, Makowski M, Peel S, Chowienczyk P, Schaeffter T, Greil G, Botnar R. Zoom imaging for rapid aortic vessel wall imaging and cardiovascular risk assessment. J Magn Reson Imaging. 2011 Aug;34(2):279-85

Statement of Conjoining Work

All work detailed herein is the primary work of Dr. Mohammad Tarique Hussain. Sub-chapters 2.1.2 and 2.1.3 are merely brief descriptions of closely related conjoining work that form the background prologue to the studies in Chapter 2.

Chapter 2.1.2

Tangcharoen T, Bell A, Hegde S, Hussain T, Beerbaum P, Schaeffter T, Razavi R, Botnar RM, Greil GF. Detection of Coronary Artery Anomalies in Infants and Young Children with Congenital Heart Disease by Using MR Imaging. Radiology. 2011 Apr;259(1):240-7.

Dr. Tangcharoen is primary author. As fourth author, Dr. Hussain's contribution to this work included data analysis and manuscript editing. Findings relevant to this thesis are described briefly in chapter 2.1.2.

Chapter 2.1.3

Uribe S, Hussain T, Valverde I, Tejos C, Irarrazaval P, Fava M, Beerbaum P, Botnar RM, Razavi R, Schaeffter T, Greil GF. Congenital Heart Disease in Children: Coronary MR Angiography during Systole and Diastole with Dual Cardiac Phase Whole-Heart Imaging. Radiology. 2011 Jul; 260(1): 232-40

Dr. Uribe is primary author. As second author of this published work, Dr Hussain's contribution to this work was study planning, data collection, analysis and manuscript editing. Findings relevant to this thesis are described briefly in chapter 2.1.3.

INTRODUCTION

Translational medicine has been defined as "***a discipline that increases the efficiency of determining the relevance of novel discoveries in the biological sciences to human disease and helps clinical researchers identify, through direct human observation, alternative hypotheses relevant to human disease. A further goal is to accelerate the rational transfer of new insights and knowledge into clinical practice for improving patients' outcomes and public health***."[1] As such, it has been identified nationally as one of the key research strategies towards delivery of improved patient care.[2]

In keeping with this definition, this thesis takes basic science developments such as coronary lumen imaging, vessel wall imaging, vessel wall delayed enhancement and reduced field-of-view imaging and implements them in clinical research. The aim is to use these techniques to answer specific clinical questions in Congenital Heart Disease, Atherosclerosis, Coronary Allograft Vasculopathy and Kawasaki disease. Ultimately these insights should be used to improve the care of these patient groups.

Among the important factors towards translation, highlighted by Lord and Trembath when setting out their translational strategy, are patient involvement, industry collaboration and multicentre collaboration. Planning and conducting this research has involved the patient support groups: "Evelina Children's Heart Organisation" and "Hearts for Kids". Results have also been presented to these patient groups. Industry collaboration with Philips Healthcare has been present from the outset with partial funding for MR imaging coming from them. Finally, we have established firm research collaboration with Great Ormond Street Hospital,

which has the biggest Paediatric Heart Transplant programme in Europe. This collaboration will be beneficial to both research groups and ultimately for patient care.

The thesis revolves around a central question: “Can we detect and grade Coronary Allograft Vasculopathy non-invasively using MRI?”

In order to answer this question, the thesis takes a stepwise approach:

Step 1: Development of Coronary Lumen Imaging

Step 2: Development of Contrast-Enhanced Vessel Wall Imaging

Step 3: Aortic Imaging as a correlate for Coronary Disease

In taking these steps, the thesis introduces new technologies and explores the implications for other type of cardiovascular disease. Ultimately, the thesis makes important contributions to congenital heart disease, atherosclerotic heart disease, Kawasaki disease and Coronary Allograft Vasculopathy.

CHAPTER 1 – Review of Imaging for Coronary Allograft Vasculopathy

1. Review of Imaging for Coronary Allograft Vasculopathy

1.1. Introduction

Coronary Allograft Vasculopathy remains one of the biggest challenges facing heart transplant medicine. It is a progressive condition, which is thought to be caused largely by chronic autoimmune-mediated endothelial damage.[3] Damaged endothelium allows cell infiltration, which is responsible for the production of cytokines, growth factors, and matrix deposition (collagen I and fibroblasts).[4] This causes a progressive thickening of the intimal layer of the coronary vessel wall. The end results are allograft ischaemia, infarction, heart failure and sudden death.

In adults, CAV, along with malignancy is the biggest cause of late death after heart transplantation.[5] In paediatric series, CAV alone is the biggest cause of late death.[6] Angiographic evidence of CAV is present in 30 to 50% of heart transplant survivors at 5 years,[5, 7] and survival is significantly reduced for those with reported CAV.[5] In children, angiographic evidence of severe CAV is associated with a mortality or retransplantation rate of over 70% at 4 years.[6] Accordingly, in both adult and children, detection at an early stage and prevention of progression is paramount. Detection of CAV, however, is made more difficult owing to a lack of ischaemic symptoms from the denervated heart. This means that the asymptomatic period is much longer and therefore, regular imaging surveillance is required. This review, addresses issues concerning different imaging modalities that have be used for the detection of CAV and particular discussion is given regarding points pertinent to imaging in children.

1.2. Angiography

Invasive coronary angiography remains the mainstay for the diagnosis of CAV in many heart-transplant centres. However, histological evidence has long been present to show that angiography is prone to underestimating disease.[8] With the advent of intravascular ultrasound (IVUS), the relative insensitivity of conventional angiography as a screening tool has been demonstrated.[9-11] In a study by *St Goar at al*, 50% of those with normal coronary angiograms were shown to have moderate or severe intimal thickening on IVUS (by Stanford grading).[10] In fact, in this study, the mean intimal thickness and the mean intimal index (the ratio of intimal area to the sum of the intimal and lumen areas) were no different between those with abnormal angiograms and those with normal angiograms but moderate to severe thickening on IVUS (thickness 0.53+0.35 mm versus 0.64+0.30 mm; index, 0.28±0.10 versus 0.34±0.10). Similarly, *Tuzcu et al* showed that the sensitivity of angiography for detection of CAV (defined by maximal intimal thickness >0.5mm on IVUS) was only 43% (specificity 95%).[11] *Spes et al*, in a study of 56 heart transplant recipients with normal coronary angiograms, demonstrated that 33 had significant CAV on IVUS (defined as mean score equivalent being greater than a mean intimal thickness of 0.3mm).[9] *Gregory et al* examined 122 coronary artery segments and, defining disease as a maximal intimal thickness >0.5mm on IVUS, demonstrated that angiography had a sensitivity of just 11% (95% CI 4 to 23%) and a negative predictive value of just 57% (47 to 66%). [12] Using the same definition as Spes, *Störk et al*, demonstrated an even lower negative predictive value of 28% (14 to 46%) and a sensitivity of 44% (29 to 60%). Hence, although angiography is highly specific for CAV and has a high positive predictive value, it is not sensitive enough and it has low negative

predictive value. As a screening tool for the early detection of CAV, it is therefore flawed. It should be stated that *Sharples et al*, using predictive modeling to assess 566 patients over a 23 year period found a higher sensitivity for angiography but this study did not have histological or IVUS correlation for comparison. [13]

The main problem with angiography is that it merely images the lumen and not the vessel wall, which is the region of pathology. CAV causes intimal thickening and fibrous changes of the whole vessel wall, frequently including the media and adventitia. Hence, compensatory Glagov-type dilatory remodeling of the artery is relatively inhibited, and the artery often undergoes constriction.[14] CAV, unlike atherosclerosis, tends to be a diffuse, concentric disease affecting large and medium size vessels as well as the microvasculature.[10, 15] This underlying pathophysiology tends to make it difficult to detect angiographically. This is reflected in wide inter-observer agreement in the reporting of diffuse or distal disease.[16] Angiography, however, remains the cornerstone of clinical imaging at many institutions due to the ease and relatively inexpensive nature compared to IVUS. The prognostic value of angiography has been clearly demonstrated,[5] and so it remains important to use the recognised nomenclature for reporting (Table 1).[17] The introduction of physiological parameters to this nomenclature such as left ventricular ejection fraction (LVEF) and restrictive physiology adds incremental value to the risk stratification but is another indication of the imperfect nature of angiography as a diagnostic test.[18, 19]

Grade	
0 (not significant)	No detectable angiographic lesion
I (mild)	Angiographic left main (LM) <50% stenosis, or primary vessel with maximum lesion of <70%, or any branch stenosis of <70% (including diffuse narrowing).
II (moderate)	Angiographic LM 50%-69% stenosis; a single primary vessel ≥70% stenosis, or isolated branch stenosis of ≥70% in branches of 2 systems.
III (severe)	Angiographic LM ≥70%, or two or more primary vessels ≥70% stenosis, or isolated branch stenosis of ≥70% in all 3 systems. Or mild/ moderate angiographic disease with LVEF <45% or evidence of significant restrictive physiology (i.e. symptomatic heart failure with echocardiographic E to A velocity ratio >2 (>1.5 in children), shortened isovolumetric relaxation time (<60 msec), shortened deceleration time (<150 msec), or restrictive hemodynamic values (Right Atrial Pressure >12mmHg, Pulmonary Capillary Wedge Pressure >25 mmHg, Cardiac Index <2 l/min/m2)

Table 1. ISHLT Consensus Grading for Coronary Allograft Vasculopathy (*Mehra et al* 2010)

For children, angiography is clinically even more important than in adults because intravascular ultrasound is largely avoided in smaller children due to the size of the coronary arteries. However, in children, published rates of angiographically defined CAV appear substantially lower than adult series at only 17% at 5 years.[6]

It may be hypothesised that the reason for this is that there is less donor atherosclerosis in younger donors and less recipient risk factors for atherosclerosis. However, this fact is hard to reconcile with the fact that CAV is an even more important cause of death or graft loss after the first year in children than in adults (in whom malignancy is more common).[5, 6] An alternative explanation is that, the pattern of disease is different with a greater burden due to concentric disease with less focal narrowing initially and hence it becomes even more difficult to diagnose angiographically. In support of this are the small paediatric IVUS studies showing only 18% to 30% sensitivity for angiography to detect CAV in children.[20, 21]

1.3. IVUS

In 1995, *Mehra et al* reported on the prognostic significance of IVUS. This study showed that, even in the presence of a normal angiogram, cardiac endpoints (death, infarction or intervention) were significantly more likely if severe intimal proliferation was present on IVUS.[22] This finding was subsequently confirmed by *Rickenbacher et al* who showed that, despite normal angiography, a mean intimal thickness of >0.3mm was associated with a significantly worse four-year survival and predicted the subsequent development of angiographic disease.[23] It has been previously demonstrated that it is not merely the presence of disease but the timing of onset and rate of progression that determines outcome.[24] Congruent with this, *Kobashigawa et al* went on to show that rapid intimal proliferation (as evidenced by an increase in intimal thickness of more than 0.5mm in the first year after heart transplantation) was an important predictor of all-cause death. [25]

IVUS is the most sensitive imaging modality for the detection of CAV, it has high image resolution and measures of intimal thickness are reproducible. In addition, the prognostic significance is described above. For these reasons, most large multicentre trials use IVUS as the gold standard to assess the effect of drug treatments on CAV. Despite this, there remain a number of concerns regarding routine clinical use. These include an inability to draw inferences on the state of the microvasculature and a lack of standardisation of technique and of image analysis. Furthermore it is costly and time-consuming. A recent consensus statement concludes that routine IVUS for clinical follow-up cannot be advocated at this time because its value as a surrogate marker remains investigational.[17] However, this consensus statement does go some way into establishing standards for carrying out IVUS. Triple vessel imaging is preferred if possible with preference to imaging of the left anterior descending artery, followed by the right coronary artery and finally the circumflex when possible. It further advises an automated pullback to enhance consistent sampling and identification of branch vessels that are used as landmarks so that serial investigations can be performed and compared. This is the technique that we use at our institution, although, due to time constraints, imaging of the left anterior descending is preformed in preference. The consensus statement falls short of providing image analysis guidance. At our institution, we aim to analyse 30 cross-sectional images evenly spaced (at approximately 1.5mm intervals) over the same segment of left anterior descending artery identified by branch points. Additionally, the images anlaysed are always taken during the mid-diastolic rest period for consistency. Maximal intimal thickness, mean intimal thickness, mean intimal index,[10] Stanford Grading[10] score and percent atheroma volume[26] are recorded. In addition, a semi-

automatic interactive edge-detection software is used (QIVUS Clinical Edition, Medis medical imaging systems) to improve reproducibility of measurements.[27] By adopting a standardised approach to performing IVUS and by using a systematic consistent analysis method, we believe that the clinical applicability for follow-up and sensitivity to change in CAV is improved.

In young children, evidence to support the use of IVUS is lacking. Unlike angiographically demonstrated CAV in children, demonstration of CAV by IVUS has not yet been convincingly shown to have any impact on prognosis.[21] However, this may be explained by small study numbers and inconsistent analysis and reporting techniques. Technical difficulties are also higher in children due to size and time limitations. Reported literature shows possible use of IVUS in children between 21-79kg, although the reported lower weight limit is 10-25kg.[20, 21] In our clinical practice, we generally avoid use of IVUS below 10 years of age.

1.4. Coronary Flow Reserve

CAV is a diffuse process with frequent involvement of large- and medium-sized vessels as well as the microvasculature.[28] Furthermore, microvascular disease, as demonstrated by histology, has been shown to be a predictor of cardiac mortality in this group of patients, independent of other risk factors, including the presence of angiographically demonstrated epicardial disease.[29] Coronary microvasculature function can be directly assessed invasively by Doppler wire (or thermodilution) coronary artery flow velocity measurements before and after direct administration of endothelial-dependent vasodilators (acetylcholine or substance P) and endothelial-independent vasodilatation (nitroglycerine, adenosine, or papaverine). The Coronary Flow Reserve (CFR) is defined as the coronary artery

averaged peak velocity during administration of vasodilator divided by the averaged peak velocity at rest. A reduction in CFR using maximal adenosine vasodilation, in the context of a normal fractional flow reserve (i.e. no epicardial stenosis) indicates microcirculatory dysfunction.[30] The Doppler wire method also provides other measures of microcirculatory function by analysis of the flow patterns ((e.g. diastolic deceleration time, systolic flow reversal) but there is less experience with the interpretation of these parameters. However, despite the proven prognostic value of detection of endothelial dysfunction using CFR in the setting of atherosclerosis,[31, 32] its significance in the setting of CAV remains unclear.

Kubrik et al, in a study of 185 patients showed that whilst microvascular dysfunction, demonstrated by CFR, was a predictor of outcome (death or adverse cardiovascular event) in the univariate analysis, it did not predict outcome in the multivariate analysis.[33] In a smaller study of 73 patients, *Hollenberg et al* showed again that microvascular dysfunction was more common in the group suffering adverse outcomes (death or angiographic evidence of CAV) than in those without adverse outcome. There was no multivariate analysis in this study.[34]

Regarding children, a small study has shown that occurrence of microvascular disease correlates with length of time since transplant.[35] Similarly, in another small study, CFR has been shown to be significantly reduced in children with histologically demonstrated microvasculopathy.[36] However, importantly this study was not able to demonstrate whether the reduction in CFR was due to epicardial or microvascular coronary disease. This was because there was only one patient in this study that had microvascular disease on histology without CAV demonstrated on angiogram.

Although prognostic value of detecting microvascular disease by histology has been demonstrated, the incremental prognostic value of performing CFR measurements is uncertain. A recent study comparing IVUS and CFR measurements, suggests that, even in early CAV, the pattern of involvement is diffuse from epicardial arteries to microvasculature and suggests therefore that IVUS alone is sensitive enough to infer microvascular involvement.[37] Furthermore, the invasive nature of CFR makes it unattractive for diagnostic use in children.

More recently, the index of microvascular resistance (IMR) has been shown to be a measure which is more independent of epicardial disease than CFR.[38] It is measured in a similar manner and defined as distal coronary pressure multiplied by the hyperaemic mean transit time (mmHg seconds).[39] One study has already demonstrated the potential value of this index as a marker for CAV but further evaluation is necessary.[15]

1.5. Single photon emission computed tomography

Single photon emission computed tomography (SPECT) is well established in the detection of ischaemia in the setting of coronary atherosclerosis and its value to guide management in this setting has been documented.[40, 41] *Ciliberto et al* demonstrated the use of quantitative evaluation of SPECT imaging with high-dose dipyridamole stress for CAV.[42] This study showed that if rest echocardiography showed no wall motion abnormalities and SPECT did not show the presence of a reversible perfusion defect, then the combined negative predictive value of this for any significant CAV was 100%. Significant CAV is defined here as luminal narrowing >50% and/or diffuse small vessel narrowing. However, this combined approach still only achieves 60% sensitivity for all angiographically demonstrated

CAV. Given the relative insensitivity of angiography, as discussed above, there would be significant concerns regarding the applicability of this approach for early detection and prevention of CAV.

Wu et al similarly showed the use of dobutamine stress perfusion with SPECT but again used angiography as the comparison.[43] Several smaller studies have also indicated the potential of SPECT in this respect[44-46].

More importantly a reversible stress perfusion defect on SPECT has been shown to be an independent predictor of mortality and graft loss after heart transplantation [42, 43, 47, 48] and two small studies have even suggested that stress SPECT imaging at 1 year post-transplant may be of early prognostic significance.[49, 50] However, the use of SPECT still needs to be moderated by concerns regarding the relative insensitivity to detect CAV when compared to IVUS and concerns regarding the use of ionising radiation.

The experience of SPECT imaging in children with CAV is extremely limited and this may in part be due to low spatial resolution, which becomes particularly relevant for smaller hearts.

1.6. Echocardiography

Both Dobutamine Stress Echocardiography (DSE) and Tissue Doppler Imaging (TDI) have been evaluated with respect to CAV. In a well-structured investigation, *Spes et al* evaluated both the diagnostic and prognostic value of DSE.[51] This showed that DSE has a poor sensitivity (47%) to detect progression of CAV as demonstrated by a combination of angiography and IVUS (specificity 72%, positive predictive value 74%, negative predictive value 44%). However, the prognostic implications of serial DSE testing are clearly shown from this study.

Serial normal DSE examinations had a 96% negative predictive value for adverse cardiac outcomes (Sensitivity 82%; Specificity 69%; Positive Predictive Value 29%). Limitations of this study include the fact that only patients with adequate trans-thoracic echocardiographic windows could be studied. Furthermore, the average length of clinical follow-up stated was only 2.7 years per patient and so the number of cardiac adverse outcomes was small (with many of the recorded adverse events being coronary interventions). In addition, IVUS was not performed in all of the patients. Despite these limitations, it is interesting to note that in patients with abnormal DSE, 90% had significant CAV by IVUS, but only 49% by angiography. This confirms that angiography is relatively insensitive in detecting CAV and infers incremental value to the addition of stress testing for institutions following only a policy of coronary luminal imaging. Furthermore, the high negative predictive value of stress testing with respect to outcome may suggest that if a strict DSE protocol is followed, a selective angiography/ IVUS policy may be adopted. This policy would be supported by findings from other DSE studies.[52-54] Furthermore, another study has also suggested that this is also true even early after transplantation and that early reproducible wall motion abnormalities on dobutamine stress are predictive of later events.[55] This offers further evidence for the use of stress testing to reduce the burden of invasive monitoring for CAV. Recent evidence suggests that strain rate imaging may be a useful quantitative aid to improve upon the qualitative visual assessment of myocardial segmental contractility during DSE.[56]

The non-invasive nature of DSE and the familiarity with echocardiography mean that DSE in children can be carried out with relative ease in most cases (with use of sedation for more difficult cases). This makes it an attractive modality in

children and studies in children have shown promise in this respect.[57-60] When angiography is used as the standard, DSE shows a sensitivity for the detection of CAV in children of 35-71%; specificity of 80-94%; positive predictive value of 45-71% and negative predictive value of 81-92%.[57, 58, 60] Furthermore, although the adverse event rate in these studies was low with a relatively short follow-up, prognostic significance of DSE has been demonstrated in children with a negative predictive value of 95-96% with respect to adverse events.[57, 58] Although utility and feasibility have been demonstrated, DSE imaging in children requires a good setup to ensure efficient intravenous access; accurate ECG monitoring; effective sedation if required; sonographer expertise in image acquisition; physician expertise in wall motion analysis; appropriate software for analysis and a specific, reproducible protocol.

A recent small study has shown the feasibility of assessing CFR by contrast-enhanced trans-thoracic echocardiography.[61] It showed both high sensitivity and specificity for the detection of significant CAV (as defined by maximal intimal thickness on IVUS >0.5mm). In a previous study with multivariate analysis, the same group has shown the prognostic value of this technique.[62] Given the uncertainty regarding the prognostic value of invasive CFR measurements, further evaluation of this technique is required to demonstrate its robustness.

Tissue Doppler Imaging has become commonplace in clinical cardiology. *Dandel et al* have demonstrated the utility of TDI for the detection of CAV.[63] In this study 293 patients underwent angiography and those with normal angiograms underwent further intravascular ultrasound to evaluate for CAV. In this study, systolic TDI parameters at the basal lateral LV wall (mitral annulus level) were found to be most predictive for CAV. Both peak systolic wall motion velocity (Sm) and time to

peak systole (TSm, using a phonogram to time the first heart sound) were significantly different between those with CAV (even if only detected on IVUS) and those without CAV. However, only the negative predictive value of TDI for angiographic disease is quoted, with more complex formulae required to exclude intravascular ultrasound or angiographic disease with only 80% probability. Nevertheless, with Sm >11cm/s and TSm > 110cm/s^2, angiographic disease can be excluded. Furthermore, in the absence of any rejection, an Sm < 10cm/s has a positive predictive value of over 97% for CAV (detected by IVUS or angiography). Concerns with this approach include interobserver variability of measurements and the influence of bundle branch block on individual TSm measurements. Given the ease of acquisition of serial measurements, TDI seems to be sensible addition to routine 2-dimensional echocardiography follow-up in the clinic. However, consistency and interpretation may vary from centre to centre.

In children, the applicability of TDI after heart transplantation has been studied in 53 children, in order to investigate the progression of TDI indices. Only 8 children had pre-terminal disease but the study did show that both tricuspid and mitral annulus peak velocities (systolic and early diastolic) are reduced in pre-terminal disease. Tricuspid annular velocities (systolic and diastolic) were shown to be earlier predictors than mitral ones. However, in this study, traditional echocardiographic measures such as ejection fraction and tricuspid regurgitation severity were also early and strong predictors of mortality respectively. Hence, although the feasibility and reproducibility of tricuspid annular velocities in children has been shown,[64] the incremental value of TDI for children remains unclear. Furthermore, a recent study in paediatric heart transplant recipients showed a poor correlation between TDI parameters and invasive haemodynamics

for both right and left ventricular indices.[65] Hence, although easily applied, interpretation of TDI indices after heart transplantation for children requires further study.

Exercise stress echocardiography has been evaluated in heart transplant recipients but has been repeatedly found to have an unacceptably low sensitivity.[66, 67] The reason for this may be the relatively poor heart rate response to exercise in transplant recipients.[68]

1.7. Pulse Wave Velocity

Carotid-Femoral pulse wave velocity (PWV) is easy to perform clinically and is a marker for the intrinsic stiffness of the aortic wall, which has been shown to be highly predictive for cardiovascular events in the setting of atherosclerosis.[69-74] The explanation given for this has been that the PWV is a measure reflecting the cumulative effect of cardiovascular risk factors on the arterial wall.[75] Furthermore increased aortic stiffness signifies adverse myocardial haemodynamic conditions including an increase in systolic blood pressure and pulse pressure with increased systolic load and decreased myocardial perfusion pressure.[76-78] The relative ease of measurement would make it an attractive adjunct to the clinic if its utility can be shown in the setting of CAV. It would be particularly beneficial in children for whom quick non-invasive markers are more acceptable. However, the pattern of blood pressure increase after cardiac transplantation in childhood is not typical to that seen due arterial stiffness (e.g. high systolic blood pressure with wider pulse pressure, as seen in elderly patients).[79] Nevertheless, a small study performed in children above 5 years of age showed a significant correlation between length of time since transplantation and PWV.[79] This finding may suggest that systemic

inflammatory insults related to CAV may also be correlated to PWV. Although numbers were too small for a meaningful multivariate analysis, the utility of PWV in these patients warrants further attention.

1.8. Multidetector Computed Tomography

In the setting of atherosclerosis, new Multidetector Computed Tomography (MDCT) facilities have been proven to have high sensitivity and specificity for the detection of angiographically significant coronary stenoses.[80] Furthermore, coronary plaque detection is also possible using MDCT and attempts are being made to characterise plaque using this imaging modality.[81, 82] In line with these findings, it has also been shown that MDCT is accurate in defining coronary stenoses in the setting of CAV.[12, 83] It has been shown that, using a 16-detector MDCT, 95% of coronary segments >1.5mm can be imaged.[83] Of the segments that were imaged, and by defining a significant coronary stenosis as >50%, MDCT was shown to have sensitivity, specificity, and positive and negative predictive values of 86%, 99%, 81%, and 99%, respectively, when compared with angiography. Only a small subsection of these patients underwent IVUS. In a separate study of 20 patients, *Gregory et al* showed that in comparison to IVUS (defining significant CAV as a maximal intimal thickness >0.5mm for a given segment), 64-detector MDCT had a sensitivity of 70%, specificity of 92%, positive predictive value of 89%, and negative predictive value of 77% for the detection of CAV.[12] It should be noted that in this study, 17% of segments (mainly distal segments) could not be analysed due to image quality and authors describe this patient group as challenging due to high BMI and high resting heart rates despite use of beta-blockers.

However, the introduction of vessel wall analysis with MDCT gives further potential strength to this imaging technique.[84, 85] Using a 16-detector MDCT and oral beta-blockers for all patients, *Romeo et al* described the analysis of lumen and vessel wall defining three groups by visual assessment ((i) normal; (ii) wall thickening without significant stenosis and (iii) stenosis (luminal stenosis >50%).[84] Again complete analysis of coronary segments was not possible in 17% (9 of 53) of patients. A further 2 patients had impaired analysis due to heavy calcification. This impact study of this is reduced, as it did not use IVUS to correlate findings of wall thickening. Nevertheless, the sensitivity of MDCT for the detection of stenosis was 83%, specificity 95%, positive predictive value 71% and negative predictive value 95%. Another small study, using 64-detector MDCT showed that it may be more sensitive for the detection of CAV than angiography alone but again, no IVUS was preformed for defining vessel wall disease.[85]

One small study directly compared a 64 channel dual source CT technology with IVUS.[86] CAV was defined as intimal thickening >0.5mm on IVUS and any visible wall thickening on CT. 27% of screened patients were excluded from the study due to impaired renal function, which is a common finding in this group of patients. Despite a high mean HR (80 bpm, range 60-100 bpm), no beta-blockers were required and image quality was adequate for analysis in 96% of all coronary segments that were larger than 1.5mm diameter on angiography. Using IVUS to define CAV, dual source CT had a sensitivity of 85%, specificity of 84%, positive predictive value of 76%, and negative predictive value of 91%.

In summary, the progress in equipment, such as increased slice number, use of dual source technology, increased gantry rotation speed and so on has made the MDCT examination time shorter, increased the success rate of examined cases and

reduced the total radiation exposure. The use of MDCT as a screening tool to reduce the number of invasive procedures therefore seems appropriate, although concerns remain regarding the radiation exposure, image degradation due to vessel calcification, use of nephrotoxic contrast agent, image acquisition at high heart rates (which appears less problematic with the latest dual source CT technology) and the image resolution achieved. Further, although comprehensive function, stress testing and myocardial scar protocols are possible using MDCT, the radiation dose involved deters extensive protocols.

With regards MDCT imaging in children, there is very little published data. Some small studies have suggested feasibility of MDCT in both Kawasaki disease and CAV but issues of resolution, high heart rates and radiation exposure remain important limitations.[87, 88]

1.9. Cardiac Magnetic Resonance (CMR)

Coronary Magnetic Resonance Angiography (CMRA) has demonstrated feasibility for the detection of stenoses in the setting of atherosclerosis,[89] and, when using tailored paediatric protocols, it is even of diagnostic use in small children with high heart rates.[90-92] However, most authors would agree that resolution and diagnostic accuracy is not as high as MDCT and indeed, one small trial looking at both modalities in the setting of CAV, confirms this statement.[93] However, the advantage of CMR is its versatility in functional imaging. A single CMR exam can give information on volumes, function, wall motion, myocardial scar, ischaemia and coronary angiography.

In the setting of atherosclerosis, adenosine stress perfusion MRI has shown non-inferiority to SPECT for the detection of myocardial ischaemia and further trials

are underway.[94] Furthermore, for dobutamine stress, MRI has been shown to perform better than echocardiography for the detection of atherosclerotic coronary stenoses.[95] Initial data for analysis using MRI, suggests that MRI may be able to quantitatively assess myocardial perfusion reserve.[96] However, this study used CFR to define significant CAV and because all the patients in the group with significant CAV had severe epicardial disease, microvascular disease could not be independently assessed.

Coronary vessel wall imaging and analysis has been shown to be feasible using MRI but this technology has not been assessed in the setting of CAV. [97-99]

Steen et al, using the robust clinical tool of myocardial late gadolinium enhancement (LGE) showed that 84% of patients with severe CAV on angiography had typical infarct-pattern subendocardial late gadolinium enhancement with a distribution consistent with the pattern of CAV on angiography.[100] Those patients with infarct-typical patterns of LGE had also showed reduced left ventricular ejection fractions at rest.

There are promising advantages of using CMR to define CAV. These include the comprehensive assessment possible; the lack of ionising radiation and the non-invasive nature. However, although less nephrotoxic than x-ray contrast media, Gadolinium-based agents remain contra-indicated in end-stage renal failure due to concerns regarding nephrogenic systemic fibrosis (NSF). Moreover, the paucity of data for CMR in the setting of CAV precludes any recommendations regarding its use at the current stage. There is no substantial data to support its use in children.

1.10. Conclusions

Despite advances described here, conventional angiography remains the main diagnostic modality of choice for the follow-up of CAV. The prognostic impact of angiography is clear but its relative insensitivity renders it flawed as a screening tool to detect and attempt to treat disease early. IVUS is currently the most sensitive imaging modality and so, is crucial in this regard for the study of disease and prevention. It is therefore important to perform and analyse/ report the IVUS in a thorough and reproducible manner. Such attention to detail for IVUS will also facilitate studies seeking to validate non-invasive imaging methods.

Sufficient data exists for the use of dobutamine stress echo (DSE) or SPECT stress perfusion in adults as a screening tool to reduce the burden of invasive testing. In children, DSE is currently preferable. CMR is a promising modality and there are clear advantages in terms of comprehensive single-modality assessment; in terms of image quality over DSE and in terms of lack of radiation over SPECT imaging. MDCT can now give both vessel wall and lumen information with acceptable accuracy in non-calcified vessels. Therefore, this modality may also be used to reduce the amount of invasive testing, although applicability to children may be limited due to high heart rates and ionising radiation.

The choice of non-invasive imaging modality to guide a selective approach to conventional angiography and IVUS, is currently guided by centre experience. In particular stress protocols whether SPECT, DSE or MRI must be performed and analysed rigorously according to accepted criteria. Operator experience, good image quality and effective patient-friendly protocols are currently more important determinants of the diagnostic power of the imaging than the actual choice of imaging modality.

In order to realise the advantages of CMR for coronary vasculopathy imaging in children, the first step in this thesis is to develop routine diagnostic quality coronary lumen imaging in children and to develop reference values for CMRA lumen dimensions. The next step is to investigate techniques for improving lumen image quality further. Once this has been elaborated, the use of direct imaging of coronary vasculopathy using contrast-enhanced techniques can be applied to specific patient groups. Finally, the development of rapid aortic imaging as a marker for coronary vasculopathy is explored.

Chapter 2 - Coronary Lumen MRI In Children

2. Coronary Lumen MRI In Children

2.1. Developing Coronary Lumen Imaging in Children: The Dual Phase approach

2.1.1. Introduction

Good coronary lumen imaging underpins successful coronary vessel wall characterisation by MR. The technique of coronary imaging in children has been well described in children with congenital heart disease.[101] In order to achieve this, a number of challenges were overcome, including cardiac and respiratory motion, and the proximity of the coronary arteries to epicardial fat and myocardium (Figure 1). Cardiac motion required synchronisation of data acquisition to the mid-diastolic rest period of the heart as identified using a high temporal resolution 4-chamber cine.[102] Compensation for respiratory motion was performed using an MR navigator, a pencil like beam, placed on the dome of the right hemi-diaphragm.[103] Data is accepted if the diaphragm-lung interface is within a window of 3 to 5 mm placed in end-expiration. Suppression of high signal from the epicardial fat was accomplished using a frequency selective small-banded pre-pulse that saturates fat signal and immediately precedes the imaging sequence.[104] Myocardial suppression was achieved using a T2 pre-pulse.[105] The combination of these imaging advances made coronary imaging possible in children. However, even in the aforementioned study by *Beerbaum et al*,[101] imaging of children less than 6 years of age was unsatisfactory due to vessel size and high heart rates. In this regard, major advances have been made by our group (detailed in study 2.1.2. and 2.1.3. below).

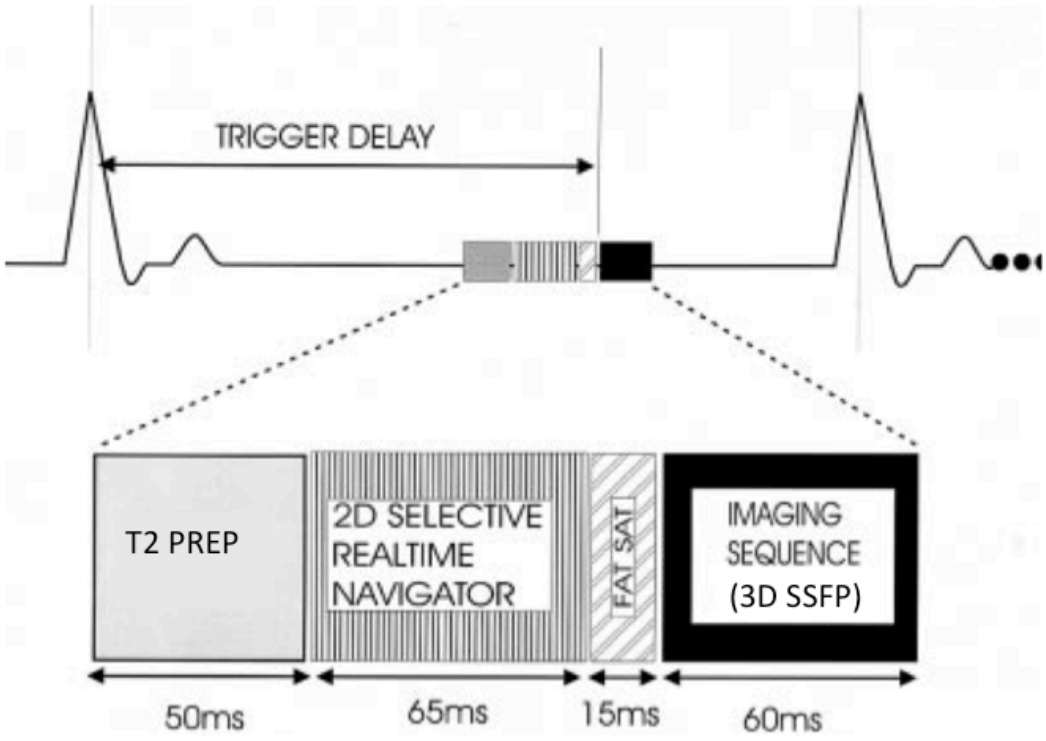

Figure 1. Schematic Showing Three-Dimensional Whole Heart Sequence

Myocardial suppression was achieved using a T2 pre-pulse (T2 PREP). Compensation for respiratory motion was performed using an MR navigator, a pencil like beam, placed on the dome of the right hemi-diaphragm (2D SELECTIVE REALTIME NAVIGATOR). Suppression of high signal from the epicardial fat was accomplished using a frequency selective small-banded pre-pulse that saturates fat signal and immediately precedes the imaging sequence (FAT SAT). The imaging sequence is a three-dimensional steady-state-free-precession acquisition.

2.1.2. Detection of Coronary Artery Anomalies in Infants and Young Children with Congenital Heart Disease Using Magnetic Resonance Imaging, *(Tangcharoen et al)*

Dr. Hussain's contribution to this work was data analysis and manuscript editing.[90] This work showed that, using a set protocol, coronary imaging in children is successful beyond 4 months of age (88% success at >4 months vs. 17% ≤4 months, $p<0.001$). There were several key improvements that may have allowed this improvement in comparison to previous studies:

- In younger patients with higher heart rates, the mid-diastolic rest period shortened whilst the end systolic rest period remained almost constant. As a consequence we acquired the whole-heart data during end systole in most of our young children and achieved diagnostic image quality in most of our patients. Another advantage of end systolic data acquisition may be the more constant duration and position of the systolic rest period within the cardiac cycle compared to the mid-diastolic rest period.[106]
- General anaesthetic allowed for a more regular pattern of breathing compared to free-breathing patients. In fact sequential breath holds in combination with a very narrow navigator window (3 mm) allowed very successful suppression of respiratory motion. The use of remifentanil as the anaesthetic agent is further advantageous in terms of heart rate control for imaging
- As coronary arteries in children are small, better intravascular contrast may have been achieved by imaging after administration of Gadolinium-based contrast agent as observed by other groups.[107]

2.1.3. Coronary MR Angiography in children with CHD During Systole and Diastole Using a Dual Cardiac Phase Whole Heart Scan *(Uribe et al)*

Dr. Hussain's contribution to this work includes study planning, data collection, analysis and manuscript editing.[92] Given our previous experience with end-systolic imaging for higher heart rates, we sought to assess a newly developed sequence, "the dual phase sequence" capable of acquiring 3D data during both end-systolic and mid-diastolic rest periods within each cardiac cycle.[108] This study showed the advantages of the novel dual phase technology. As outlined by *Tangcharoen et al*, the ideal rest period needs to be predicted prospectively for the single phase technology. With the dual phase technology, it was nicely demonstrated that within the same patient, different segments of the coronary artery may be better visualised either in an end-systolic or mid-diastolic phase. However, contrary to our initial hypothesis, it was not possible to predict which rest period would be optimal for a given segment at a given heart rate. Hence it is hypothesised that, in fact, the dual cardiac phase offers further improved coronary artery visualisation due to the possibility of retrospectively choosing the best cardiac phase for each segment. This development also has wider implications for patients with congenital heart disease and this is investigated in section 2.1.4 below.

2.1.4. 3D Dual-Phase Whole-Heart Magnetic Resonance Imaging: Clinical Implications for Congenital Heart Disease

2.1.4.1. Advances in Knowledge

1. A recently developed dual cardiac phase technique for whole heart imaging is able to image in both systolic and diastolic rest periods in approximately the same time as a standard single phase sequence.

2. For 3D whole-heart steady-state-free-precession imaging, cardiac chambers (ventricles and atria) and pulmonary veins are better imaged in systole whereas the great vessels are better imaged in diastole.

3. 3D dual phase whole heart imaging offers a higher rate of diagnostic quality imaging for all cardiac structures in congenital heart disease than either systolic or diastolic imaging alone.

4. 3D dual phase imaging is able to depict changes in diameter of structures in congenital heart disease through the cardiac cycle and so is better for the planning of interventional procedures than the standard single phase technique.

5. Arterial stenoses have better image quality in diastole but for, interventional planning, should be measured in systole and both can be achieved with 3D dual phase whole-heart imaging.

2.1.4.2. Implications for Patient Care

1. To improve rates of diagnostic image quality and to allow accurate measurements for interventions, 3D angiography in congenital heart disease should be performed in both systolic and diastolic rest periods.

2. The 3D dual phase whole-heart technique is able to image in both systolic and diastolic rest periods in approximately the same time as a standard single phase sequence.

2.1.4.3. ABSTRACT

Purpose: To identify which rest phase (systolic or diastolic) is optimum for assessing or measuring cardiac structures in the setting of 3D whole-heart imaging in congenital heart disease (CHD).

Materials and Methods: The study was approved by the Institutional Review Board and informed consent obtained. 50 children (26 male) underwent 3D dual phase whole-heart imaging. Cardiac structures were analysed for contrast-to-noise ratio (CNR) and image quality (IQ). Cross-Sectional measurements were taken of the aortic arch, right ventricular outflow tract (RVOT) and pulmonary arteries. Normally distributed variables were compared by paired t-tests and categorical data by Wilcoxon signed-ranks test.

Results: CNR and IQ were significantly (all $p<0.05$) greater in systole for the cardiac chambers (RA (mean CNR = 8.9 vs. 7.5: sum of IQ ranks = 438 vs. 91), LA (CNR = 8.0 vs. 5.3: IQ = 1006 vs. 29), RV (CNR = 10.6 vs. 8.2: IQ=131 vs. 23) & LV (CNR = 9.4 vs. 7.7: IQ = 125 vs. 28)) and pulmonary veins (CNR = 6.2 vs. 4.9: IQ = 914 vs. 32). Conversely, diastolic CNR was significantly higher in the Aorta (9.2 vs. 8.2: $p=0.013$) and diastolic IQ was higher for the branch pulmonary arteries (LPA = 238 vs. 62: $p=0.007$)(RPA = 219 vs. 35: $p<0.001$) and for post-arterial stenosis imaging (164 vs. 7:$p<0.001$). All aortic arch and RVOT cross-sectional measurements were significantly ($p<0.05$) greater in systole (Narrowest-point-of-arch = 70 vs. 53mm2; Descending-Aorta= 71 vs. 58mm2; Transverse-arch = 293

vs. 275mm2; valvar-RVOT = 291 vs. 268mm2; supravalvar-RVOT = 337 vs. 280mm2; pre-bifurcation-RVOT = 329 vs. 259mm2) Conclusion: Certain structures in CHD are better imaged in systole and others in diastole and therefore, the dual phase approach allows a higher overall success rate. This approach is also able to depict diameter changes between systole and diastole and is therefore preferable to standard single phase sequences for the planning of interventional procedures.

2.1.4.4. Introduction

A single phase 3-dimensional (3D) steady-state-free precession (SSFP) whole-heart approach with respiratory navigator gating and ECG triggering is now frequently used and has proven utility for diagnostic imaging in children with congenital heart disease (CHD).[101] It is common practice to perform this imaging in the diastolic rest period. In young children with high heart rates, utilisation of the systolic rest period for such imaging has been demonstrated to be successful.[90] Recent advances have allowed acquisition of the 3D whole-heart data set in both end-systole and mid-diastole, in a single free-breathing sequence in approximately the same time as the traditional single phase sequence. This sequence has been termed the '3D dual phase whole-heart sequence'.[92] The relevance of this technique has been demonstrated for coronary imaging, ventricular function and volumetric assessment.[92] However, its utility has not been assessed in the wider setting of congenital heart disease.

The dual phase 3D whole-heart sequence offers not only the opportunity to study which heart phase is optimum for each structure but also affords the clinical opportunity to retrospectively select either phase for the assessment of anatomy.

An important parameter for assessing anatomy is the vessel sharpness. This is particularly relevant when measuring vessel size for planning of interventions. Vessel sharpness using the ECG-gated 3D whole-heart approach at end-diastole has been shown to be superior compared to non-gated conventional magnetic resonance angiography.[109]. However, it may be more appropriate to image at end-systole for the purposes of certain interventions (e.g. implantation of valve bearing stents), because this gives the maximum arterial diameter.[110] The 3D dual phase approach may also be able to detect changes in diameter between systole and diastole in order to appropriately plan intervention.

The purpose of this study was to identify which rest phase (systolic or diastolic) is optimum for assessing or measuring cardiac structures in the setting of 3D whole-heart imaging in congenital heart disease.

2.1.4.5. Methods

2.1.4.5.1. Participants

Children undergoing 3D whole-heart imaging for clinical reasons as part of a cardiovascular MRI were included in the study. The study was approved by the local Institutional Review Board (IRB 08/H0810/058) and informed consent was obtained. 50 children participated in this study. The mean age was 4 years 10 months (range 5 days to 18 years) and this was not different between male (mean age 4.7 years, range 2 weeks to 16 years) and female (mean age 5.1 years, range 5 days to 18 years) patients (p=0.35 by independent samples t-test). All children were in sinus rhythm. 42 underwent imaging while under general anesthesia with use of an anaesthetic delivery system (Aestiva/5; Datex-Ohmeda (GE Healthcare,

WI, USA) with pressure-controlled ventilation (routine protocol for young or uncooperative children at our institution). After gas induction, general anesthesia was continued with a continuous intravenous infusion of remifentanil. All anaesthetic procedures were completed without adverse effects.

2.1.4.5.2. MRI Protocol

Cardiac MRI was performed using a 1.5 Tesla Achieva clinical MR scanner (Philips Healthcare, Best, NL). 3D dual phase sequence was used for all cases.[108] As with standard 3D SSFP sequences,[101] the dual phase sequence is respiratory-gated and ECG-triggered with a fat saturation pre-pulse to null fat signal and a T_2 pre-pulse to improve the myocardium to blood pool contrast.[108] Imaging was acquired in a sagittal orientation (repetition time (TR) /echo time (TE) = 3.4/1.7 ms, flip angle 90°, 60-120 slices, isotropic resolution of 1-1.5 mm^3, acquisition window of 60 -75 ms). For children below 3 years of age, a two-element coil was used (Flex M or Flex S). For older children, a five-element cardiac coil was used. Parallel imaging with a SENSitivity Encoding (SENSE) acceleration factor of 2 in the antero-posterior direction was also used. Trigger delays were set for end-systole and mid-diastole. The cardiac rest periods were assessed with a high temporal resolution, balanced steady-state free precession (SSFP), four-chamber cine (TR= 3.1–3.6 ms, TE = 1.6–1.8 ms, flip angle 60°, 6-mm-thick sections, 240-300 mm field of view, 60–80 phases). The sequence employs navigators for each cardiac phase with a respiratory gating window of 3 mm and data is only accepted if both navigators, in any given cardiac cycle, fall within this gating window.

2.1.4.5.3. Image analysis

Image processing and reformatting were performed with commercially available analysis software (View Forum; Philips Healthcare). All cardiac chambers and great vessels were quantitatively analysed for contrast-to-noise ratio (CNR) and qualitatively analysed for image quality (IQ).

2.1.4.5.3.1. Image quality measurements

A consensus reading was performed for IQ on reformatted angiograms of each structure in a blinded and random order by 2 readers (TH and DL: both with >3 years experience of cardiovascular MRI). Prior to the analysis, a trial assessment of five angiograms was performed for quality assurance. Study images were first reviewed independently and then disagreement was discussed before the final grade was given. Image quality was scored according to the system described by *McConnell et al*: 0 indicates that the structure was not visible; 1 visible but with markedly blurred borders; 2 visible with moderately blurred borders; 3 visible with mildly blurred borders and 4 visible with sharply defined borders.[111] Using this, a score of 2 or more out of 4 was considered diagnostic quality (definition adapted from *Greil et al*).[112, 113]

2.1.4.5.3.2. Contrast to noise measurements

Regions of interest (ROIs) were defined to determine the signal (S) from blood (S_{Blood}) and reference tissue ($S_{Myocardium}$). ROIs were drawn by both observers independently (TH & DL) on images reformatted in the transverse plane. Noise (N) was estimated by the standard deviation in both of these respective ROIs, as parallel imaging was used.[113] Blood pool ROIs were drawn in the superior vena

cava (SVC), right atrium (RA), right ventricle (RV), main pulmonary artery (MPA), left pulmonary artery (LPA), right pulmonary artery (RPA), pulmonary veins (PV's), left atrium (LA), left ventricle (LV) and aorta (Ao). Similarly placed ROI's were positioned in identically reformatted systolic and diastolic images. Additional blood pool ROI's were drawn in any location post-arterial stenosis (e.g. post-coarctation or post pulmonary artery stenosis) and in structures pertinent to specific congenital defects (lateral tunnels in total cavo-pulmonary connection; modified Blalock-Taussig shunts (BT); Glenn anastomoses and Damus-Kaye-Stansel (DKS) anastomoses).

CNR was defined by using the following equation:

$CNR = (S_{Blood} - S_{Myocardium})/(0.5 \cdot (N_{Blood} + N_{Myocardium}))$, where all variables are means.[114]

2.1.4.5.3.3. Cross-Sectional Measurements

Measurements of the aortic arch, branch pulmonary arteries or right ventricular outflow tract (RVOT) were performed as clinically indicated. These cases were chosen to in order to answer the following clinically pertinent question: in the setting of branch pulmonary artery stenoses, repaired coarctation or right-ventricular outflow tract surgery, is it important to measure in the correct rest period for interventional planning?

For the aortic arch, cross-sectional area was measured at the narrowest point (isthmus or coarctation site); at the transverse arch (between left common carotid and left subclavian) and at the descending aorta, level with the dome of the

diaphragm (Figure 2). For the branch pulmonary arteries, measurements were repeated at the narrowest point and at the distal vessel prior to bifurcation (or trifurcation) (Figure 2). RVOT dimensions were measured at valvar, supravalvar and pre-bifurcation levels. In all cases, care was taken to ensure measurements were in the exact corresponding positions in both systole and diastole (see (Figure 2)).

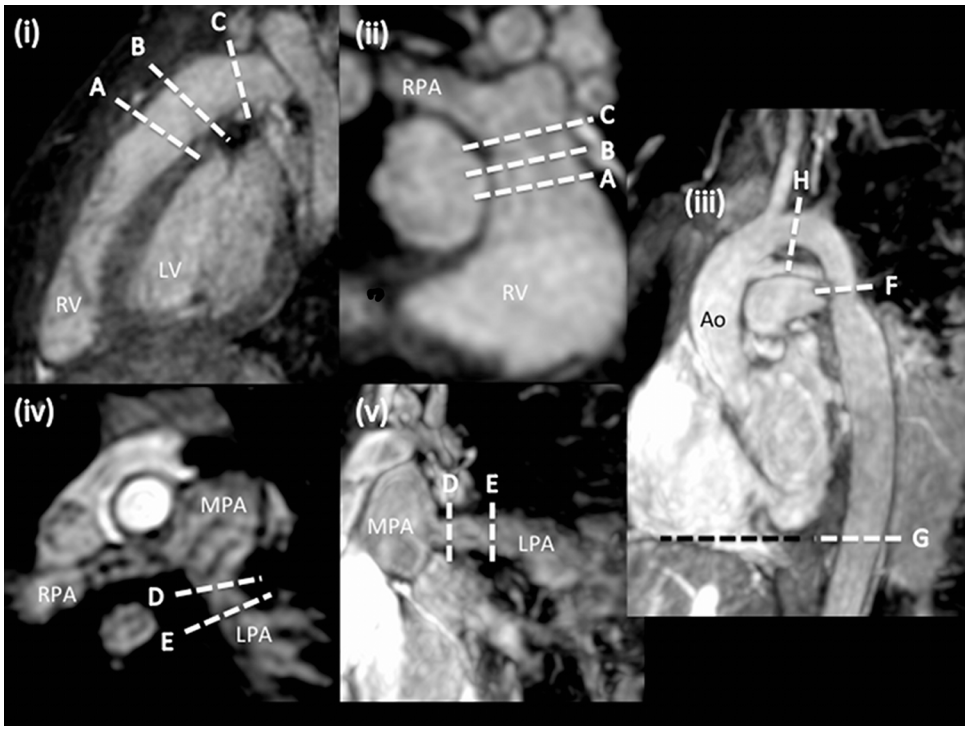

Figure 2. Measurement levels for Dual Phase Study

(i) shows right ventricular outflow tract (RVOT) in sagittal plane (RV = right ventricle; LV = left ventricle)

(ii) shows right ventricular outflow tract in coronal plane (RPA= right pulmonary artery)

(iii) shows arch in oblique sagittal (Ao = Aorta)

(iv) shows branch pulmonary arteries in transverse plane (MPA = main pulmonary artery; LPA = left pulmonary artery)

(v) shows left pulmonary artery in sagittal plane

Dashed line represent levels at which measurements were taken:

A: RVOT at valvar level

B: RVOT at supravalvar level

C: RVOT at pre-bifurcation level

D: LPA at the narrowest point

E: LPA at the distal vessel

F: Aortic Arch at the narrowest point (isthmus or coarctation site)

G: Descending aorta, level with the dome of the diaphragm

H: Transverse arch (between left common carotid and left subclavian)

2.1.4.5.4. Statistics

IQ scores represent categorical data and were tested using non-parametric statistical procedures. Remaining variables were visually assessed with histogram plots and formally tested for normality using Kolmogorov-Smirnov tests for normality. Normally distributed variables were compared by paired t-tests and remaining variables were assessed by Wilcoxon signed ranks test. A repeated measures analysis of variance models for CNR was constructed in order to account for within-subject and between-subject variability arising from testing multiple segments over two phases in each patient. Levene's test was used to assess the assumption for homogeneity of variance. Assumptions of sphericity were formally tested using Mauchly's test but rejected. Hence, results given use the Greenhouse-

Geisser model. The Bonferroni correction is used to correct for multiple comparisons. Statistical analysis was performed on SPSS (version 19) 2010.

As we are unaware of similar data from previous studies, prospective power analysis was not possible. However, post hoc analysis shows that for a significance level of 5% and with 80% power, 50 cases enables us to be able to detect a change in CNR of approximately 10% in the aorta. A 10% difference was felt to be appropriate from a clinical perspective.

2.1.4.6. Results

2.1.4.6.1. Participants

50 children (26 male) underwent 3D dual phase SSFP imaging. The mean age was 4 years 10 months (range 5 days to 18 years) and this was not different between male (mean age 4.7 years) and female (mean age 5.1 years) patients (p=0.35 by independent samples t-test). Diagnoses and RV volumes are given in (Table 2). The mean HR was 90 bpm (range 56 to 139 bpm). Navigator efficiency and total time taken for the dual phase sequence are given in (Table 3).

Table 2. Diagnoses of Patients for Dual Phase Congenital Heart Disease Study

HR Rate	Time Taken (s)	Navigator Efficiency
<80	611 ± 218	36 ± 6%
80to100	526 ± 277	42 ± 13%
>80	454 ± 184	47 ± 10%
Total	532 ± 237	41% ± 11%

Table 3. Time Taken for Dual Phase Imaging.

Values given as mean ± standard deviation.

Diagnosis	N	RV in Diastole	RV in Systole
Pulmonary Atresia, VSD	6	85 ±19	39 ±13
Hypoplastic Left Heart Syndrome	6	94 ±14	43 ±21
Tetralogy of Fallot	13	85 ±31	42 ±19
Coarctation of the aorta	3	54 ±19	26 ±12
Heterotaxy syndrome, Univentricular AV connection, Solitary RV, Aortic Atresia	1	183	123
Transposition, VSD, Pulmonary Stenosis	1	83	34
Double Inlet Left Ventricle	2		
Unbalanced AVSD	3	78 ±29	39 ±18
Coarctation and VSD	2	85 ±1	25 ±1
Aortic Stenosis	2	77 ±8	29 ±13
Congenitally Corrected Transposition, VSD	1	64	26
Mitral Valve Hypoplasia and VSD	1	75	18
Vascular ring	1	84	45
Total Anomalous Pulmonary Venous Drainage (TAPVD)	1	178	38
Ebstein's Anomaly	1	138	98
Pulmonary Stenosis	2	62 ±3	27 ±2
Truncus Arteriosus	1	70	17
Heterotaxy Syndrome, TAPVD, AVSD, Pulmonary atresia	1	54	25
Pulmonary Stenosis and VSD	2	100 ±47	44 ±33

2.1.4.6.2. Image Quality

Dual phase yielded diagnostic quality imaging for all chambers and great vessels in one or other cardiac phase in 38 out of 50 patients. Systolic imaging alone had diagnostic image quality for all segments in 31 cases and diastolic imaging alone had diagnostic quality in 26 cases. A summary of non-diagnostic segments is given in (Figure 3). Two points are notable from this figure: that end-systole was more successful for the imaging of the LA and PV's and that the combination of the two phases is clearly more successful from a segment to segment basis compared to either phase alone.

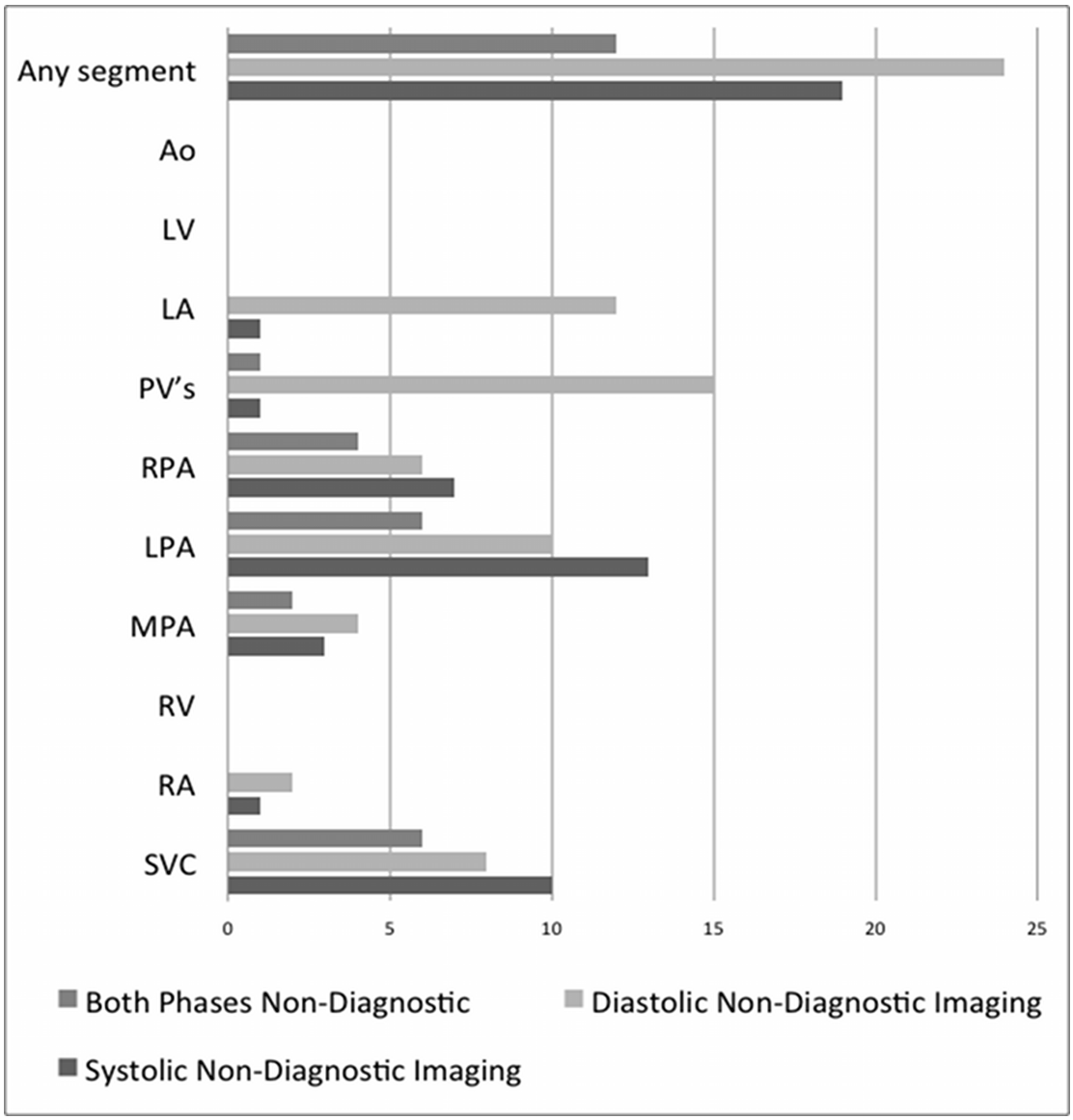

Figure 3. Summary of segments with non-diagnostic IQ

Using the Wilcoxon Signed Ranks test, IQ was significantly greater in systole for the four cardiac chambers (RA, LA, RV & LV) and for the PV's. Conversely, diastolic IQ was significantly greater for the branch pulmonary arteries and for post-arterial stenosis imaging. Mean rank values and p-values are given in (Table 4). Clearly, RVOT obstruction and pulmonary arterial stenosis may influence IQ of the branch pulmonary arteries but the relationship between superior image quality in diastole and the branch pulmonary arteries, remains true even if RVOT obstruction and pulmonary arterial stenosis cases are excluded (p=0.02 by

Wilcoxon Signed Rank test for RPA IQ between systole and diastole) but not for the LPA (p=0.13 by Wilcoxon Signed Rank test for IQ between systole and diastole).

		N	Mean Rank	Sum of Ranks
SVC (p=0.201)	Diastole Better	12	10.29	123.5
	Systole Better	7	9.5	66.5
RA (p=0.001)§	Diastole Better	5	18.1	90.5
	Systole Better	27	16.2	437.5
RV (p=0.006)§	Diastole Better	3	7.5	22.5
	Systole Better	14	9.32	130.5
MPA (p=0.439)	Diastole Better	9	8	72
	Systole Better	6	8	48
LPA (p=0.007)¶	Diastole Better	19	12.53	238
	Systole Better	5	12.4	62
RPA (p=0.001)¶	Diastole Better	19	11.5	218.5
	Systole Better	3	11.5	34.5
PV's (p<0.001)§	Diastole Better	2	16	32
	Systole Better	41	22.29	914
LA (p<0.001)§	Diastole Better	2	14.5	29
	Systole Better	43	23.4	1006
LV (p=0.015)§	Diastole Better	4	7	28
	Systole Better	13	9.62	125
Ao (p=0.127)	Diastole Better	12	9.75	117
	Systole Better	6	9	54
BT (p=1.00)	Diastole Better	0	0	0
	Systole Better	0	0	0
DKS (p=0.705)	Diastole Better	2	2	4
	Systole Better	2	3	6
Glenn (p=0.157)	Diastole Better	0	0	0
	Systole Better	2	1.5	3
Lateral Tunnel	Diastole Better	0	0	0
	Systole Better	0	0	0
Post-stenosis (p<0.001)¶	Diastole Better	16	10.25	164
	Systole Better	2	3.5	7

p-values are given for differences between phases. ¶ indicates diastole significantly better. § indicates systole significantly better

Table 4. Image Quality of Cardiac segments for Dual Phase Congenital Heart Disease Study

2.1.4.6.3. Contrast-to-noise Ratio

All CNR measurements were normally distributed using Kolmogorov-Smirnov tests for normality. Similar to the pattern for IQ, CNR was also significantly higher in systole for cardiac chambers (LA, RA, LV and RV) and for the PV's. Diastolic CNR was significantly higher in the Aorta and for the Glenn anastomosis. However it should be noted that the number of Glenn anastomoses was small (n=5). CNR results are given in (Table 5). There were no significant differences for the CNR at arterial post-stenosis sites between systolic and diastolic images. Similarly, exclusion of arterial stenosis cases from the analysis does not influence the given results for branch pulmonary arteries.

	Segment	Cardiac Phase	Mean	N	Std. Deviation	p-values
1	SVC	(diastole)	5.1	45	2.5	0.796
		(systole)	5.2	45	1.9	
2	RA	(diastole)	7.5	49	2.3	<0.001§
		(systole)	8.9	49	2.4	
3	RV	(diastole)	8.2	49	2.4	<0.001§
		(systole)	10.6	49	2.6	
4	MPA	(diastole)	6.6	33	3.3	0.194
		(systole)	7.4	33	2.2	
5	LPA	(diastole)	4.7	43	2.7	0.448
		(systole)	4.5	43	1.9	
6	RPA	(diastole)	4.6	44	2.6	0.082
		(systole)	5.2	44	1.9	
7	PV's	(diastole)	4.9	48	2.4	0.001§
		(systole)	6.2	48	2.7	
8	LA	(diastole)	5.3	49	2	<0.001§
		(systole)	8	49	2.7	
9	LV	(diastole)	7.7	46	2.8	0.002§
		(systole)	9.4	46	3	
10	Ao	(diastole)	9.2	50	2.9	0.013¶
		(systole)	8.2	50	2.3	
11	BT	(diastole)	1.4	3	1.6	0.359
		(systole)	2.6	3	2.2	
12	DKS	(diastole)	5.2	3	2	0.409
		(systole)	6.7	3	0.5	
13	Glenn	(diastole)	7.3	5	1.4	0.008
		(systole)	5.4	5	2.1	
14	Lateral Tunnel	(diastole)	8.4	1	NA	NA
		(systole)	8.7	1	NA	
15	Post Stent	(diastole)	6	14	3.1	0.445
		(systole)	5.4	14	2.8	

p-values are given for differences between phases. ¶ indicates diastole significantly better. § indicates systole significantly better

Table 5. CNR of Cardiac segments for Dual Phase Congenital Heart Disease Study

Only major segments (SVC, RA, RV, LPA, RPA, PV's, LA, LV and Ao) are included in the repeated measures ANOVA model, in order to have adequate (n=33) numbers with complete segmental analyses. The model is constructed using CNR as a

measure (which has been already formally tested to pass assumptions of normality) and within-subject variables are given as segment (SVC, RA, RV, LPA, RPA, PV's, LA, LV and Ao) and heart phase (systole or diastole). Between subjects, the heart rate variable is tested by grouping heart rates (three groups <80; 80 to 100 & >100 bpm). All data passes Levene's test of Homogeneity of Variance, showing that this assumption is met. Assumptions of sphericity have also been formally tested and rejected (Mauchly's test). Hence results given use the Greenhouse-Geisser model. The Bonferroni correction is used to correct for multiple comparisons.

The model demonstrates that the systolic CNR (mean 7.2) is higher than the diastolic CNR (mean 6.3) ($p=0.007$). There is no interaction between this relationship and HR ($p=0.10$). As described in the univariate analysis, the ANOVA model confirms that this relationship between the CNR and heart phase is significantly altered according to the segment imaged ($p<0.001$).

2.1.4.7. Cross-Sectional Measurements

In 16 cases, right ventricular outflow tract measurements were clinically indicated. This included 8 cases of repaired tetralogy of Fallot; 5 cases of pulmonary atresia and ventricular septal defect (VSD) repaired with homograft; 1 transposition, VSD, pulmonary stenosis (PS) after Rastelli procedure; 1 repaired truncus arteriosus and one mixed valvar and supravalvar PS. Systolic RVOT areas were shown to be significantly greater than diastolic areas (mean at valvar level 2.91 vs. 2.68 cm^2 ($p=0.01$); supravalvar level 3.37 vs. 2.80 cm^2 ($p<0.001$); pre-bifurcation 3.29 vs. 2.59 cm^2 ($p=0.003$)) (see (Table 6)). In 10 cases, the aortic arch measurements were clinically important (previous arch repairs). At all levels, systolic

measurements were greater than diastolic (mean in systole vs. diastole = 0.70 vs. 0.53 cm^2 at narrowest point (p=0.009); 0.71 vs. 0.58 cm^2 at diaphragm (p=0.023) and 2.93 vs. 2.75 cm^2 at transverse arch (p=0.016) (see (Table 6) 15 cases had branch pulmonary artery stenoses of varying severity. Although mean areas were slightly higher in systole both at the narrowing (0.57 vs. 0.49 cm2 in diastole) and distally (0.75 vs. 0.68 cm2 in diastole), this did not reach significance (p=0.30 and 0.21 respectively) (see (Table 6)).

Segment	Level	Phase	N	Mean Area (mm^3)	S.D.	p-value
Arch	Narrowest Point	Systole	10	70.34	34.79	0.009*
		Diastole	10	52.60	24.57	
	Descending Aorta	Systole	10	70.71	49.36	0.023*
		Diastole	10	57.93	36.31	
	Transverse arch	Systole	10	293.13	514.80	0.016*
		Diastole	10	274.95	517.92	
Branch PA's	Narrowest Point	Systole	15	56.79	56.45	0.213
		Diastole	15	49.25	47.29	
	Distal Vessel	Systole	15	75.01	54.28	0.307
		Diastole	15	68.16	40.80	
RVOT	Valvar level	Systole	16	291.44	119.58	0.01*
		Diastole	16	268.04	111.56	
	Supravalvar	Systole	16	336.56	167.65	<0.001*
		Diastole	16	279.75	150.04	
	Pre-bifurcation	Systole	16	328.56	265.58	0.003*
		Diastole	16	259.25	214.45	

* denotes statistically significant differences using paired t-test to compare

Table 6. Cross-Sectional Measurements of Cardiac segments for Dual Phase Congenital Heart Disease Study

2.1.4.8. Discussion

The original approach to 3D whole-heart imaging in children to image coronary arteries, as suggested by *Tangcharoen et al*, is to use the systolic rest period at higher heart rates when assessed to be longer than the diastolic rest period.[90] However, this approach does not acknowledge that certain structures may be inherently better imaged at a specific cardiac phase.

We have shown that regardless of heart rate, systole offers better imaging for many cardiac segments in congenital heart disease. In particular, cardiac chambers (RA, RV, LA & LV) and pulmonary veins had both higher CNR and IQ scores at end-systole (see (Figure 4)). The reason for this may be due to different blood exchange rates during the two rest periods. For example, in healthy individuals, the systolic flow rate (and waveform) is of higher amplitude than diastole in the pulmonary veins.

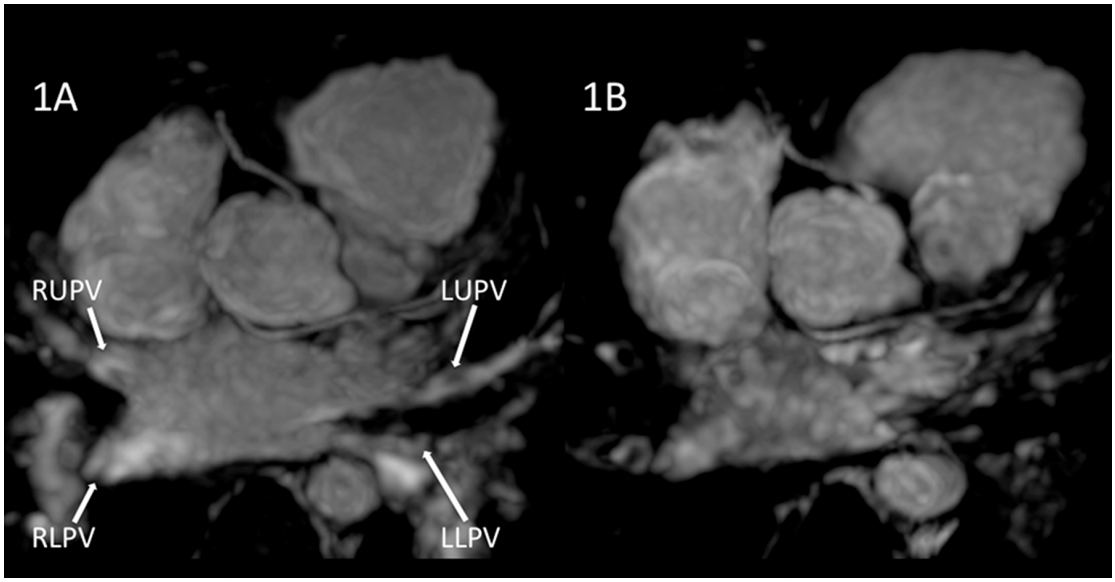

Figure 4. A 6-yr-old patient, status post repair of Tetralogy of Fallot. Identical formatting showing thick slab (1.6 cm) depicting pulmonary veins. Systolic pulmonary vein imaging (A) has superior IQ (grade 2 vs. 1) and CNR

(5.3 vs. 4.9) to the diastolic image (B). (RUPV – right upper pulmonary vein; RLPV – right lower pulmonary vein; LUPV – left lower pulmonary vein and LLPV – left lower pulmonary vein).

However, diastolic imaging appears preferable for arterial imaging with higher CNR values for the Aorta and higher IQ scores for the branch pulmonary arteries (see (Figure 5)). The reason for this may be simply that, although end-systole is a cardiac rest period, arterial motion is still present whereas mid-diastole offers a more stable combined arterial and cardiac rest period.

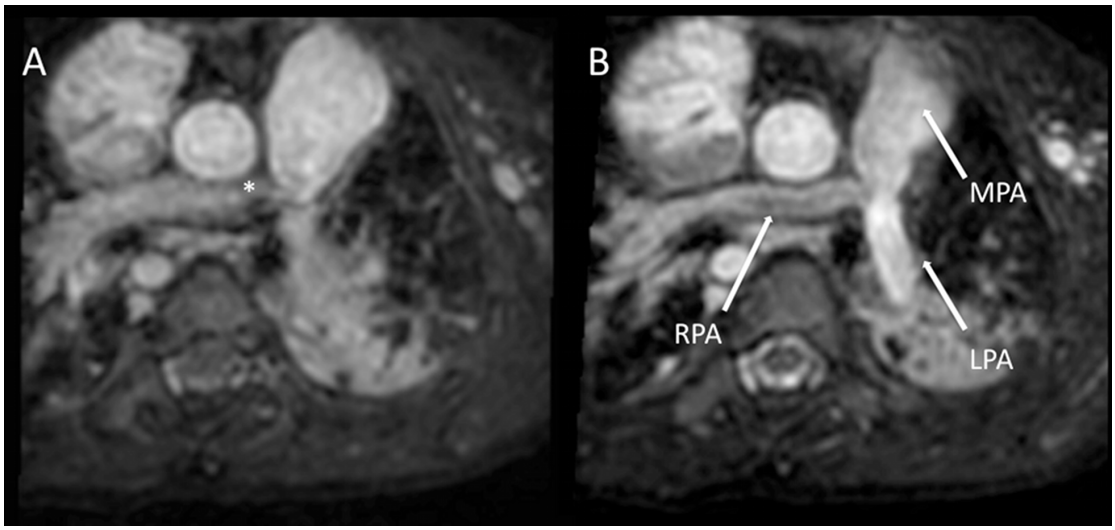

Figure 5. A 4-year-old patient, after repair of tetralogy of Fallot.

Identical formatting to demonstrate pulmonary artery and branches (arrows). This is only appreciated in the diastolic image (B) and not in the systolic image (A), which shows image disturbance due to flow turbulence (asterix). (RPA – right pulmonary artery; LPA – left pulmonary artery and MPA – main pulmonary artery)

Furthermore, to support this, we were able to show that the dual phase approach was advantageous in demonstrating a higher rate of diagnostic quality imaging than either phase alone.

The issue of imaging arterial stenosis is best considered separately. We demonstrated superior image quality in diastole for imaging arterial stenoses (e.g. Coarctation: see (Figure 6)). However, x-ray angiographic measurements are typically done in systole for two reasons: (i) Contrast medium from the injection fills the artery in systole (ii) the wider systolic diameter is taken for intervention so that stent sizes are not under-estimated leading to possible embolisation. For these purposes, we have further shown the ability of dual phase imaging to demonstrate the deformations of the RVOT and aortic arch though the cardiac cycle, using similar definitions as recently used to illustrate four-dimensional computed tomography.[110] Although systolic mean areas were higher for stenosed branch pulmonary arteries (both at the narrowing and distally), we were not able to demonstrate a significant difference. This can be explained by a number of factors. First, amongst our 15 branch pulmonary artery stenoses, there were 3 with venous flow (cavopulmonary connections) and 2 with continuous flow (BT shunts). Branch pulmonary arteries with such venous or continuous flow would not be subject to the same systolic deformation. Furthermore, in the setting of significant branch stenosis (at least 3 further cases), pulmonary arterial flow is known to be redistributed to the unaffected artery and, in the stenotic artery, pulsatility is reduced. In short, we were underpowered in this study to be able to demonstrate the ability of dual phase imaging to depict deformation of stenotic branch pulmonary arteries. Despite this, dual phase imaging has clear advantages for interventional planning over standard 3D single phase sequences, because

diastolic images, with superior image quality, can be used for diagnostic purposes and systolic images can be used for measurements.

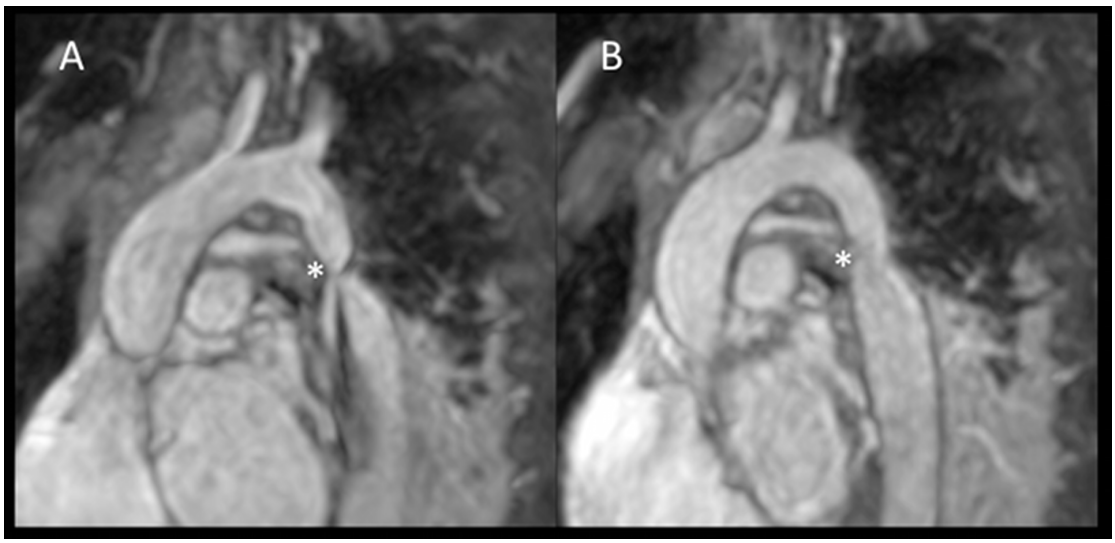

Figure 6. A 1-year old patient with a coarctation.

The asterix depicts the site of narrowing. The systolic image (A) is of lower quality than the diastolic image (B) with depiction of the stenotic flow jet in systole.

Magnetic resonance contrast angiography measurements are now routinely used for the planning of both surgical and trans-catheter intervention. It has been shown recently that the accuracy of these measurements may be improved by using identical angulations for formatting the MRI data, as used in the x-ray angiography.[115] However, this approach is still limited in accuracy compared to 3D whole-heart imaging, because standard MR contrast angiography is not ECG-gated and therefore subject to blurring due to cardiac motion.[109] As demonstrated by *Potthast et al*, routine clinical 3D whole-heart imaging is done in diastole.[109] In some ways, our study lends support to this because we show that diastole has

superior arterial image quality. However, systolic imaging is vital, especially when considering interventions of the RVOT.[110] 3D whole-heart imaging is time-consuming and the disparity between this and prior statements can only be resolved by use of dual phase imaging. Using this sequence, we can provide ECG-gated 3D imaging in both cardiac rest periods in a single sequence taking approximately the same time as the standard single phase approach. We can then also format the systolic images using approximated equivalents for subsequent x-ray angiography, as suggested by *Valverde et al*.[115]

Although, we have described findings in arterial stenosis, we only had one patient with an aneurysmal segment. The suggestion from this case (Figure 7) is that systole may provide better image quality, perhaps due to more disordered flow in diastole (swirling).

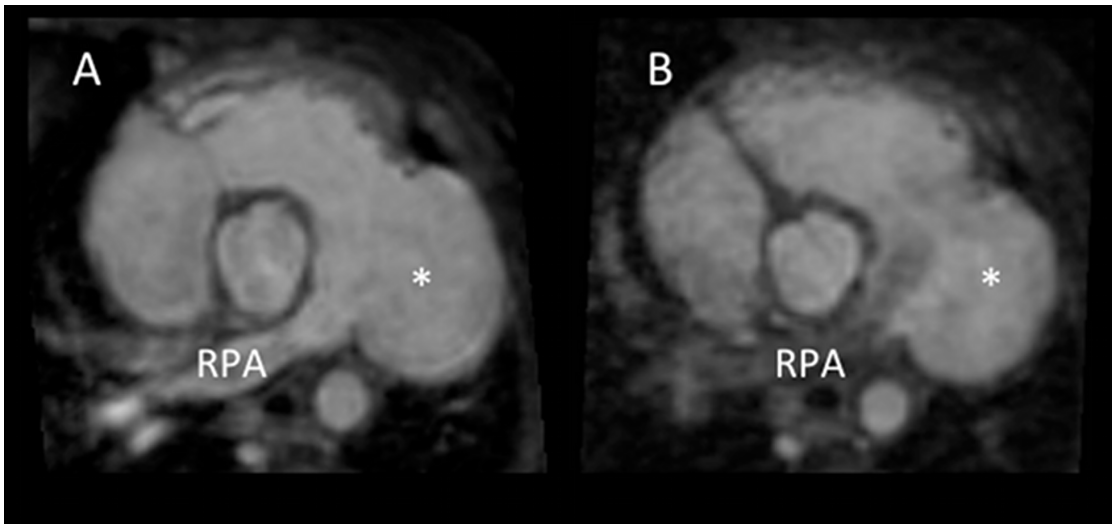

Figure 7. A right ventricular outflow tract aneurysm (*) is shown in a 9 months old patient after trans-annular patch repair of Tetralogy of Fallot.

Systole A; Diastole B

The superiority of systolic image quality (A) is clear. This may be due to diastolic blood (B) swirling in the aneurysm, perhaps heightened by pulmonary regurgitation. (RPA – right pulmonary artery)

The effect of blood flow velocities on image quality may be partially explained by the use of a Cartesian readout for 3D whole-heart imaging. The dual phase sequence that is described here did not benefit from flow compensation gradients. Perhaps, other trajectories with fully velocity compensate gradients may reduce the IQ and CNR differences between systole and diastole.[116-118]

As mentioned previously,[119] another theoretical limitation of dual phase imaging is the possible reduction of signal-to-noise ratio due to the acquisition of two cardiac phases during a single cardiac cycle when compared with the signal-to-noise ratio obtained with a single phase whole-heart sequence. In addition, the application of two T2 preparation pulses may also influence the contrast to some extent. However, these effects are likely to affect both cardiac phases similarly.

This study does not include a direct comparison between single phase and dual phase approaches. However, dual phase imaging is now part of the routine protocol at our institution and we have not noted any image degradation in comparison to the previous single phase approach. This experience is supported by comparison of two recent publications using 3D whole-heart SSFP. *Uribe et al*, using 3D dual phase whole-heart SSFP imaging measured image quality quantitatively (by vessel sharpness) for the left (LCA) and right coronary artery (RCA) systems.[92] Values for the best phase were 40% ± 10% for the LCA and 40% ± 10% for the RCA. Thirty children (28 under general anaesthesia) were studied with a mean age of 5 years (range 0-16 years). Using a very similar protocol but using a single phase approach (using the phase with the longest user-defined rest period), *Tangcharoen et al* imaged 100 children under general anaesthesia.[90] This data is divided into age groups and the oldest group (range 5-11 years) is comparable and comprised 32 children. The mean vessel sharpness for LCA (32%

± 0.24) was not significantly different to data from *Uribe et al* (p=0.09 by two-tailed independent samples t-test). Similarly, there was no significant difference for RCA vessel sharpness (41% ± 18%; p=0.79). The combination of experience and quantitative analyses from these studies leads us to believe that, although SNR may be theoretically reduced, image quality is not significantly different between dual phase imaging and each of the corresponding single phase acquisitions.

In summary, the dual phase sequence should become the routine 3D whole-heart sequence for children with congenital heart disease. The utility of this sequence has already ben shown for the imaging of coronary arteries.[119] **We demonstrate here that the dual phase sequence improves the overall success rate in achieving diagnostic image quality, and is particularly useful for interventional planning**. Similar results can be achieved using time-resolved 3D computed tomography[110] but this would further increase the amount of radiation used compared to single rest-period multi-detector computed tomography and would result in inferior diagnostic physiological information with respect to cardiovascular MRI.

2.2. Coronary artery size and origin imaging in children: a comparative study of MRI and trans-thoracic echocardiography

2.2.1. Introduction

In infants, it is appreciated that currently, echocardiography is the first line imaging method for delineation of the origin and course of the proximal portion of the coronary arteries.[120] However, echocardiographic imaging becomes progressively more difficult in children and adolescents due to size and poorer transthoracic ultrasound windows.

Normal values exist for coronary dimensions using echocardiography,[121, 122] but no such references exist for coronary magnetic resonance angiography (CMRA). The difficulty exists in producing normal MRI data is that young children and infants would require sedation or general anaesthesia. This information, however, may be gained by cross-referencing MRI and echo data, so that MR dimensions can be validated systematically against echo-derived dimensions. This will be important for clinical settings, such as Kawasaki disease (or coronary allograft vasculopathy), where MRI is used for longitudinal follow up of coronary arteries.

In the setting of aneurysmal coronary segments and larger coronary arteries (in adults, >3mm), it has already been shown that CMRA is very accurate.[91] The purpose here is to be able to develop a reference for coronary dimensions in children to be able to identify whether the segment in question is indeed dilated. This is particularly important for longitudinal follow-up and when echocardiographic windows are poor.

2.2.2. Methods

Institutional Review Board approval was obtained for this study (reference 07/Q0704/3). The inclusion criterion was any patient undergoing a clinical cardiovascular MRI with 3d-whole heart acquisition under general anaesthesia at our institution. Written, informed consent was obtained appropriately in each case. Enrolled patients underwent dual phase whole-heart 3D balanced steady state free precession (SSFP) imaging and echocardiography under general anaesthesia.

2.2.2.1. MRI

Cardiac MRI was performed using a 1.5 Tesla Achieva clinical MR scanner (Philips Healthcare, Best, NL). The 3d whole heart approach, described by *Beerbaum et al*[101] was implemented with noticeable changes. It has been recently demonstrated that dual phase imaging (end-systole and mid-diastole) can improve coronary imaging by providing the ability to retrospectively select the optimum phase to be used for analysis.[92] Hence this approach was used for this study.

As with standard 3D SSFP sequences, the dual phase sequence is respiratory-gated and ECG-triggered with a fat saturation pre-pulse to null fat signal and a T_2 pre-pulse to improve the myocardium to blood pool contrast.[123] Imaging was acquired in a sagittal orientation (repetition time (TR) /echo time (TE) = 3.4/1.7 ms, flip angle 90°, 60-120 slices, isotropic resolution of 1-1.5 mm^3, acquisition window of 60 -75 ms). For children below 3 years of age, a two-element coil was used (Flex M or Flex S). For older children, a five-element cardiac coil was used. Parallel imaging with a SENSitivity Encoding (SENSE) acceleration factor of 2 in the antero-posterior direction was also used. Trigger delays were set for end-systole

and mid-diastole. The cardiac rest periods were assessed with a high temporal resolution, balanced steady-state free precession (SSFP), four-chamber cine (TR= 3.1–3.6 ms, TE = 1.6–1.8 ms, no. of lines acquired per heart beat = 8 to 20, flip angle 60°, 6-mm-thick sections, 240-300 mm field of view, 60–80 phases). The dual phase sequence employs navigators for each cardiac phase with a respiratory gating window of 3 mm and data is only accepted if both navigators, in any given cardiac cycle, fall within this gating window.

In addition, it has been shown that an automated programme is capable of more accurate definitions of cardiac rest periods than visual inspection.[124] It was therefore hoped that clearer definitions for cardiac rest-periods would produce a similar effect. The mid-diastolic period was taken from cessation of movement of RCA (i.e. pause in visible filling of RV) to the beginning of atrial systole. This stringent definition covers both RCA and LAD diastolic rest periods.[102] The end-systolic period was taken from cessation of movement of the RCA (corresponding to lowest RV volume) to just before the beginning of opening of the tricuspid valve. Coronary dimensions were assessed manually at the same points as the echocardiographic measurements. The number of proximal LAD branches imaged was also recorded in order to give an estimate of distal coronary tree visualisation. Coronary origins were classified as abnormal if there was operator certainty from both echo and MRI. In the case where modalities disagreed, reference was made either to earlier diagnostic catheterisation or to previous surgical notes.

2.2.2.2. Echocardiography

The Washington protocol for coronary dimensions was followed.[122] This protocol was chosen in preference as the measurement process is clearly defined. Images of

the proximal coronary arteries (right coronary artery (RCA), left mainstem (LM) and left anterior descending (LAD)) were recorded as digital cines using short axis (in preference but alternatively, modified superiorly-tilted long-axis view for LAD was used). Operator assessment of coronary origins was recorded and stored cines were used to assess coronary dimensions.

Measurements of the RCA, LAD and LM were made from inner edge to inner edge, excluding points of branching.[125] LM was measured at its mid-point and the LAD/ RCA will be measured 0.2 to 0.5 mm from its origin.[122] Measurements and imaging were performed by three experienced operators (SM, AB and KB, all with >5 years experience in coronary echocardiography in congenital heart disease).

Current echocardiographic data does not specify the point of the cardiac cycle (systole or diastole) over which measurements should be taken.[122] Therefore, for each coronary measurement, it was also recorded as to which phase the measurement was taken, in order to compare fairly to MRI. The number of proximal LAD branches imaged was also recorded in order to give an estimate of distal coronary tree visualisation.

2.2.2.3. Statistical Methods

First, bland-Altman plots were used to assess agreement between MRI and echocardiography for coronary dimensions. Using information gleaned from this analysis, a regression analysis was carried out in order to describe the exact relationship between MRI and echocardiographic measurements. Best curve fit estimation, using scatter plot and comparison of root mean squared error of model estimates, was performed to choose the most appropriate model.

Distal coronary visualisation, assessed by number of LAD branches visualised, was compared between modalities using Wilcoxon Signed Ranks test.

A repeated measures analysis of variance models for coronary dimensions was constructed in order to assess if the coronary distensibility in children results in different dimensions according to cardiac phase. A repeated measures model was used in order to account for within-subject and between-subject variability arising from testing multiple segments over two phases in each patient. Assumptions of sphericity were formally tested, and accepted, using Mauchly's test. The Bonferroni correction is used to correct for multiple comparisons.

Statistical analyses were performed on SPSS (version 19) 2010. Variables are described using mean ± standard deviation (SD)

2.2.3. Results

2.2.3.1. Subjects

50 children participated in this study with a mean age of 4 ± 4.4 years (range 18 days to 18 years). This included 24 boys (mean age 4.5 ± 4.6 years) and 26 girls (mean age 3.6 ± 4.3 years; no significant age difference according to sex, p=0.46 by independent samples t-test). Mean weight was 15.47 ± 11.6 kg (range 3.7 to 52 kg) and mean height was 94 ± 29 cm. 48 children underwent imaging for follow-up of congenital heart disease, 1 child for cardiomyopathy and 1 for resolved Kawasaki disease.

2.2.3.2. Reference Values

Bland-Altman plots (Figure 8)(Figure 9) and (Figure 10) and show a systematic bias between echocardiographic and MRI measurements for all coronary measurements (i.e. as the coronary artery gets larger, the greater the discrepancy between echocardiography and MRI).

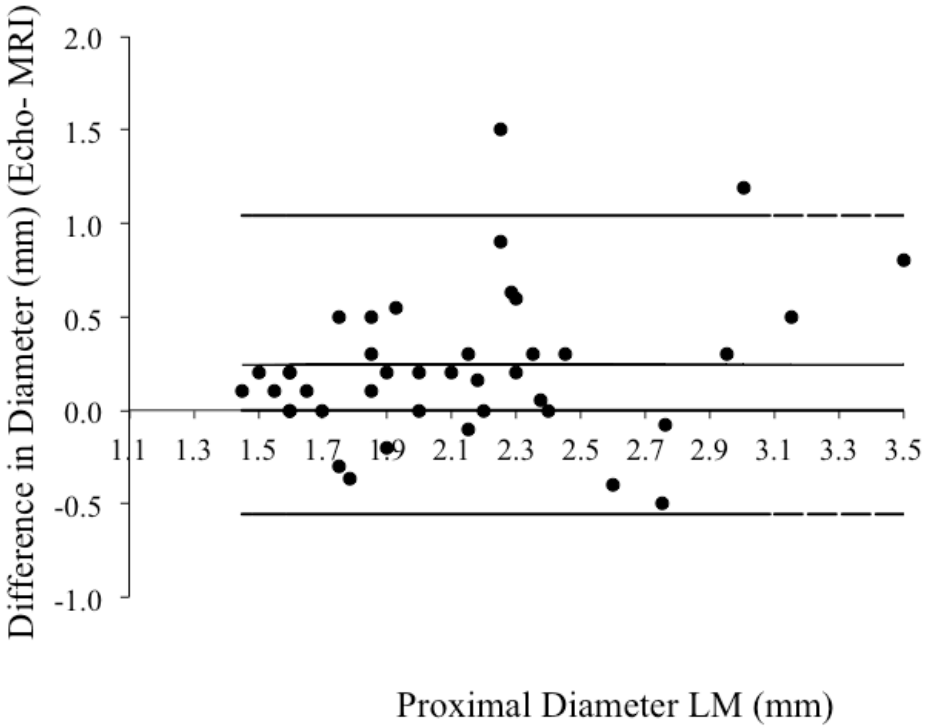

Figure 8. Bland Altman Mean vs. Difference plots for Echo and MRI LM measurements

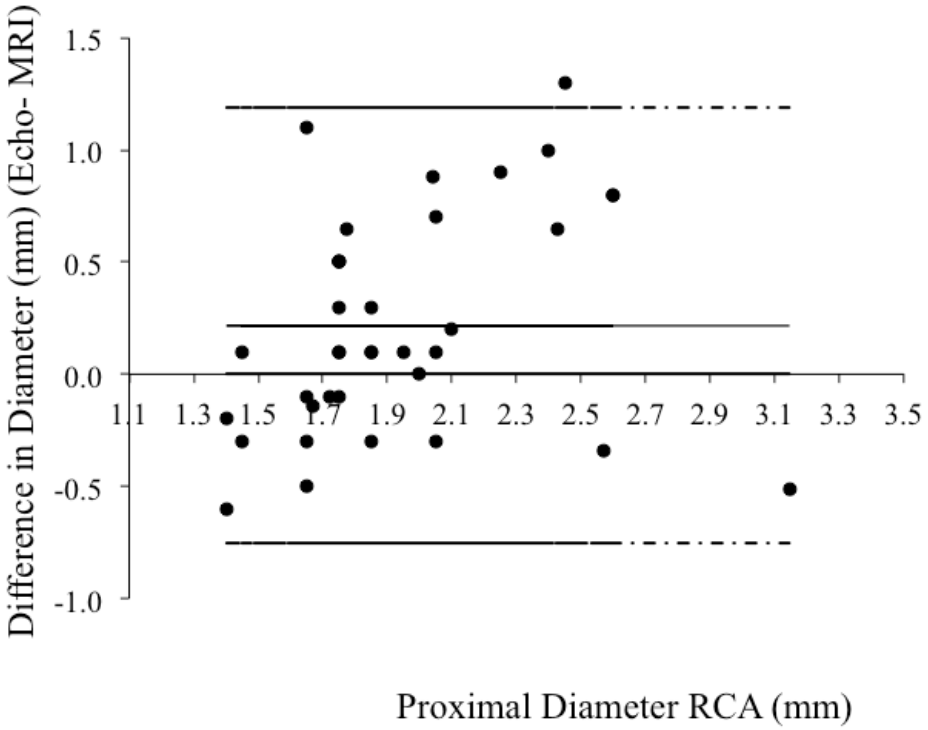

Figure 9. Bland Altman Mean vs. Difference plots for Echo and MRI RCA measurements

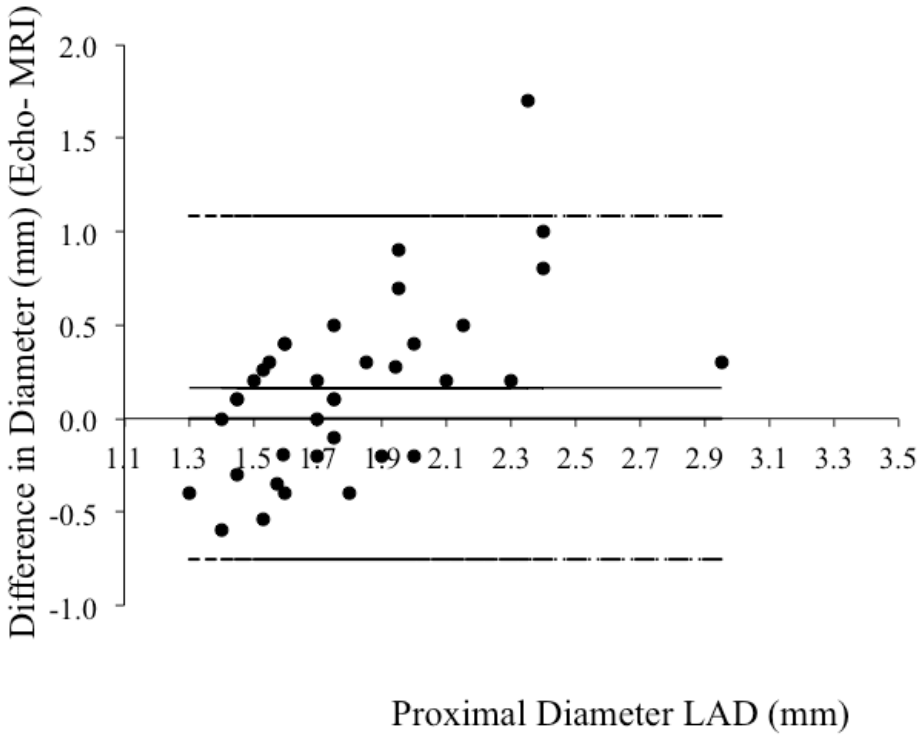

Figure 10. Bland Altman Mean vs. Difference plots for Echo and MRI LAD measurements

Regression analyses show significant linear associations for the relationship between MRI and echocardiography dimensions. (R^2 for RCA was 0.44, p=0.007; for LM R^2 was 0.58, p<0.001 and for LAD, R^2 was 0.21, p=0.005). Regression equations to calculate echo values from MRI are given below with confidence intervals for coefficients given below the equations. (Table 7) shows the range of MRI values over which these reference equations have been calculated.

Table 7. Summary of CMRA coronary measurements

MRI diameters	N	Minimum	Maximum	Mean	Std. Deviation
LAD values (mm)	47	1.4000	2.8000	1.7	.28
RCA (mm)	47	1.1000	3.4000	1.8	.37
LM (mm)	47	1.4000	3.1000	2.0	.47

RCA	Echo diameter =	0.6 (MRI diameter) + (0.2, 1)	1 (0.2, 1.7)
LM	Echo diameter =	1x (MRI diameter) + 0.3 (0.7, 1.2)	(-0.3, 0.8)
LAD	Echo diameter =	0.5 x (MRI diameter) + (0.3, 1.3)	0.8 (-0.5, 1.5)

However, this may be more usefully summarised by ignoring the segment imaged, removing outliers and pooling data. If this is done we get a simple message: there is indeed a systematic bias for CMRA dimensions between 1 and 2.5mm. This is demonstrated on the Bland-Altman plot (Figure 11) and on the regression analysis, which shows a significant linear relationship (R^2 =0.12, $p<0.001$):

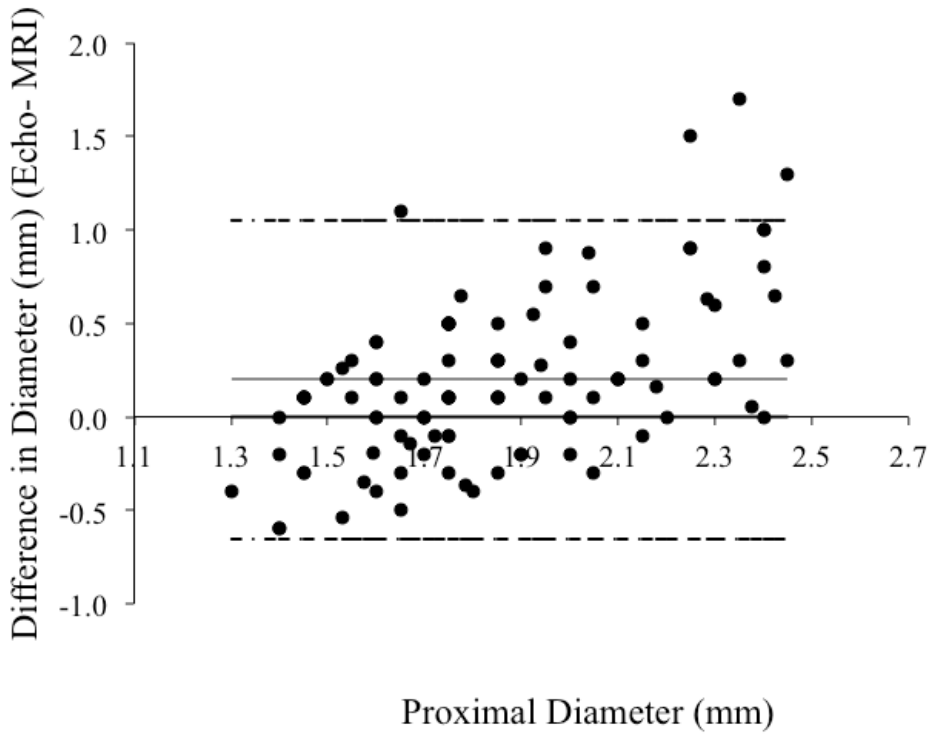

Figure 11. Bland Altman Mean vs. Difference plots for all Echo and MRI measurements with outliers excluded

Echo diameter = 0.6 x (MRI diameter) + 0.8

(0.3, 1.4) (0.3, 1)

Quadratic and cubic regression analyses were also performed but these did not improve the root mean squared error of the model estimates and hence, the linear relationship is presented here.

CMRA evaluation

Operator certainty regarding the origin of the three main coronary arteries (RCA, LAD and left circumflex (LCx)) was achieved in 47 out of 50 cases for MRI. The three uncertain cases were infant below a year of age (3 months, 9 months and 11 months) and with heart rates >100 bpm. In comparison, certainty was achieved in 41 out of 50 cases for echo. The uncertain cases were older patients (mean 4.8 years, range 9 months to 18 years). In two cases, MRI detected abnormalities in coronary origin classified as normal on echocardiography. These two cases had confirmed abnormalities on surgery. Both were slightly older children (13 months and 8 years age respectively).

In total, there were 6 abnormal coronary origins. 5 out of 6 were identified by MRI ((Figure 12)(Figure 13)(Figure 14)(Figure 15) and (Figure 16)) and the remaining one was classified as unsure. 4 out of 6 were correctly identified on echocardiogram with the remaining two, incorrectly classified as normal as described above.

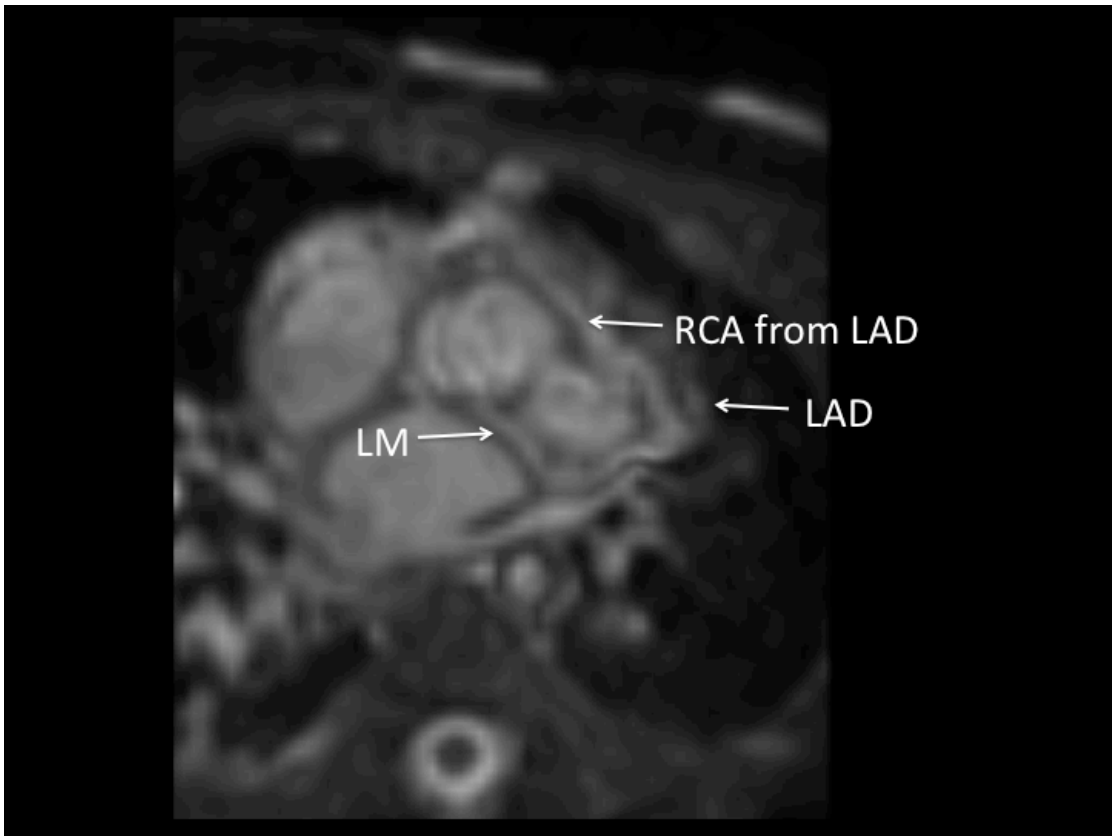

Figure 12. 3 month old with Ventriculo-Arterial discordance and RCA arises from LAD

Also seen on echocardiogram

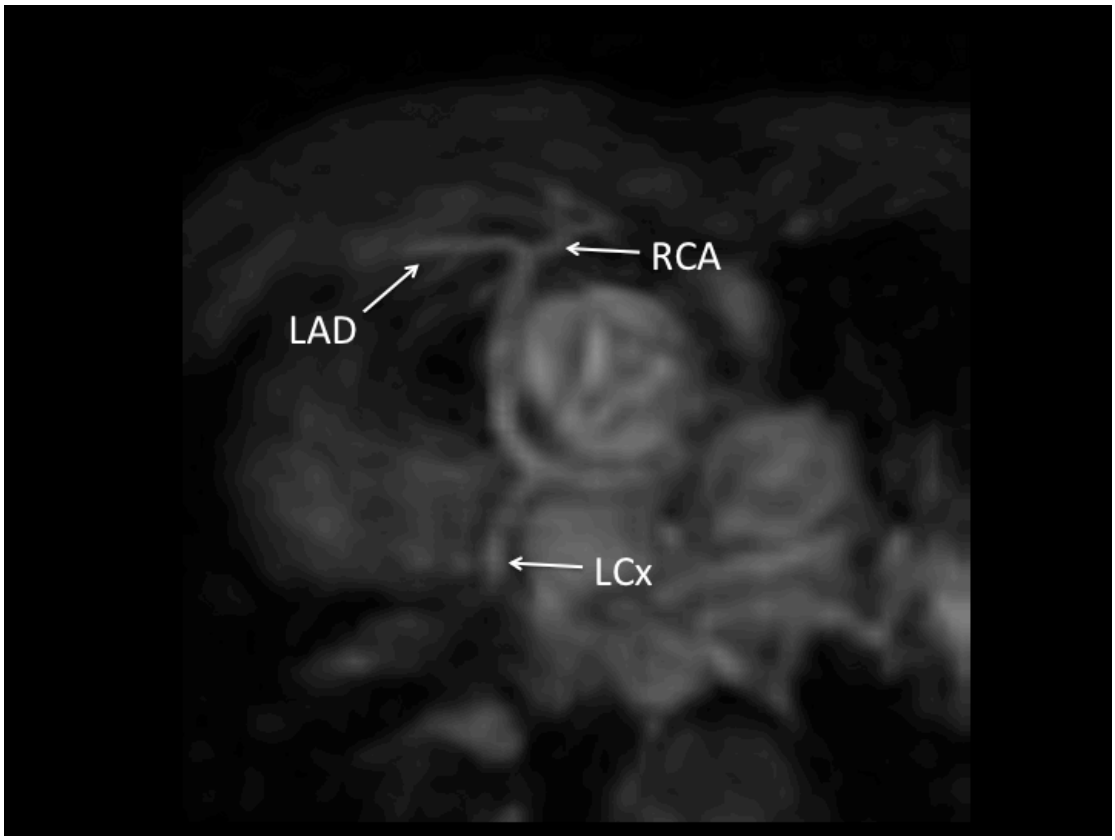

Figure 13. 3year old girl with Dextrocardia and Tricuspid Atresia. Single Coronary artery.

Also seen on echocardiogram

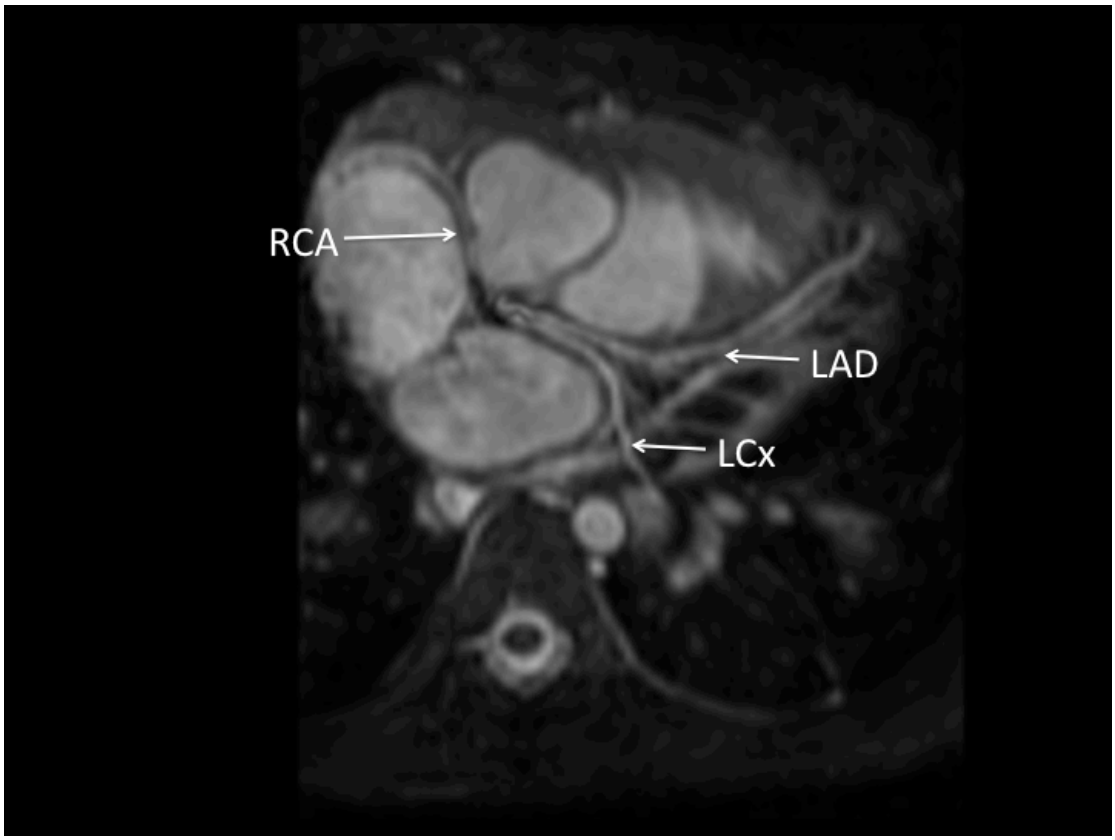

Figure 14. 8 year old boy with ventriculo-arterial discordance showing single coronary artery.

Not seen on echocardiogram.

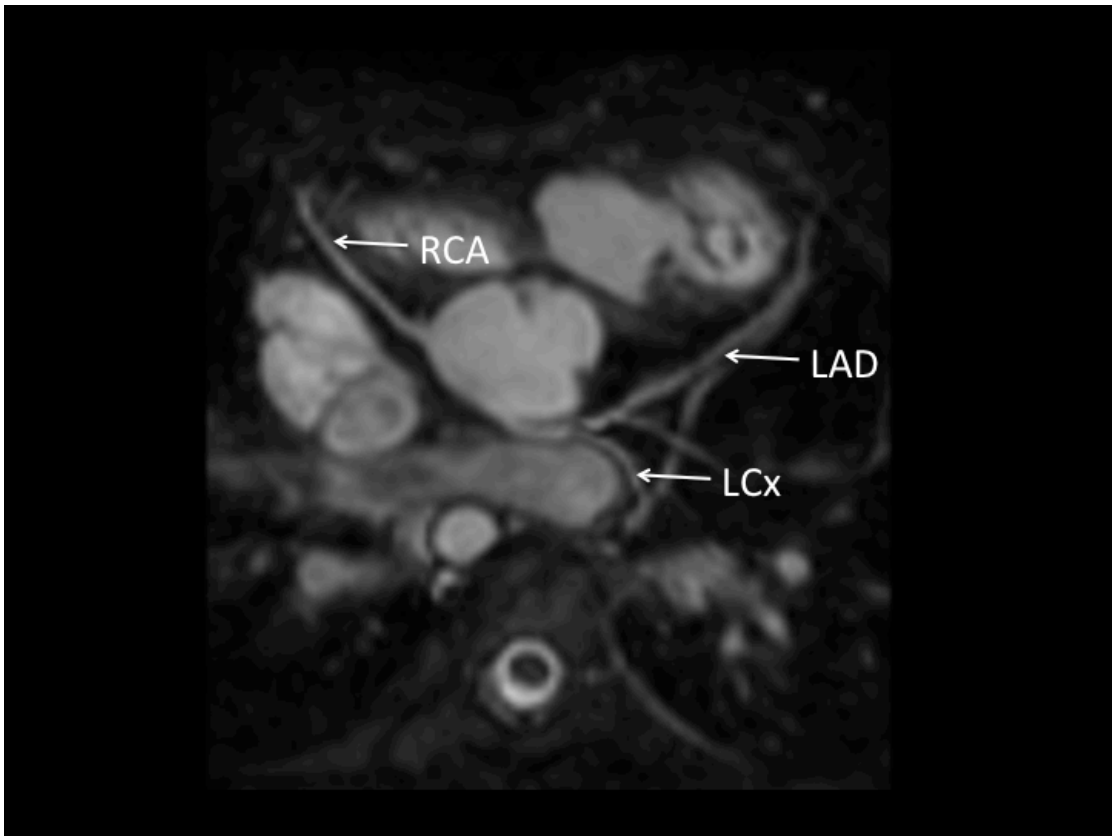

Figure 15. 7 year old girl with repaired pulmonary atresia and ventricular septal defect. RCA arises from posterior non-coronary cusp

Also seen on echocardiogram

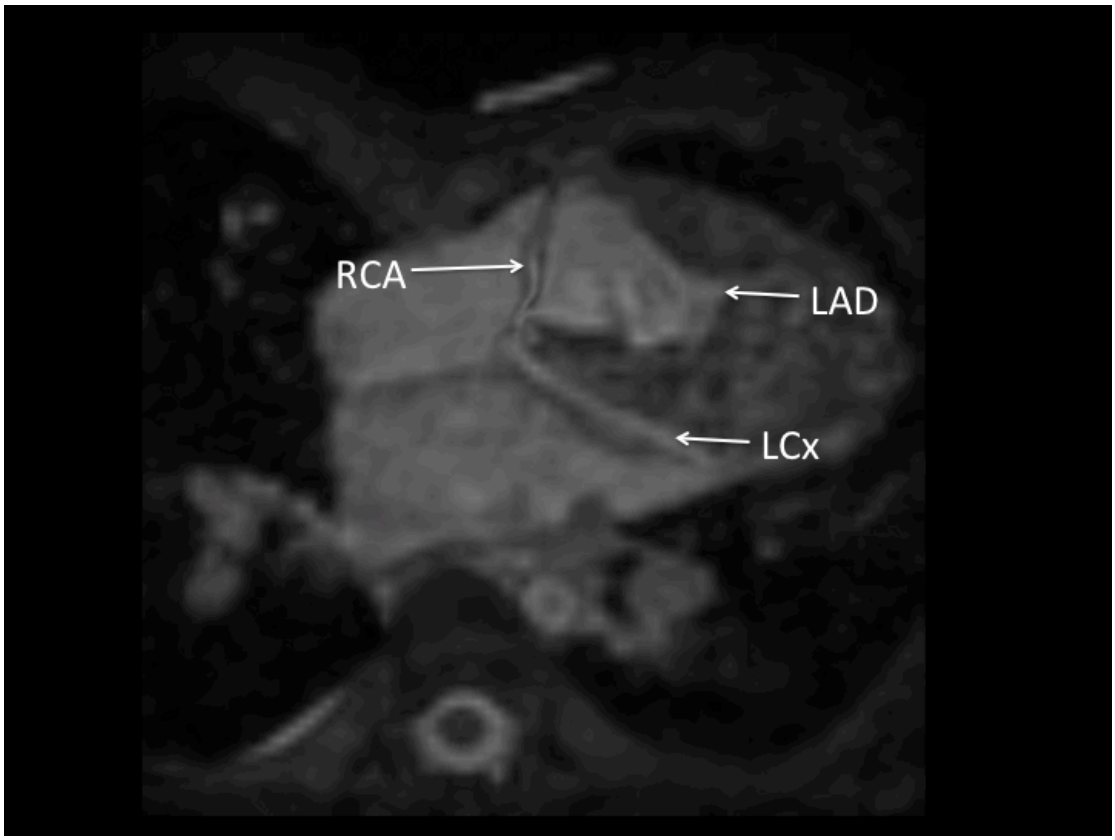

Figure 16. 13 months old boy showing LCx arising from RCA.

Not seen on echocardiography.

Overall, CMRA performed better than echocardiography in terms of distal visualisation of the coronary tree, as defined by number of proximal LAD branches imaged ($p = 0.001$ by Wilcoxon Signed Ranks test). The median number of LAD branches on MRI was 1 (interquartile range 0 to 2) and on echo was 0 (interquartile range 0 to 1).

CMRA measurements did vary according to cardiac phase. The repeated measures model demonstrates that the systolic coronary dimension (estimated marginal mean 1.90 ± 0.05 mm) is greater than the diastolic measurement (estimated marginal mean 1.84 ± 0.05 mm ($p=0.002$).

2.2.3.3. Discussion

This study has important implications for the follow-up of Kawasaki disease in particular. It is demonstrated here that CMRA measurements between 1 to 2.5mm have a systematic bias when compared to echocardiographic measurements. We can now correct for this by using the regression equation given above and so we are able to use published z-score values for echocardiography.[122] MRI is particularly useful for follow-up of Kawasaki Disease and Coronary Allograft Vasculopathy as anatomic evaluation can be combined with functional evaluation with pharmacological stress testing. Hence, this study now allows full evaluation by including coronary reference values. In the past, clinicians have merely assumed that dimensions were normal on CMRA if they equated to normal published echocardiographic z-scores. This study shows that this assumption is erroneous, as may be expected because echocardiography relies on high contrast in the vessel wall and low contrast in the lumen, whereas CMRA is the opposite. Although 'black-blood' coronary MRI exists[97] and contrast-enhanced echocardiography exists, the purpose of this study was to evaluate the commonly used clinical echocardiographic and MRI techniques.

Bland-Altman analysis with outliers included (Figure 17), show a trend towards greater accuracy with measurements above 2.5mm. This is supported by a previous in adults and adolescents with coronary aneurysms showing good CMRA accuracy for coronary measurements above 3mm.[91] The figure also shows a systematic bias for values below 2.5mm. A trend is shown for greater underestimation of diameter by MRI with respect to echo as the diameter increases (as described above for Figure 11). Hence, it is suggested that only measurements below 2.5mm should be corrected currently.

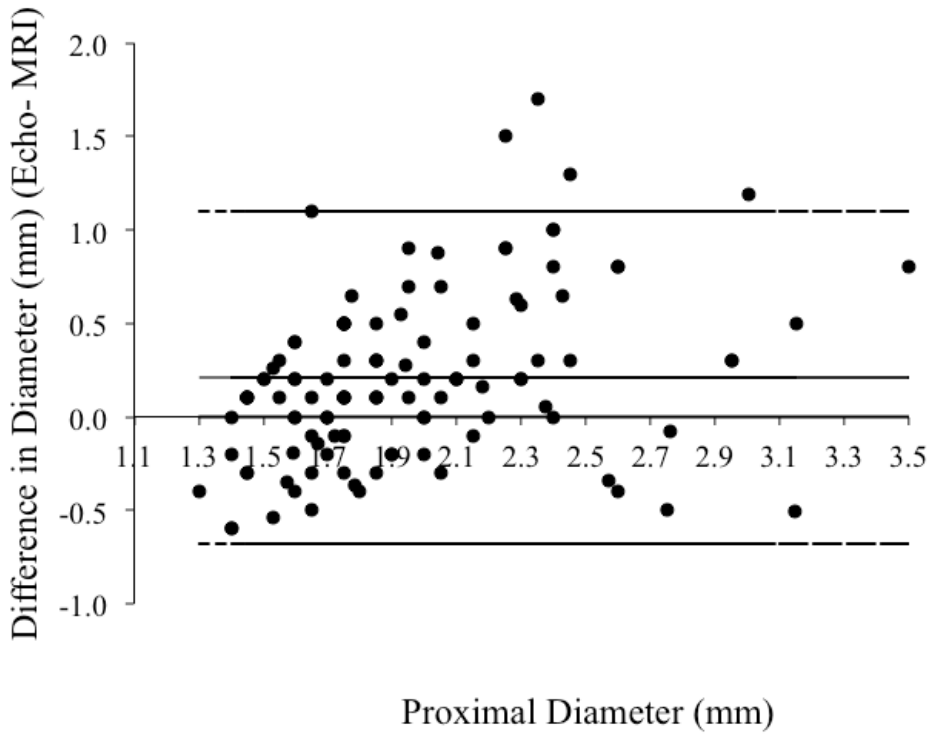

Figure 17. Bland Altman Mean vs. Difference plots for all Echo and MRI measurements

In keeping with previous studies, this study shows an excellent (94%) success rate for CMRA detection of coronary origins in children.[90, 92] Infants with high heart rates remain challenging and echocardiography remains the modality of choice for this age group. This study also shows that distal coronary tree imaging in children is superior with CMRA in comparison to echocardiography. This is another useful point of note from this study for clinical follow up of coronary disease in children.

Unfortunately, coronary distensibility in children has been largely neglected. Although an important recognised variable in adults,[126] this factor has been ignored when generating echocardiographic normal values for coronary dimensions in children. The given reference study,[122] was chosen specifically as precise details are given regarding how the measurements were taken. Even this

study neglected to mention whether values are to be taken in systole or diastole. From clinical experience, it is usually difficult to get clear pictures for each segment in both phases and so it is understandable that this is not stressed. However, our data from the dual phase CMRA measurements shows that dimensions do indeed vary according to phase. Future normal values for echocardiography in children should note this finding and provide phase-specific references.

Intra- and inter-observer error for both echocardiography and CMRA have been previously investigated and shown to be low in these studies.[92, 122] Both techniques are reliable and it is hoped that, in the future, specific normative coronary dimensions for CMRA are available. The difficulty imaging normal volunteers in this age group has precluded this to date. Hence, until such data becomes available, the regression equation given should be used to correct measurements when using echocardiographic data to derive z-scores.

Chapter 3 – Studies Relevant to Coronary Magnetic Resonance Angiography

3. Studies Relevant to Coronary Magnetic Resonance Angiography

As detailed in chapter 2, good coronary lumen imaging underpins successful coronary vessel wall characterisation by MR. The dual phase approach is clearly an important development in this respect. This chapter explores two potential further improvements: use of 3.0 Tesla field strength (chapter 3.1) and use of sublingual nitroglycerin (chapter 3.2).

3.1. Coronary Magnetic Resonance Angiography: In vivo comparison of image quality at 1.5 Tesla versus 3.0 Tesla with Parallel Radiofrequency Transmission.

3.1.1. Abstract

Background: Coronary plaque and thrombus characterisation at 3 Tesla (T) holds great potential for clinical benefit but problems still exist with coronary lumen image quality at 3T. Parallel radiofrequency transmission (Tx) can improve B1 field homogeneity and reduce B1 attenuation artefacts. The purpose of this study is to investigate if, in comparison to 1.5T imaging, balanced steady-state free precession (SSFP) coronary magnetic resonance angiography (CMRA) image quality at 3T can be maintained by use of Tx.

Methods: Ten subjects (7 male) underwent balanced-SSFP CMRA at 3T and 1.5T. Targeted CMRA of the left coronary system was performed using free-breathing, cardiac-triggered, T2-prepared, 3d balanced-SSFP. At 3.0T, a B1 volume shim, utilising Tx technology, was applied. Proximal vessel diameter; SNR; CNR; vessel

sharpness; vessel length; number of proximal left anterior descending (LAD) branches visualised; number of left coronary artery segments visualised and qualitative image quality (IQ) scores (0 to 4) were recorded. Paired t-tests were used for comparisons but categorical variables were compared using Wilcoxon Signed Ranks Test.

Results: As expected, SNR values were significantly higher at 3T (33 vs. 23; p=0.01) and there was a trend towards higher CNR (17 vs. 14; p=0.06). This resulted in better distal visualisation with a greater visualised length of LAD at 3T (8.4 vs. 7.1cm; p=0.03). It also resulted in non-inferiority when compared with 1.5T for visualisation of first-order branches (median 2.5 at 3.0T and 2.0 at 1.5T; p=0.92) and of coronary segments (median for both = 10; p=0.86).
However, vessel sharpness was reduced at 3T (37% vs. 43%; p=0.011) and IQ scores were worse (median 3.0 vs. 4.0; p=0.011). The reduction in image quality resulted in an overestimation of vessel size at 3T in comparison to 1.5T (mean bias = 0.2mm; p=0.049).

Conclusions: This study shows that, despite implementation of parallel transmit technology, balanced-SSFP CMRA at 3T is still inferior to 1.5T imaging. Parallel transmit should be combined with other recent technological advances to achieve superior imaging at 3T.

3.1.2. Introduction

Despite many medical advances in the last twenty years, atherosclerosis remains the leading cause of mortality in developed nations.[127, 128] Coronary magnetic resonance angiography (CMRA) is a valuable tool for the non-invasive detection of significant proximal or mid coronary artery disease.[129] However, the real strength behind cardiac magnetic resonance imaging currently, does not lie in coronary lumen angiography but in the functional and pathophysiological assessment of coronary disease.[130] Furthermore, coronary lumen imaging to detect stenoses is a poor predictor of future coronary events.[131] Approximately 60-70% of acute coronary syndromes are caused by stenosis of less than 50% of the luminal diameter due to compensatory positive vessel wall remodeling.[132] Hence, non-invasive coronary vessel wall imaging has the potential to identify the true disease burden and become the next big clinical development for cardiac magnetic resonance imaging.[97-99] T1 weighted imaging and late gadolinium enhancement on MRI have already been proven to demonstrate symptomatic carotid plaques with intra-plaque hemorrhage or thin fibrous cap respectively.[133] Late gadolinium enhancement and T1 weighted imaging for coronary vessel wall disease therefore have great potential and have already been shown to be feasible with important clinical implications.[134-136] These techniques do, however, rely on high SNR and high image resolution. Therefore, the advantages of high-field imaging at 3.0 Tesla may benefit these approaches. Feasibility studies for coronary plaque and thrombus characterisation at 3.0 Tesla have already been demonstrated.[134, 137] Good quality luminal imaging is, however, a pre-requisite both as a roadmap for coronary vessel wall imaging and for stenosis quantification.[133-137]

Current limitations of CMRA lumen imaging at 1.5 Tesla include residual motion and signal-to-noise (SNR) constraints. Since SNR is proportional to the static magnetic field (B0), imaging at 3 T should theoretically increase SNR. Although *Stuber et al*, found an increase in SNR and CNR in CMRA images at 3T, there was no clinically meaningful increase in image quality, measured as vessel sharpness, or in distal coronary artery imaging, measured by length of vessel visualised.[138] One possible explanation is the difficulty in achieving uniform radiofrequency (RF) excitation over the entire field of view (FOV) at higher field strengths resulting in a reduction of image quality (e.g. B1 attenuation artefacts).

Balanced steady-state free precession (SSFP) sequences have been demonstrated to give superior CNR and SNR values compared with gradient-echo sequences.[139] More recently, imaging at 3T using balanced-SSFP was found to increase SNR by over 50%.[140] However, this study also found inconsistent image quality at 3.0 Tesla due to off-resonance artefacts. The issue arises because higher field strengths are associated with increased susceptibility-induced resonance frequency shifts to which balanced-SSFP sequences are particularly susceptible.[141]

Multi-channel RF transmission (Tx) can be used to improve the RF (B1 field) homogeneity in high-field MRI.[142] More accurate knowledge of the local B1 field also allows for improved management of the local specific absorption rate (SAR), thereby enabling shorter repetition times (TR) to be employed.[143] This may improve image quality by reducing artefact levels, as demonstrated recently in a small study comparing balanced-SSFP cine images with and without the use of Tx.[144]

The purpose of this study is to investigate if balanced-SSFP CMRA image quality is maintained by use of Tx when moving to 3.0 Tesla imaging in order to ultimately realise the potential advantages of high field MRI for coronary lumen imaging.

3.1.3. Methods

3.1.3.1. Image Acquisition

Ten (7 male) healthy volunteers were first imaged in supine position on a 3T Achieva clinical scanner (Philips Healthcare, Best, Netherlands; gradient amplitude 30 mT/m and slew rate 200 mT/m/sec) using a 32-element cardiac phased-array receiver coil. Imaging was then repeated on a 1.5T Achieva clinical scanner (Philips Healthcare, Best, Netherlands; gradient amplitude 30 mT/m and slew rate 150 mT/m/sec) using a similar 32-element cardiac phased-array receiver coil. At both scanners, an initial survey and reference scan was acquired to obtain coil sensitivity maps. At the 3.0 Tesla scanner, an additional B1 calibration scan was performed between the survey and reference scans in order to calculate the patient-specific absorption rate and allow for B1 volume shimming. Following this, the cardiac rest period was ascertained using a high temporal resolution, balanced-SSFP, two-dimensional cine MR sequence in a four-chamber view orientation. (Imaging parameters included: repetition time = 2.4 ms, echo time = 1.2 ms, flip angle = 60° at 1.5T and 40° at 3T, slice thickness = 10mm, FOV = 300-350 mm, 80 cardiac phases, echo train length = 11 at 1.5T and 22 at 3.0T, temporal resolution = 10 to 16 ms/ frame). The mid-diastolic rest period, ascertained from the cine images, was used to define the acquisition window for the subsequent CMRA.

First, a rapid whole-heart CMRA was performed as a roadmap for a subsequent 3-point plan-scan for a targeted double-oblique CMRA parallel to the native left coronary artery system.[145] It was performed with a previously described navigator-gated free-breathing and cardiac-triggered T2-prepared three-dimensional (3D) balanced-SSFP sequence allowing visualisation of the anatomy of the coronary artery lumen.[146] At 3.0 Tesla, a volume B1 shim was applied utilising the parallel RF transmit technology. Imaging parameters included the following: FOV = 270x270 mm, matrix = 216x216, acquired in-plane resolution = 1.25x1.25 mm (reconstructed 0.75x0.75 mm), reconstructed slice thickness = 1.5 mm (acquired thickness = 3 mm overcontiguous slices), acquisition window = 80 to 100 ms, repetition time (TR) /echo time (TE) = 5.2 ms/2.6 ms, flip angle = 90° at 1.5T and 70° at 3.0T; start-up cycles = 5, and number of slices = 20. Parallel imaging techniques such as sensitivity encoding (SENSE) were not used to allow for SNR measurements.

3.1.3.2. Image analysis

For quantitative analysis, the targeted left CMRA images were reformatted along the major axis of the left coronary artery system and analysed using "Soap-Bubble" software (Release 5.0, Philips Healthcare, Best, Netherlands).[147] Using this semi-automatic software, proximal vessel diameter of the combined left main and anterior descending artery; SNR; Contrast-to-Noise Ratio (CNR) and vessel sharpness were measured. The local vessel sharpness was calculated as a percentage by normalising the magnitude of the local change in signal intensity at the selected vessel border to the average signal intensity of the centerline of the selected vessel by using a Deriche algorithm.[148] The SNR was calculated as:

$$SNR = (SI_{Blood}) / (SD_{Air})$$

where SI_{Blood} is the mean signal intensity in a user-specified region of interest (ROI) in the ascending aorta and SD_{Air} is the standard deviation of the signal in a ROI defined anterior to the chest wall.[138]

Subsequently, the CNR between blood in the ascending aorta (at the level of the coronary ostia) and muscle was calculated as:

$$CNR = (SI_{Blood} - SI_{Muscle})/SD_{Air}$$

Where SI_{Muscle} is the signal intensity in a ROI defined in the muscle of the left ventricular free wall.[138]

In order to measure distal coverage and branches, the length of left anterior descending artery (LAD), the number of proximal first-order LAD branches and the number of left coronary artery segments visualised were recorded. Segments were defined as 11 left coronary system segments using the modified 16-segment American Heart Association (AHA) coronary tree classification (Figure 18).[149] Segments were defined as having been visualised if the proximal portions were seen.

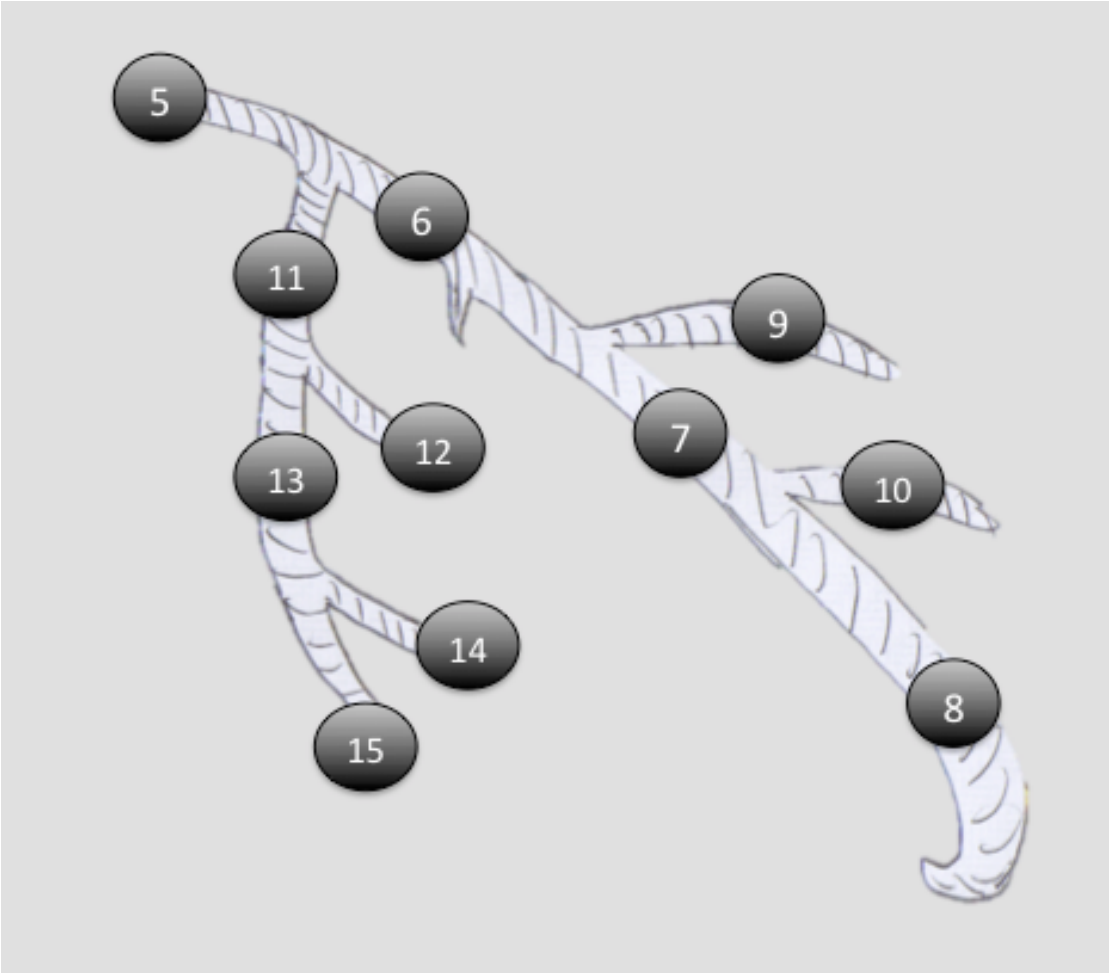

Figure 18. Segmental anatomy of the left coronary artery system using a modified AHA classification.

5=main stem; 6=LAD proximal; 7=LAD mid; 8=LAD distal; 9=first diagonal; 10=second diagonal; 11=LCX proximal; 12=obtuse marginal; 13=LCX distal; 14=LCX posterolateral branch; 15=LCX posterodescendens branch; (LCX=left circumflex artery; LAD=left anterior descending coronary artery)

Finally, a qualitative analysis was undertaken by means of a consensus reading for image quality scoring on all the angiograms in a blinded and random order by two readers (T.H. and G.F.G. (>3 years and 10 years respectively of CMRA experience)).

The two readers first reviewed the images independently and any disagreement was then discussed before the final grade was given. The following scoring system was used: 0 indicates that the coronary artery was not visible; 1 visible but with markedly blurred borders; 2 visible with moderately blurred borders; 3 visible with mildly blurred borders and 4 visible with sharply defined borders.[111]

3.1.3.3. Data analysis

Variables were visually assessed on frequency plots for normality and then formally assessed for normality of distribution using the Kolmogorov-Smirnov test. Image quality scores (IQ); number of first-order LAD branches and number of left coronary segments imaged were assumed to have a non-parametric distribution.

Measurements were compared by paired t-test analysis for normally distributed variables and Wilcoxon signed rank tests for categorical variables (p values < 0.05 indicated rejection of the null hypothesis). Agreement between 3.0 Tesla and 1.5 Tesla CMRA for proximal LAD diameter was assessed using Bland-Altman analysis. Using an 80% power level, a 2-tailed significance level of 5% and an SD of 7 for vessel wall sharpness from previous data,[138] to show a significant change of vessel sharpness of 15%, 10 paired cases are required.

Statistical analysis was performed on SPSS version 19 (Release 19.0.0, IBM Software Group, New York, USA).

3.1.4. Results

All ten healthy subjects (7 male) underwent CMRA at both scanners. Mean age was 32 years (range 25 to 39), mean weight was 71kg (range 48 to 90) and mean

height was 170 cm (range 154 to 193). The mean time between scans was 23 days (range 1 to 70 days). There was no difference in mean heart rate between scans (mean 63 bpm at 3.0 Tesla and 62 bpm at 1.5 Tesla; p= 0.65 by paired t-test)

Vessel sharpness; proximal vessel diameter; LAD length imaged; SNR and CNR were assessed visually with frequency plots and were further formally tested for normality using the Kolmogorov-Smirnov test ($p>0.2$ for all). Based on this assessment, all five variables were assumed to be normally distributed.

As expected SNR values were significantly higher at 3.0 Tesla (33 vs. 23; p=0.008 by paired t-test) and there was a trend towards higher CNR (17 at 3.0T vs. 14 at 1.5T; p=0.060). This resulted in better distal visualisation as given by a slightly greater visualised length of LAD at 3.0 T (8.4 cm vs. 7.1 cm; p=0.03). It also resulted in non-inferiority when compared with 1.5 Tesla for first-order branch visualisation (median at 3.0 Tesla, 2.5 branches seen and median at 1.5 Tesla, 2.0 branches seen; p=0.92 by Wilcoxon Signed Ranks Test) and for number of segments seen (median at both field strengths = 10 segments; p=0.86 by Wilcoxon Signed Ranks Test).

However, vessel sharpness was found to be inferior at 3T (37% at 3.0 Tesla and 43% at 1.5 Tesla; p=0.011 by paired t-test). Qualitative IQ scores were also inferior (median 3.0 at 3.0 Tesla and 4.0 at 1.5 Tesla; p=0.011 by Wilcoxon Signed Ranks Test). This resulted in an overestimation of vessel size at 3T compared with 1.5 T (mean bias = 0.2mm; p=0.049; 95% limits of agreement on Bland-Altman analysis were 0.35 to -0.75mm) (Figure 19). Results are summarised in (Table 8) and (Table 9). Sample images are shown in (Figure 20) and (Figure 21).

Table 8. Normally distributed variables for 1.5T vs. 3T study.

Tested using 2-tailed paired t-tests. * denotes significant differences ($p<0.05$)

Measure	3.0 Tesla (mean ± SD)	1.5 Tesla (mean ± SD)	p-value
Vessel Sharpness (%)	37 ± 6	43 ± 6	**0.011***
Vessel Length (cm)	8.4 ± 1.2	7.1 ± 1.7	**0.027***
CNR	17 ± 4	14 ± 6	0.060
SNR	33 ± 7	23 ± 10	**0.008***

Table 9. Non-parametric tests for 1.5T vs. 3T study.

P-values are given for paired differences using Wilcoxon Signed Ranks Test. *denotes a significant difference ($p<0.05$)

Measure	3.0 Tesla median (interquartile range)	1.5 Tesla median (interquartile range)	p-value
Number of left coronary segments imaged	10 (8.25 to 11)	10 (8.75 to 10)	0.86
Number of first-order LAD branches imaged	2.5 (1 to 3.25)	2.0 (1.75 to 3.25)	0.92
Image Quality Score	3.0 (2 to 3.25)	4.0 (3.75 to 4)	**0.011***

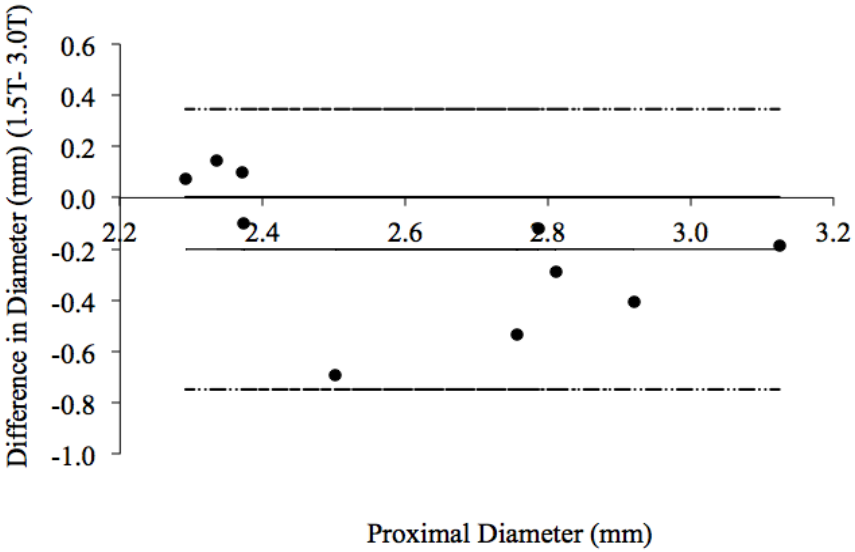

Figure 19. Bland-Altman Plots for agreement between vessel diameter measurement at 3.0 Tesla and 1.5 Tesla.

Dashed line represents 95% level of agreement and solid line centre-line represents the mean bias. There is a significant mean bias of 0.2mm (p=0.049) toward overestimation of vessel diameter. This may be explained by a lower image quality and vessel sharpness at 3.0 Tesla leading to problems with partial-volume effects which result in overestimation of vessel diameter

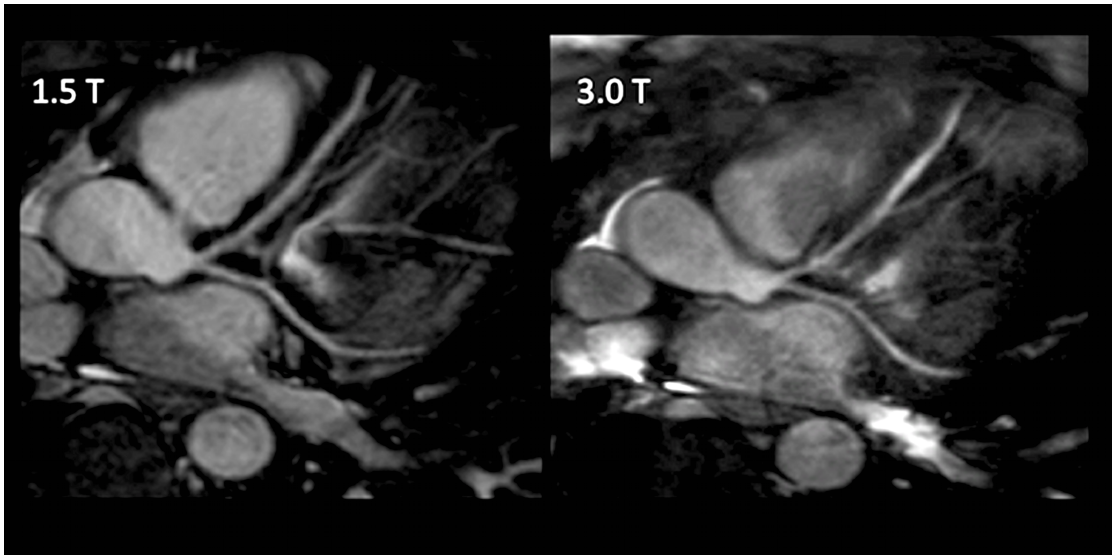

Figure 20. Sample Images showing left coronary system of same volunteer at 1.5 Tesla (T) on left and 3.0 T on right.

Images have been reformatted using "Soap-Bubble".

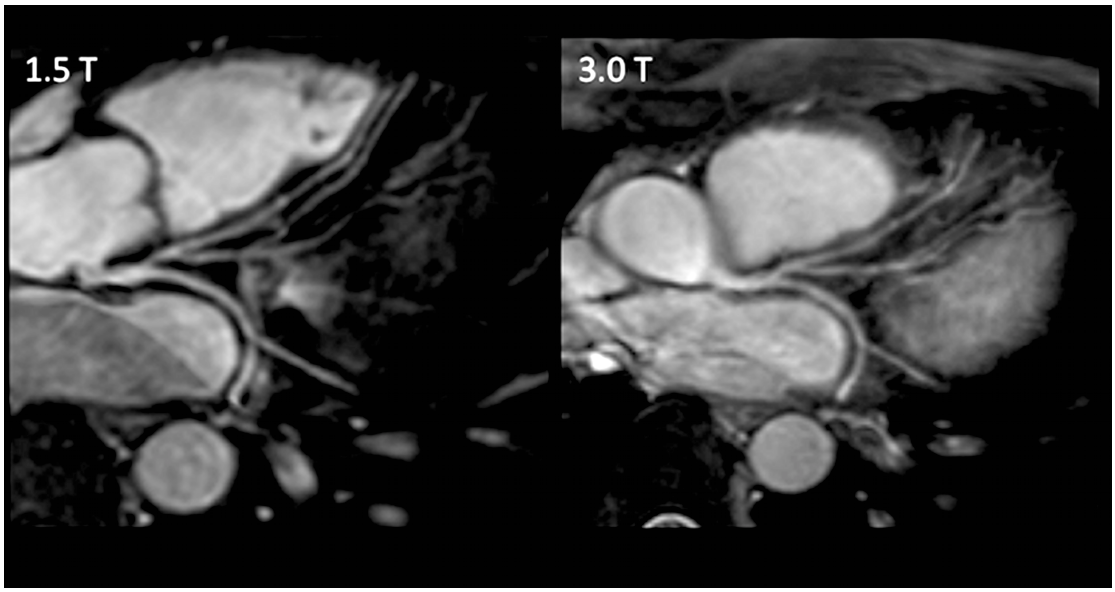

Figure 21. Further sample Images showing left coronary system of same volunteer at 1.5 Tesla (T) on left and 3.0 T on right.

Images have been reformatted using "Soap-Bubble".

3.1.5. Discussion

Congruent with previous studies, we have shown that the SNR of CMRA is increased at 3.0 Tesla compared with 1.5 Tesla.[138, 150] We have further shown a trend towards increase in CNR. In this preliminary study of healthy subjects, the use of balanced-SSFP at 3.0T using parallel transmit technology allowed improved visualisation of the more distal coronary tree compared with 1.5 Tesla (length of LAD visualised 8.4 cm vs. 7.1cm).

However, improvements in B1 homogeneity afforded by parallel transmit technology did not result in better image quality. Qualitative (IQ) and quantitative (vessel sharpness) measures of image quality were in fact reduced at 3.0 Tesla compared with 1.5 Tesla imaging. More worryingly, this results in a small but significant overestimation of lumen size (mean bias 0.2mm). This is likely to be the

result of partial volume effects (intra-voxel dephasing) that occurs due to a reduction in vessel sharpness as demonstrated in (Figure 20) and (Figure 21).

This study is important as it shows that, despite advantages in T1 weighted imaging and late gadolinium enhancement imaging at 3.0 Tesla,[134, 137] the pre-requisite of good lumen imaging is not being adequately met.

Overall, our findings suggest that parallel transmit technology alone is not sufficient to achieve balanced-SSFP CMRA image quality at 3.0 Tesla comparable with 1.5 Tesla. We can, however, only draw conclusions from the specific sequence tested. Sequences are being developed such as the method to alternate repetition times resulting in an alteration of the spectral response of SSFP.[151] Hence, wider band spacing can be achieved, relaxing the TR limitation. This approach, termed 'wideband SSFP' has already been shown to suppress off-resonance related banding artefacts and hence improve image quality. The combination with parallel transmit technology may achieve the full potential of SSFP CMRA at 3.0 Tesla. This could ultimately be combined with improved motion compensation. Novel 2D and 3D self-navigator techniques have recently been described and have already been shown to improve CMRA image quality and even shorten the scan duration.[152, 153]

It seems probable that a combination of these approaches will soon achieve improved CMRA image quality at 3.0 Tesla compared with lower field strengths. We have shown that parallel transmit technology is only one step towards that goal.

3.1.6. Conclusion

This study shows that despite implementation of parallel transmit technology, balanced-SSFP CMRA image quality at 3.0 Tesla is still inferior to 1.5 Tesla

imaging. Parallel transmit combined with other recent technological advances may allow superior imaging at 3.0 Tesla.

3.2. Combined Coronary Lumen and Vessel Wall Magnetic Resonance Imaging with i-T2prep: Influence of Nitroglycerin

3.2.1. Abstract

Background: It has been shown that sublingual nitroglycerin (NTG) improves image quality of coronary lumen magnetic resonance angiography. The purpose of the study was to investigate the influence of sublingual NTG on coronary lumen and vessel wall image quality using a combined, single sequence approach (i-T2prep), which is able to image both coronary lumen and vessel wall within the known time-frame of action of sublingual NTG

Methods: Ten healthy volunteers underwent right coronary artery (RCA) lumen and vessel wall imaging using the i-T2prep sequence before and after administration of NTG. Lumen and vessel wall image quality was assessed qualitatively (scale 0 to 4: 0 being not visible and 4 being visible without any blurring) and quantitatively (using vessel wall sharpness). Vessel lumen and wall diameters and length were also measured using dedicated semi-automatic software, "Soap-Bubble". Normally distributed variables were assessed using paired t-tests and remaining variables were assessed using Wilcoxon signed ranks test.

Results: NTG induced coronary vasodilatation (RCA lumen diameter increased from 2.16 ± 0.32 to 2.52 ± 0.59mm; p=0.036). As a result, visualised RCA lumen length (9.8 ± 2.6 to 11.4 ± 3.3 cm; p=0.025) and qualitative lumen image quality

(median 3 (interquartile range 2 - 3.25) vs. median 3 (interquartile range 3 – 4); p=0.046) both improved. Vessel wall imaging also demonstrated a significant improvement in vessel wall sharpness after NTG (24.8 vs. 27.3%; p=0.036).

Conclusions: This study demonstrates the benefits of NTG for coronary lumen and vessel wall imaging using a combined sequence, i-T2prep. The methodology described here has great potential for future pathophysiological studies.

3.2.2. Introduction

Sublingual nitroglycerin (NTG) has been recently shown to improve subjective image quality for coronary magnetic resonance angiography (CMRA) without influencing signal-to-noise or contrast-to-noise ratios.[154] Increase in luminal diameter is thought to result in a better delineation of the coronary arteries and a reduction of artefacts. Such improvements are welcome because CMRA is a valuable tool for the non-invasive and radiation-free detection of significant proximal or mid coronary artery disease.[89] However, coronary lumen imaging to detect stenoses is a poor predictor of future coronary events.[131] Approximately 60-70% of acute coronary syndromes are caused by stenosis of less than 50% of the luminal diameter due to compensatory positive vessel wall remodeling.[132] Hence, coronary vessel wall imaging is required to provide the true disease burden and such screening has been demonstrated using non-invasive black-blood MRI.[97-99] In this study, we sought to investigate the influence of NTG on a combined protocol, i-T2prep (interleaved T2prep), for coronary lumen and vessel wall imaging.

The pharmacodynamics of NTG suggests that peak blood levels are reached by 2 minutes of administration, that this level falls to 50% by 7 minutes and that it is

barely detectable by 20 minutes.[155] This timing means that it is impractical to utilise effects for both coronary lumen and vessel wall imaging given the relatively long imaging times for these free-breathing sequences. Therefore, we used a coronary vessel wall sequence based on the differences in T2 relaxation time of arterial blood and surrounding tissues. The technique is based on the acquisition and weighted subtraction of two 3D coronary steady-state free-precession (SSFP) data sets, one obtained with a T2 preparation prepulse (T2prep-ON) and the second without (T2prep-OFF). The weighted subtraction allows for nulling of the signal of arterial blood while maintaining the signal of myocardium and the vessel wall.[156] The two acquisitions are interleaved over 2 heartbeats. Data are only accepted if both the T2prep-ON and T2prep-OFF acquisition were within the gating window thus allowing for identical positions and reducing misregistration artefacts. The resulting sequence (i-T2prep) is ideal for the purposes of our study allowing identical influence of NTG on both CMRA (using the acquisition with T2prep-ON) and vessel wall (using the i-T2prep weighted subtraction). Additionally, having a single sequence that can be completed within the time frame of action of sublingual NTG, eases the practicalities of administration.

The purpose of the study was to investigate the influence of sublingual NTG on coronary lumen and vessel wall imaging using the combined, single sequence, i-T2prep approach.

3.2.3. Methods

3.2.3.1. Subjects

Institutional Review Board (IRB) approval was obtained prior to commencement of recruitment (IRB reference number 07/Q0702/62). Ten healthy volunteers took part in the study after written, informed consent was obtained. i-T2prep MRI was performed before and directly after administration of 800 micrograms of sublingual NTG.

3.2.3.2. MRI

Cardiac MRI was performed using a 1.5 Tesla (T) Achieva clinical MR scanner (Philips Healthcare, Best, NL) equipped with a 32-element cardiac phased-array receiver coil. An initial survey and reference scan was acquired for subsequent positioning of the imaging volume & navigator and to obtain coil sensitivity maps. Following this, the mid-diastolic cardiac rest period was ascertained using a high temporal resolution, balanced-SSFP, two-dimensional cine MR sequence in a four-chamber view orientation. (Imaging parameters included: repetition time = 2.4 ms, echo time = 1.2 ms, flip angle = 60° at 1.5T, slice thickness = 10mm, FOV = 300-350 mm, 80 cardiac phases, temporal resolution = 10 to 16 ms/ frame). The mid-diastolic rest period, ascertained from the cine images, was used to define the acquisition window for the subsequent CMRA.

First, a rapid whole-heart CMRA was performed as a roadmap for a subsequent 3-point plan-scan to set a targeted double-oblique geometry parallel to the native right coronary artery (RCA) system. RCA geometry was used for the ECG-triggered and navigator-gated i-T2prep 3D SSFP gradient echo sequence. Imaging parameters

included flip angle = 70°; TE/TR = 2.7/5.4 ms; acquired matrix = 280x280; slice thickness = 2 mm; 20 slices acquired; acquired resolution = 1x1 mm and reconstructed resolution = 0.3x0.3 mm. The acquisition window and trigger delay were defined as assessed using the 4-chamber cine. A diaphragmatic 1D respiratory navigator[157, 158] and a fat suppression pre-pulse preceded the imaging sequence. A 7 mm respiratory navigator window was used but data was only accepted if consecutive T2prep-ON and T2prep-OFF acquisitions were both within the window. The T2 preparation pre-pulse[105] had a duration of 80 ms and consisted of 2 non-selective, adiabatic, 180° refocusing pulses.

The i-T2prep sequence was repeated, starting exactly 1 minute and 45 seconds after the administration of 800 micrograms of sublingual NTG. Vessel wall images were obtained by subtraction of T2prep-ON from T2prep-OFF images using custom-made software implemented in Matlab (Release 2009b, version 7.9, Mathworks, Natick, MA, USA). A multiplication factor of 1.28 was used for T2prep-ON images to achieve consistent blood signal subtraction.

3.2.3.3. Image Analysis

For quantitative analysis, the targeted RCA lumen and vessel wall images were reformatted along the major axis of the RCA and analysed using "Soap-Bubble" software (Release 5.0, Philips Healthcare, Best, Netherlands).[147] Using this semi-automatic software, length of RCA lumen visualised, proximal vessel diameter, and vessel sharpness were measured. The local vessel sharpness was calculated by "Soap-Bubble" as a percentage by normalising the magnitude of the local change in signal intensity at the selected vessel border to the average signal intensity of the centerline of the selected vessel by using a Deriche algorithm.[148]

Similarly, images reformatted in the RCA plane were used to measure anterior and posterior vessel wall length, vessel wall sharpness and vessel wall thickness. Combined anterior and posterior wall length, mean anterior and posterior wall sharpness and mean wall thickness was used for analysis.

Finally, a qualitative analysis was undertaken by means of a consensus reading for image quality scoring on all the reformatted lumen and vessel wall images in a blinded and random order by two readers (T.H. and G.F.G. (>3years & >10 years of CMRA experience respectively). The two readers first reviewed the images independently and any disagreement was then discussed before the final grade was given. The following scoring system was used: 0 indicates that the coronary artery was not visible; 1 visible but with markedly blurred borders; 2 visible with moderately blurred borders; 3 visible with mildly blurred borders and 4 visible with sharply defined borders.[111]

3.2.3.4. Statistical Methods

Variables were visually assessed on frequency plots for normality and then formally assessed for normality of distribution using the Kolmogorov-Smirnov test. Normally distributed variables are described in the format mean ± standard deviation (SD). It was assumed that image quality scores (IQ), being categorical data, were not normally distributed.

Measurements were compared by paired t-test analysis for normally distributed variables and Wilcoxon signed rank tests for remaining variables. p values < 0.05 indicated rejection of the null hypothesis.

There was little data regarding the i-T2prep sequence, around which to plan study numbers. However, post-hoc testing was performed using a 2-tailed significance

level of 5% and an SD of 3.2 for difference in vessel wall sharpness, as indicated by our data. Taking a meaningful change of vessel wall sharpness to be 10%, post-hoc analysis revealed that the study had a 60% power level.

Statistical analysis was performed on SPSS version 19 (Release 19.0.0, IBM Software Group, New York, USA).

3.2.4. Results

3.2.4.1. Subjects

Ten subjects (5 male) successfully participated in the study without any adverse events. Mean age was 38.7 ± 6.8 years and mean weight was 71.4 ± 11.4 kg. Mean total time taken for i-T2prep acquisition was 7.5 ± 1.5 minutes (mean navigator efficiency = 47 ± 10%). All post-NTG i-T2prep acquisitions were started at 1 minute and 45 seconds after administration and all were finished by 12 minutes. Mean heart rate at rest was 63 bpm and, as expected, there was a small but significant rise to 69 bpm with NTG ($p=0.002$).

3.2.4.2. Image analysis

Vessel sharpness, proximal vessel diameter, RCA length imaged, vessel wall sharpness, vessel wall length and vessel wall diameter were assessed visually with frequency plots and were further formally tested for normality using the Kolmogorov-Smirnov test ($p>0.2$ for all). Based on this assessment, these variables were assumed to be normally distributed.

After NTG administration, coronary lumen imaging demonstrated a significant increase in RCA diameter (2.16 ± 0.32 to 2.52 ± 0.59mm; $p=0.036$), RCA length

visualised (9.8 ± 2.6 to 11.4 ± 3.3 cm; p=0.025) and qualitative image quality (median 3 (interquartile range 2 – 3.25) vs. median 3 (interquartile range 3 – 4); p=0.046). There was no difference in vessel sharpness (see (Table 10) and (Table 11) and (Figure 22)).

Table 10. NTG Summary Statistics for normally distributed variables Tested using 2-tailed paired t-tests. * denotes significant differences (p<0.05)

Measure	median at rest (interquatile range)	median after NTG (interquatile range)	p-value
Lumen Image Quality Score	3.0 (2 to 3.25)	3.0 (3 to 4)	**0.046***
Vessel Wall Image Quality Score	3.0 (1.75 to 4)	3.5 (1.75 to 4)	0.317

Table 11. NTG Study Summary of Categorical Variables.

P-values are given for paired differences using Wilcoxon Signed Ranks Test.

***denotes a significant difference (p<0.05)**

Measure	Rest (mean ± s.d.)	NTG (mean ± s.d.)	p-value
Vessel Lumen Sharpness (%)	47 ± 9	45 ± 12	0.333
Vessel Lumen Length (cm)	9.8 ± 2.6	11.4 ± 3.3	**0.025***
Vessel Lumen Diameter (mm)	2.16 ± 0.32	2.52 ± 0.59	**0.036***
Vessel Wall Sharpness (%)	24.9 ± 14.2	27.4 ± 15.3	**0.039***
Vessel Wall Length (cm)	9.8 ± 4.1	10.4 ± 3.4	0.412
Vessel Wall Diameter (mm)	1.07 ± 0.27	1.02 ± 0.23	0.253

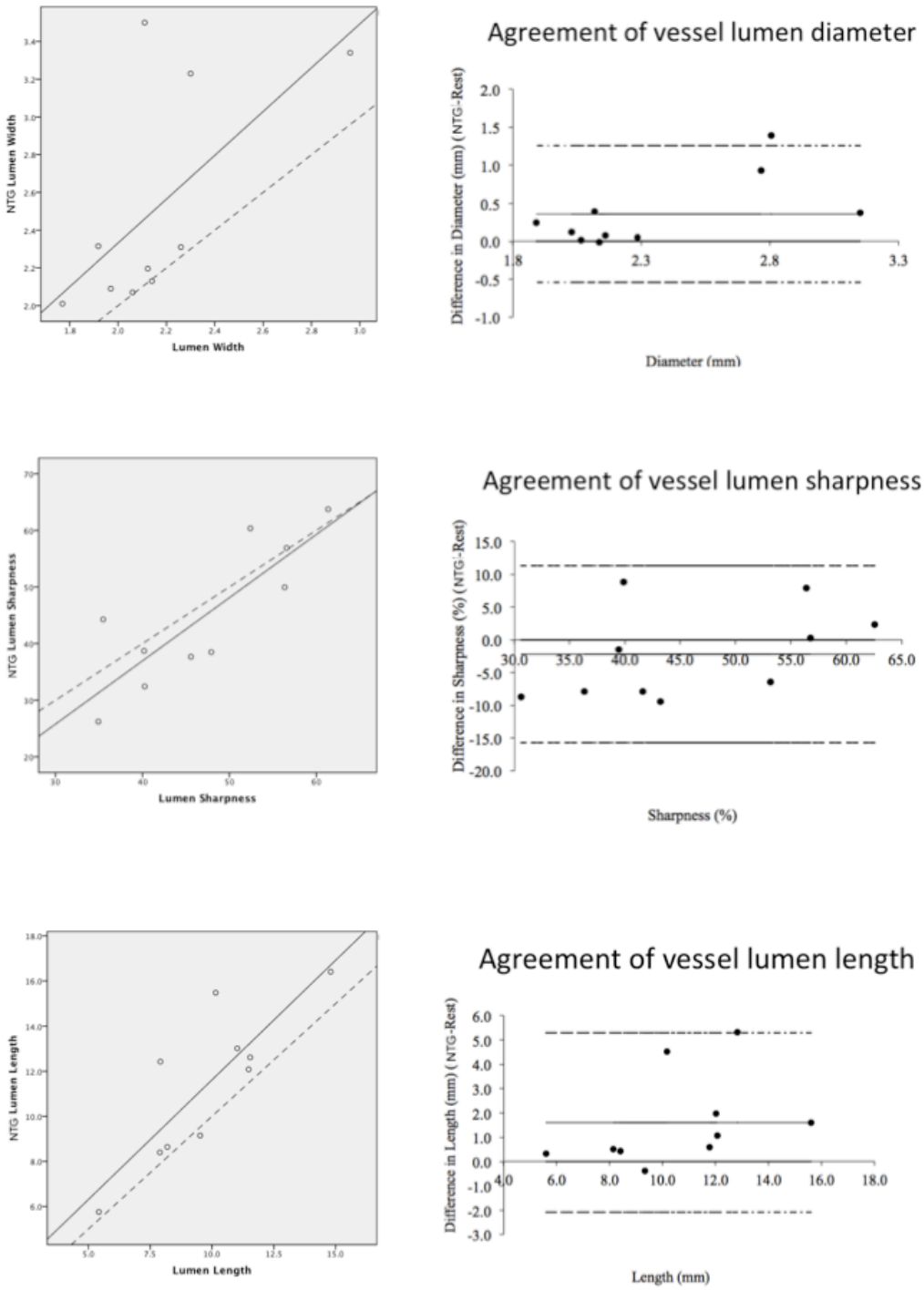

Figure 22. Linear correlation of vessel lumen parameters

Linear correlation of vessel lumen parameters before and after NTG administration. Dotted line is the line of equivalence, whereas the solid line

plot is the regression line of best fit. Corresponding Bland-Altman agreement plots are shown on the right. After NTG administration, coronary lumen imaging demonstrated significant increase in RCA diameter (2.16 ± 0.32 to 2.52 ± 0.59mm; p=0.036) and RCA length visualised (9.8 ± 2.6 to 11.4 ± 3.3 cm; p=0.025). This is demonstrated with a separate regression lines above the line of equivalence. It is also shown in the agreement plot with the mean bias being clearly above 0. There was no significant difference in vessel lumen sharpness.

Vessel wall imaging demonstrated a significant improvement in vessel wall sharpness after NTG (24.8 to 27.3%; p=0.036). Vessel wall length visualised, vessel wall thickness and vessel wall image quality score showed no differences after NTG administration (see (Table 10) and (Table 11) and (Figure 23)).

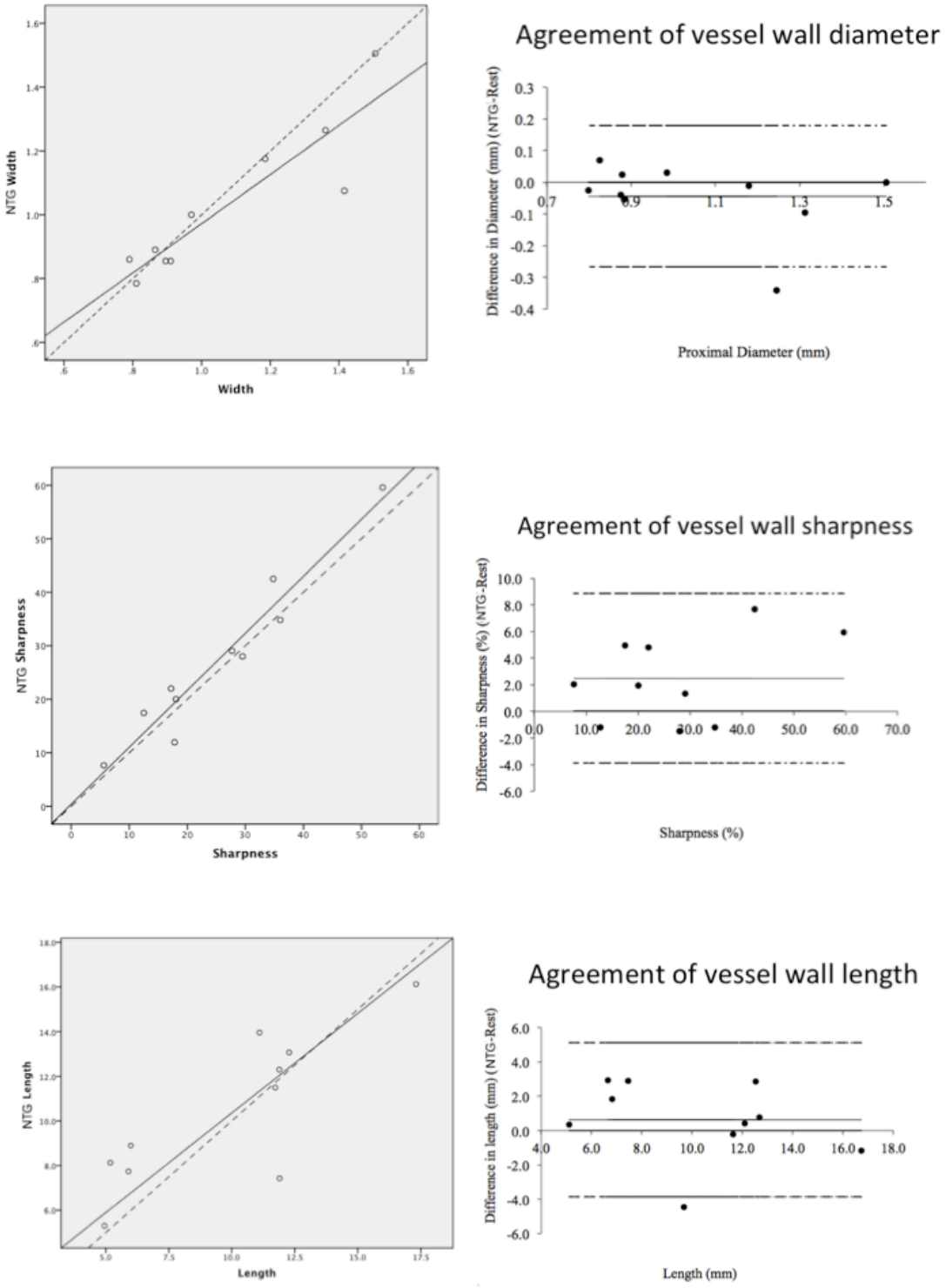

Figure 23. Linear correlation of vessel wall parameters

Linear correlation of vessel wall parameters before and after NTG administration. Dotted line is the line of equivalence, whereas the solid line

plot is the regression line of best fit. Corresponding Bland-Altman agreement plots are shown on the right. Vessel wall imaging demonstrated a significant improvement in vessel wall sharpness after NTG (24.8 to 27.3%; p=0.036). This is demonstrated with a separate regression line above the line of equivalence. It is also shown in the agreement plot with the mean bias being clearly above 0. Vessel wall length visualised and vessel wall diameter showed no significant differences after NTG administration.

Interestingly, 4 subjects showed little change in vessel diameter (<5%) with NTG. These four subjects showed a mean increase in vessel wall sharpness of only 2.7% compared to 20.8% for subjects that had >5% increase in vessel diameter.

All study images are shown in (Figure 24) and (Figure 25). Mean vessel wall thickness with GTN was almost identical to previously published MRI black-blood values for healthy individuals (1.0 ± 0.2 mm using i-T2prep and 1.0 ± 0.2mm for previous black-blood sequence).[99]

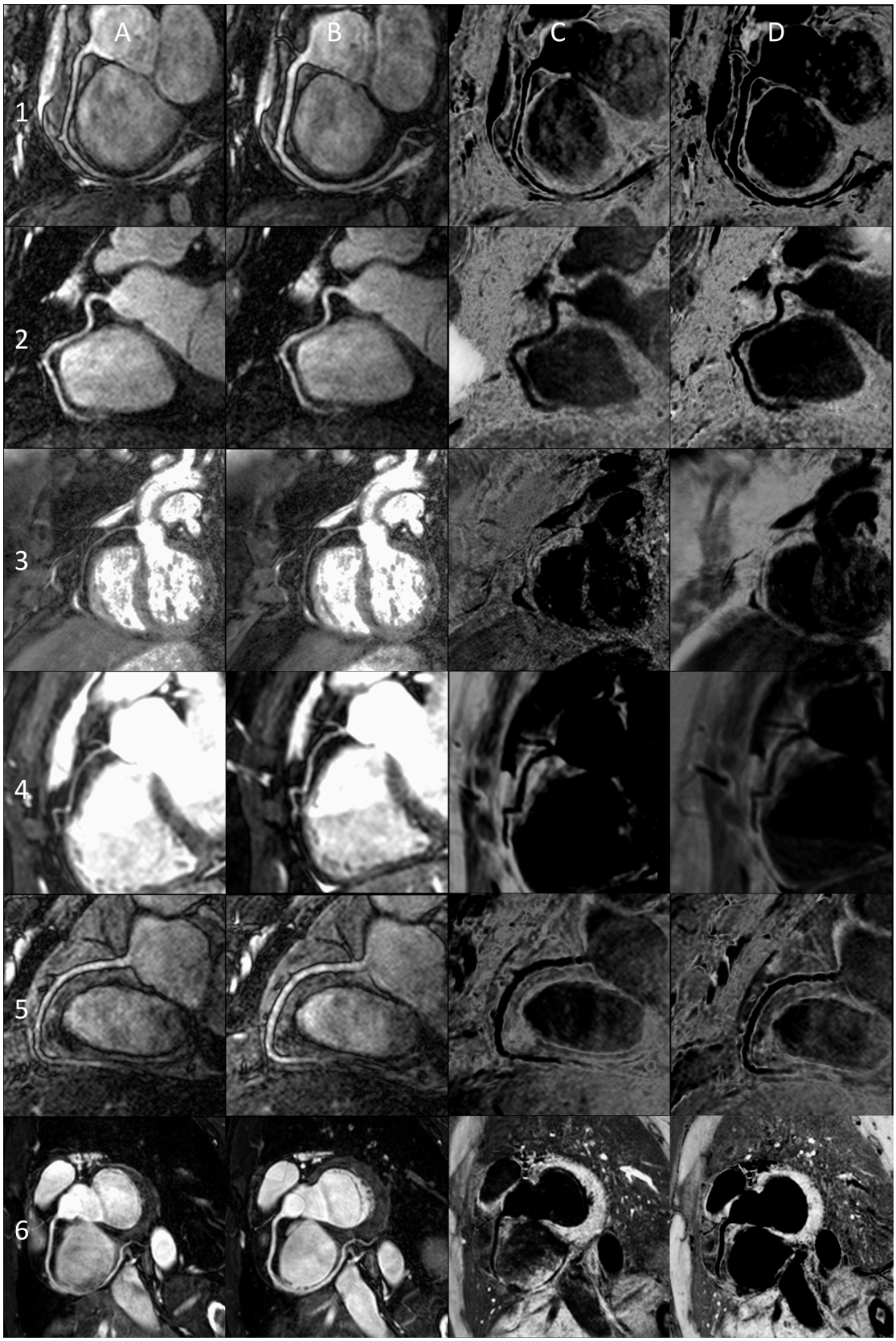

Figure 24. NTG Volunteer Images

Rows 1 to 6 represent individual volunteers. Images are reformatted to show the major axis of the RCA. Column A represents RCA lumen CMRA.

Column B is the repeated lumen CMRA using NTG. Column C represents subtraction RCA vessel wall images. Column D represents the repeat subtraction image using NTG.

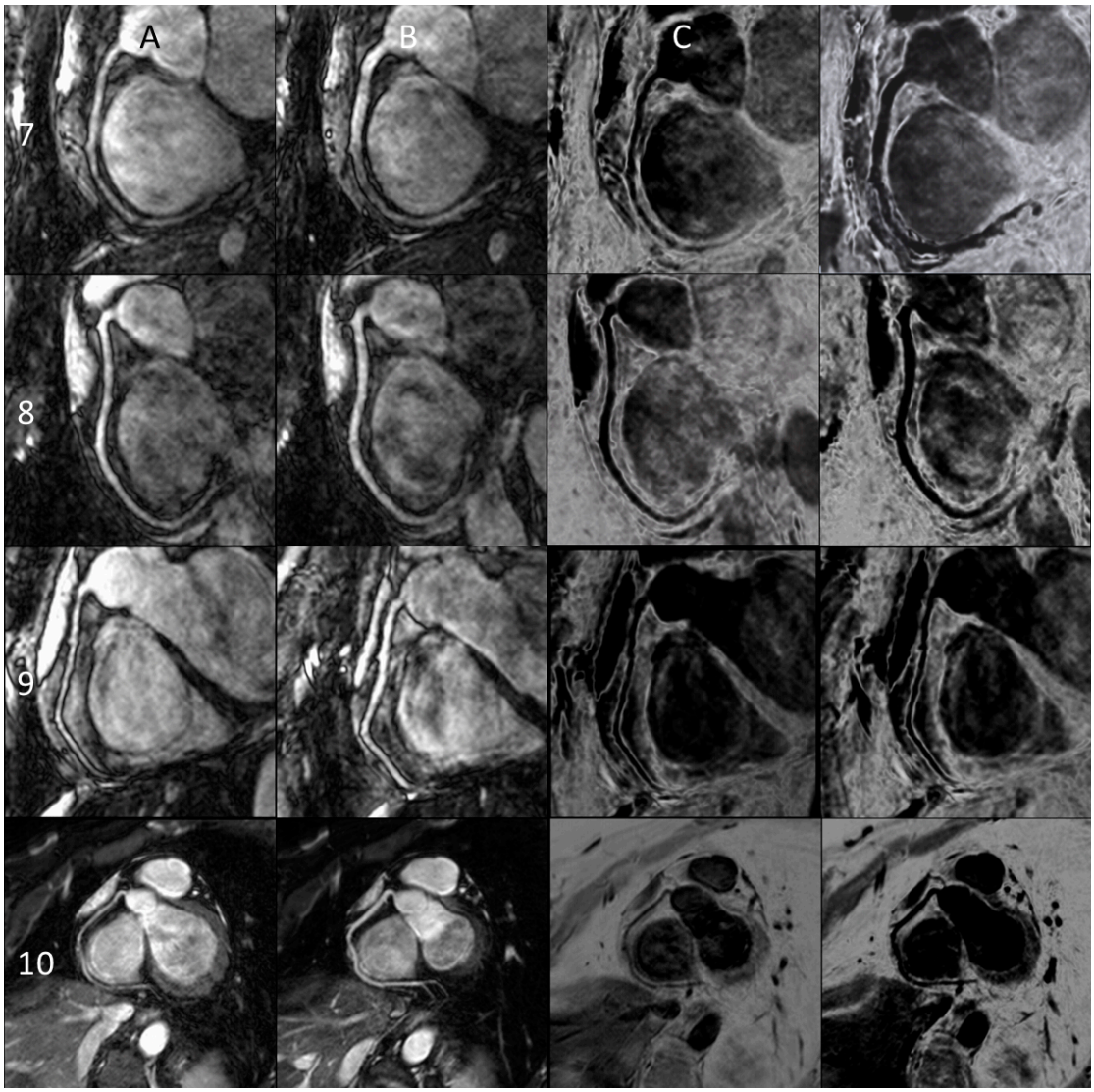

Figure 25. Further NTG Volunteer Images

Rows 7 to 10 represent individual volunteers. Images are reformatted to show the major axis of the RCA. Column A represents RCA lumen CMRA. Column B is the repeated lumen CMRA using NTG. Column C represents subtraction RCA vessel wall images. Column D represents the repeat subtraction image using NTG.

3.2.5. Discussion

We have shown that NTG improves qualitative image quality for coronary lumen imaging. This is congruent with the experience of other investigators.[154] Qualitative CMRA lumen image quality using i-T2prep sequences is similar to previous CMRA sequences that have a proven value in the detection of proximal or mid vessel stenosis.[89] Vessel sharpness with the i-T2prep sequence was 47 ± 9% compared to 46 ± 10% for the previous study.[89] Furthermore, we were able to show a mean increase in vessel diameter of 16.7% using NTG. We believe that this was responsible for a greater visualised length of RCA (mean 11.4cm vs. 9.8cm). This is important as it allows for detection of more distal stenoses.

In regard to vessel wall imaging, we have shown that the quantitative measure of image quality (vessel wall sharpness) is increased by 10%. This is likely due to the increase in vessel diameter, which results in better separation between anterior and posterior vessel walls. This is supported by the data showing no meaningful mean increase in vessel wall sharpness in those individuals showing no significant increase in vessel diameter after NTG.

Volunteers were in supine position during the entire period of peak action of NTG. This, no doubt, contributed to very few reported symptoms but there remained a small but significant reflex increase in heart rate due to NTG. This is one limitation of the study as heart rate increase is not desirable in the context of coronary imaging. Hence, a combination with a beta-receptor antagonist would be preferable for future studies. Furthermore, although successful vessel wall imaging has been demonstrated, this study included healthy volunteers and future studies using the i-T2prep sequence will need to focus on the quantification of coronary

plaque. However, (Figure 24) and (Figure 25), suggest that the sequence is robust enough for this purpose.

One limitation is that the subtraction algorithm may unduly influence the resulting vessel wall thickness. On practical terms, ensuring complete arterial blood suppression minimizes this potential error. Arterial blood suppression using a simulation for this sequence has been performed previously and the optimum value shown to lie between 1.2 and 1.3.[159] Validation of this sequence and this subtraction weighting value has also been performed on the Aortic vessel wall. *Andia et al* showed excellent agreement between vessel wall measures using a previously validated dual-inversion recovery black-blood turbo-spin-echo sequence and this novel i-T2prep sequence. Hence, in this study a weighting factor was used of 1.28, which achieved consistent arterial blood suppression for all our cases. Additionally, the vessel wall thickness obtained using i-T2prep in this study of healthy volunteers was identical to a previous black-blood coronary vessel wall imaging sequence, which has been validated to be able to show vessel wall disease.[99, 160] In the long term, further validation with invasive imaging would lend further credence to this type of coronary vessel wall imaging. Another limitation was that, as an exploratory study of this sequence, there was insufficient published data to prospectively select the sample-size required. However, we were able to show a meaningful 10% increase in vessel wall sharpness with our given sample size.

The methodology of this study is important. Like the previous study,[154] the imaging in this study was started at the known time for peak blood concentrations of NTG. This enabled both vessel lumen and vessel wall imaging to be performed within the window of action of sublingual NTG. The study sequence, i-T2prep was

also ideal for these purposes, with the interleaving allowing identical timing of effect for both lumen and vessel wall imaging. The methodology used here has great potential for the pathophysiological assessment of coronary disease. It has been previously shown that impaired NTG-induced coronary vasodilatation is associated with advanced atherosclerosis in an asymptomatic older population.[161] The protocol described would allow us to identify the influence of atherosclerotic plaque on endothelium-independent vasodilatation on a segment-to-segment basis. Combining the protocol with methods to quantify calcification would allow us to answer whether calcified or soft plaques differ in their effects on this type of vasodilatation.[162] Moreover, impairment of endothelial-dependent coronary vasodilatation has been shown to be an early marker of atherosclerosis.[31] The relationship between endothelium dependent vasodilatation and NTG-induced direct vasodilatation is not entirely clear but this could be assessed further using this protocol and thereby directly relating it to vessel wall disease.

In conclusion, we have demonstrated the benefits of NTG for coronary lumen and vessel wall imaging using a combined sequence, i-T2prep. The methodology described here has great potential for future pathophysiological studies of coronary artery disease.

Chapter 4 - Contrast-Enhanced Inversion Prepared Coronary Vessel Wall Imaging for Coronary Vasculopathy

4. Contrast-Enhanced Inversion Prepared Coronary Vessel Wall Imaging for Coronary Vasculopathy

4.1. Detection and Grading of Coronary Allograft Vasculopathy in Children using Contrast-Enhanced Magnetic Resonance Imaging of the Coronary Vessel Wall

4.1.1. Abstract

Background: Coronary Allograft Vasculopathy (CAV) is the leading cause of late death after heart transplantation in children. It is poorly detected by conventional angiography. Intravascular ultrasound (IVUS) is invasive and costly. The purpose here is to show that MRI late gadolinium enhancement (LGE) of the coronary vessel wall can detect and grade CAV.

Methods and Results: 12 children (5 male, mean age 15.1 years (range 12-17)) underwent coronary angiography, IVUS and MRI. Maximal intimal thickness (MIT) and mean intimal index (MII) were recorded. MRI included coronary magnetic resonance angiogram (CMRA) and LGE vessel wall imaging. Mean time post-transplant was 4.5 years (range 0.5-12). No patient had angiographic disease. Two patients had Stanford grade 4 CAV on IVUS. MIT was 0.50 ± 0.29mm and MII was 17.5 ± 5.7%. On MRI, mean diameter of enhancement of vessel wall was 5.38 ± 2.39 mm and mean enhancement index (indexed to vessel lumen size) was 0.53 ± 0.42. Correlation of LGE with MIT using Pearson's coefficient was 0.81 ($p=0.001$) and with MII was 0.62 ($p=0.03$). If disease on MRI was defined as enhancement diameter > 7.5mm, sensitivity and specificity values of 100% are obtained for the detection of significant CAV.

Conclusion: This study has shown that imaging CAV with MRI is possible in paediatric transplant recipients. The late gadolinium enhancement scores correlate well with traditional IVUS measures. These promising results warrant larger studies to confirm the utility of this technique. This approach may enable closer follow-up and better prevention of CAV in children.

4.1.2. Introduction

Coronary Allograft Vasculopathy (CAV) is the leading cause of late death or graft loss after heart transplantation in children.[6] It is a progressive condition, which is thought to be caused largely by chronic autoimmune-mediated endothelial damage.[3] Damaged endothelium allows cell infiltration, which is responsible for the production of cytokines, growth factors, and matrix deposition (collagen I and fibroblasts).[4] This results in a progressive thickening of the intima, which is poorly detected by conventional angiography.[8] Rapid progression is the most important predictor for all-cause death in this patient group[25] and warrants a change in treatment. Intravascular ultrasound (IVUS) is a much more sensitive imaging modality and is therefore desirable for the early detection of CAV.[9-11] However, it is invasive, costly and it is not technically feasible in small children. This limits how closely CAV can be monitored, especially in children.

Gadolinium DTPA is a paramagnetic contrast agent used for MRI, which is known to be deposited in diseased tissue with abundant fibrosis and extracellular matrix.[163-165] It is this property of Gadolinium that has previously been shown to be useful to demonstrate coronary vessel wall disease.[135] In this study, we examine the utility of late gadolinium enhancement for the non-invasive detection and grading of CAV.

4.1.3. Methods

Institutional Review Board approval was obtained prior to commencing the study (Research Ethics Committee reference number 09/H0713/53). Written, informed consent was obtained from the patient and/or parent accordingly. Patients older than 10 years undergoing annual review after orthotopic heart transplantation were invited to take part in the study. Participants underwent cardiac MRI followed by their routine conventional X-ray angiography and IVUS, one day later. Additionally, 10 volunteers undergoing cardiac MRI for clinical purposes also underwent coronary delayed enhancement to serve as a control group. These volunteers were young adults and adolescents without any history of coronary disease or any major cardiovascular risk factors (i.e. smoking, hypertension, dyslipidaemia, diabetes or family history of early disease). These volunteers were referred either for the exclusion of hereditary cardiomyopathy or for follow-up of surgically corrected congenital heart disease. Volunteers were excluded if there was any evidence of cardiomyopathy, reduced ventricular function, significant residual lesion, prior history of coarctation repair or history of arterial switch procedure. Separate Institutional Review Board approval and written, informed consent was obtained for these volunteers (Research Ethics Committee reference number 09/H0802/078).

4.1.3.1. MRI Sequences

Cardiac Magnetic Resonance was performed using a 1.5 Tesla Achieva clinical MR scanner (Philips Healthcare, Best, NL). Images were obtained using a 32-element cardiac phased-array receiver coil. Prior to entering the scan room, 0.2 mmol/kg

body weight of a Gadolinium-based contrast medium (Gadovist, Bayer Schering, Berlin, Germany) was administered intravenously. Subsequently, an initial survey and reference scan were acquired to obtain coil sensitivity maps. Following this, the cardiac rest periods were ascertained using a high temporal resolution, balanced steady-state free precession (SSFP), two-dimensional cine MR sequence in a four-chamber view orientation. (Imaging parameters included: repetition time = 2.4 ms, echo time = 1.2 ms, flip angle = 60°, slice thickness = 10mm, field-of-view = 300-350 mm, 80 cardiac phases, TFE factor = 6, temporal resolution = 8 to 11 ms/ frame). The mid-diastolic rest period ascertained from the cine images was used to define the acquisition window for the subsequent coronary lumen and vessel wall scans.

Targeted coronary bright-blood Magnetic Resonance Angiography (CMRA) was performed with a previously described navigator-gated free-breathing and cardiac-triggered T2-prepared three-dimensional (3D) steady-state free precession sequence allowing visualisation of the anatomy of the coronary artery lumen.[146] Adaptations of the technique for imaging in children have also been described and implemented here.[90, 92, 101] First, a rapid whole-heart CMRA was performed as a roadmap for a subsequent 3-point plan-scan for a targeted double-oblique CMRA parallel to the native left coronary artery system.[145] Then, using an identical imaging plane and spatial resolution as the targeted CMRA, a coronary late gadolinium enhancement (LGE) sequence was performed. This was performed 30-40 minutes after the administration of gadolinium. This sequence is a navigator-gated, vector ECG-triggered, fat-suppressed T1-weighted 3D gradient-echo inversion-recovery sequence.[135, 166, 167] Imaging parameters included the following: field of view = 270x270 mm, matrix = 216x216, acquired in-plane

resolution = 1.25x1.25 mm, reconstructed slice thickness = 1.5 mm (acquired thickness = 3 mm), acquisition window = 80 to 100 ms, repetition time/echo time = 4.9 ms/1.6 ms, flip angle = 30°; start-up cycles = 5, and number of slices = 20. The patient-specific inversion time was adjusted to null blood signal with a preceding Look Locker sequence.[168] Typical inversion times were 180 to 240ms.

4.1.3.2. MR Image Analysis

CMRA images were analysed using a semi-automatic vessel analysis tool (Soap-Bubble, Release 5.0).[147] This was used to measure the mean coronary artery diameter and the combined length of left main and left anterior descending that was imaged. LGE has been used to quantify atrial scar burden in the setting of atrial fibrillation.[169] The technique described by Oakes at al[169] for atrial wall enhancement was adapted for coronary vessel wall quantification. Visualisation and segmentation of the MRI were performed with OsiriX version 3.9.1. LGE was defined as areas in the vessel wall with a signal intensity that is significantly (>2 standard deviations (SD)) higher than normal non-enhancing vessel wall. The ascending aorta (distal to anastomosis site) or the descending aorta was used as the reference for normal vessel wall. A threshold filter (mean signal of normal vessel + 2 SD) is then applied to the LGE images. Using the coronary MRA as an overlay roadmap, the volume of coronary vessel wall enhancement was then measured (Figure 26). Using this volume and Soap-Bubble measurements, mean enhancement area (=volume/length imaged), enhancement diameter (assuming circular area) and mean enhancement index (=enhancement area/coronary mean cross sectional area) were derived and recorded. As well as quantifying the

volume of enhancement, the position of areas of vessel wall enhancement was recorded, as the distance from major branches.

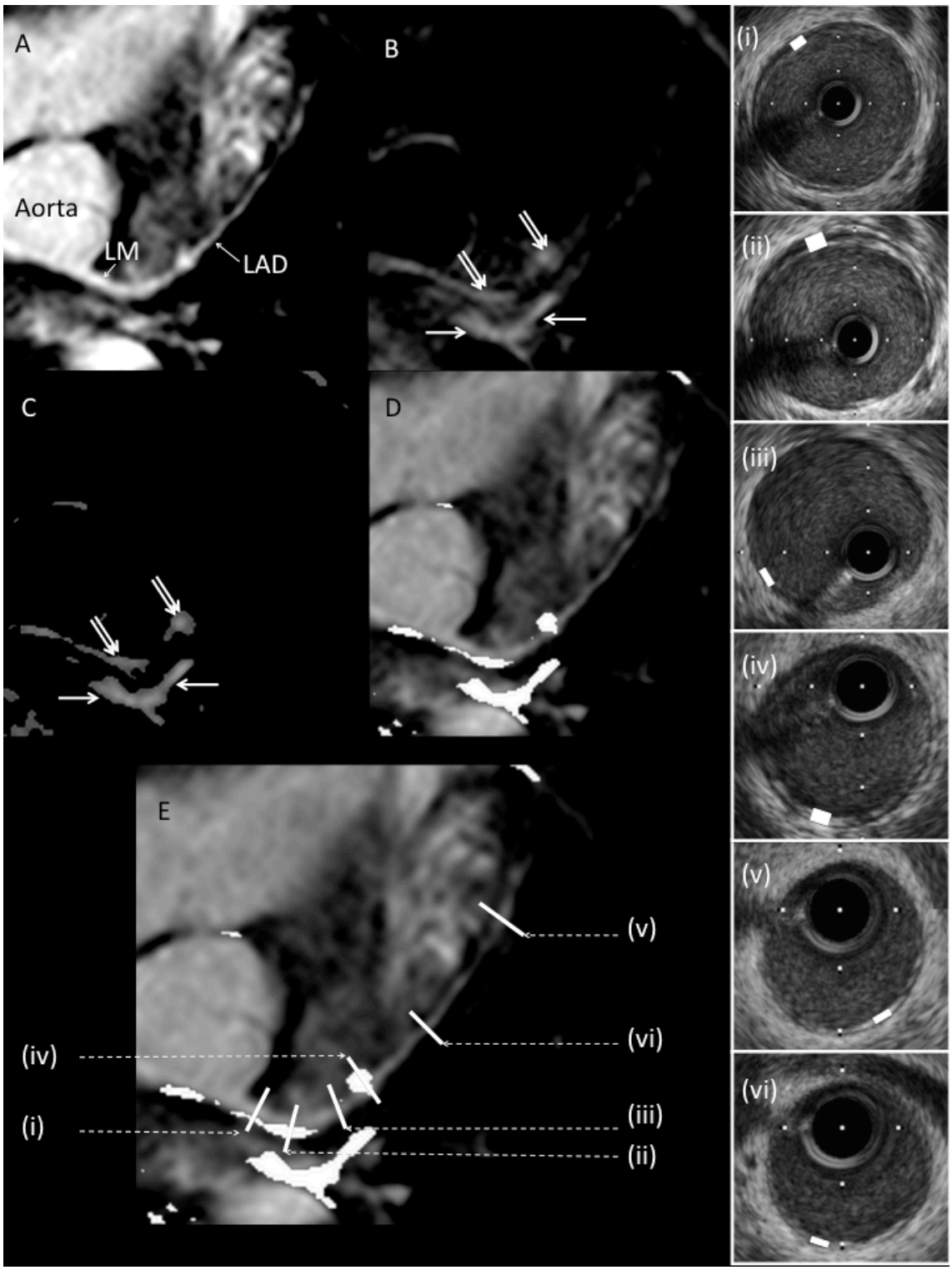

Figure 26. Anatomical Correlation of Late Gadolinum Enhancement and Intravascular Ultrasound

A – Coronary Magnetic Resonance Angiogram showing left mainstem coronary artery (LM) and left anterior descending (LAD)

B – Late Gadolinium Enhancement of same slice as image A. Double arrows show areas of marked enhancement occurring in the coronary vessel wall. Single arrows show enhancement in a pulmonary vein as it enters the left atrium (This area may show enhancement also, either because of the presence of an anastamosis line in the left atrium close to the pulmonary vein ostium or due to venous labelling as explained in the text above).

C – Late Gadolinium Enhancement images after threshold applied. Double arrows show areas of marked enhancement occurring in the coronary vessel wall. Single arrows show enhancement in the left upper pulmonary vein as it enters the left atrium

D – Overlay of image C on image A. Overlay shows how areas of enhancement pertaining to the coronary vessel wall can be clearly identified and differentiated from pulmonary vein or left atrial enhancement.

E – Image D showing positions of intravascular ultrasound images (i) to (vi)

Intravascular ultrasound images (i) to (vi) show intimal thickness corresponding to areas on image E. The white rectangles in images (i) to (vi) represent the maximal thickness of the intimal layer. In this particular case there is good anatomical correlation between areas of enhancement and areas of intimal thickening as shown in the sample of intravascular ultrasound images

All LGE measurements were repeated to calculate the intra-observer and inter-observer variability in analysis. Two observers, experienced in cardiovascular

MRI, (GG and TH (both >3yrs cardiovascular MRI experience) analysed data in an independent manner, blinded to the angiography and IVUS results.

4.1.3.3. Conventional X-ray Angiography and Intravascular Ultrasound

Conventional Angiography and IVUS was undertaken on the day following the MRI scan. Catheterisation is performed under general anaesthesia for children and adolescents, according to institutional protocol, but for older adolescents or young adults, performance under local anaesthesia is encouraged. Catheterisation and IVUS were only performed as clinically indicated for annual review. CAV on angiography is defined as mild, moderate or severe according to published criteria.[7] Angiograms were reported by a single experienced observer but any abnormalities were confirmed by a second experienced observer.

IVUS was performed in the left anterior descending coronary artery with automated pullback at 0.5mm/s. Typically, the imaging has a temporal resolution of 30 frames/second. A suitable length of vessel was imaged to allow analysis of at least 30 cross-sectional images evenly spaced (at approximately 1.5mm intervals) over the same segment of left anterior descending artery that was analysed at the previous annual review (identified by branch points). Additionally, the images analysed were always taken during the mid-diastolic rest period for consistency. Maximal intimal thickness, mean intimal index, and Stanford Grading score (Table 12) were recorded.[10] Mean intimal index is defined as the ratio of the mean intimal area to the sum of the mean intimal and luminal areas. In addition, a semi-automatic interactive edge-detection software was used (QIVUS Clinical Edition, Medis medical imaging systems) to improve reproducibility of measurements.[27] Finally, the position of the most affected regions (regions with thickness greater

than twice the mean intimal thickness for that patient) of the left main and anterior descending coronary artery were recorded, using distance from major side branches.

Table 12. Stanford score table

Severity is graded based on the site with the most severe disease.

GRADE	SEVERITY	INTIMAL THICKNESS
I	Minimal	<0.3mm & <180 degrees
II	Mild	<0.3mm & >180 degrees
III	Moderate	0.3-0.5mm OR 0.5-1mm & <180 degrees
IV	Severe	>1mm OR 0.5-1mm & >180 degrees

4.1.3.4. Data Analysis

First an anatomical comparison was made between areas of enhancement on MRI and the location of prominent thickening on IVUS. Variables are then formally assessed for normality of distribution using the Kolmogorov-Smirnov test. Then specific bivariate correlation was performed between enhancement index (MRI) and intimal index (IVUS). Further bivariate correlation was made between enhancement diameter and maximal intimal thickness.

Finally, sensitivity and specificity for LGE for the detection of CAV compared with IVUS and conventional angiography were calculated. For these purposes, significant CAV is defined as that present on X-ray angiogram or scored as Stanford grade IV on IVUS.

Inter- and intra-observer variability in enhancement scoring are further assessed by Bland-Altman analyses. Comparison against control enhancement scores was further performed using independent t-tests.

4.1.4. Results

Twelve children (5 male) took part in this study with a mean age of 15 years and 1 month (range 12 to 17 years). Mean follow-up time was 4.5 years post-transplant (range 6 months to 12 years). On IVUS, Maximal Intimal Thickness (MIT) was 0.50 ± 0.29mm and Mean Intimal Index (MII) was 17.5 ± 5.7%. On MRI, mean enhancement diameter was 5.38 ± 2.39 mm and mean enhancement index was 0.53 ± 0.42. All four variables (MIT, MII, Enhancement diameter & Enhancement index) were assessed visually with frequency plots and were further formally tested for normality using the Kolmogorov-Smirnov test (p= 0.56, 0.47, 0.19 and 0.23 respectively). Based on this assessment, all four variables were assumed to be normally distributed.

Eleven patients underwent angiography and IVUS within 48 hours of the MRI procedure. One patient had their procedure delayed by eight weeks due to initial technical failure. No patient had angiographic evidence of CAV but two had Stanford grade 4 disease on IVUS.

4.1.4.1. Anatomical Assessment

For the 12 patients, there were 17 coronary artery segments classified as being the most affected regions on IVUS. Similarly, 17 regions of enhancement were identified on MRI. In 11 regions (mean intimal thickness 0.51mm), there was anatomical correlation (to within 1mm for location from a major branch-point) between areas of IVUS depicted thickening and enhancement noted in the MRI (Figure 26). 6 IVUS regions classified as worst affected areas had no reciprocal enhancement on MRI. The mean intimal thickness of those 6 regions (0.44 mm) was not significantly different to the 11 matched areas (p=0.69 by independent t-test). Conversely, there were 6 areas of late enhancement on MRI that were not reciprocally identified by IVUS. The mean intimal thickness on IVUS corresponding to those areas (0.28 mm) was significantly less than the 11 matched areas (p=0.04).

4.1.4.2. Quantitative assessment

Enhancement diameter on MRI showed a significant positive correlation with Maximal Intimal Thickness on IVUS (Pearson's Correlation coefficient 0.81, p=0.001) (Figure 27). Similarly, the enhancement index on MRI showed significant positive correlation with the Mean Intimal Index on IVUS (Pearson's Correlation coefficient 0.62, p=0.03) (Figure 28).

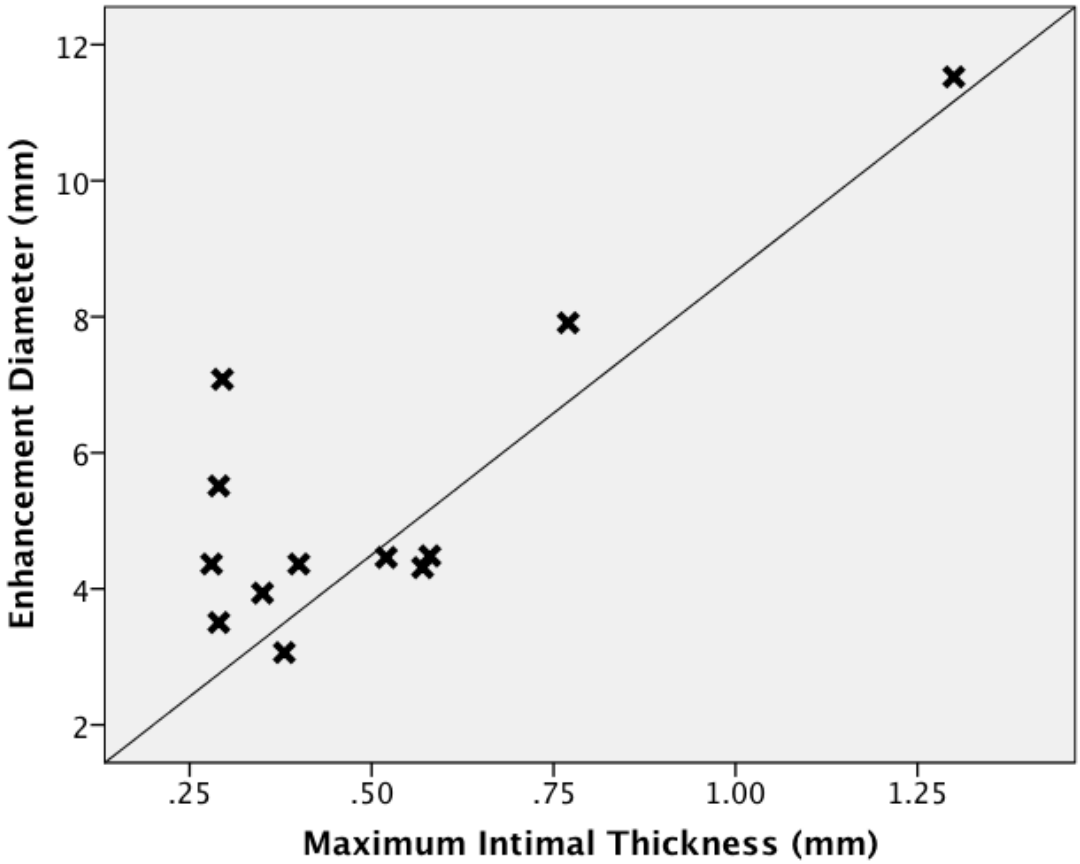

Figure 27. Scatter plot for Correlation of Enhancement Diameter on MRI against Maximal Intimal Thickness on IVUS.

It shows individual values and regression line. Pearson's Correlation coefficient 0.81, p=0.001

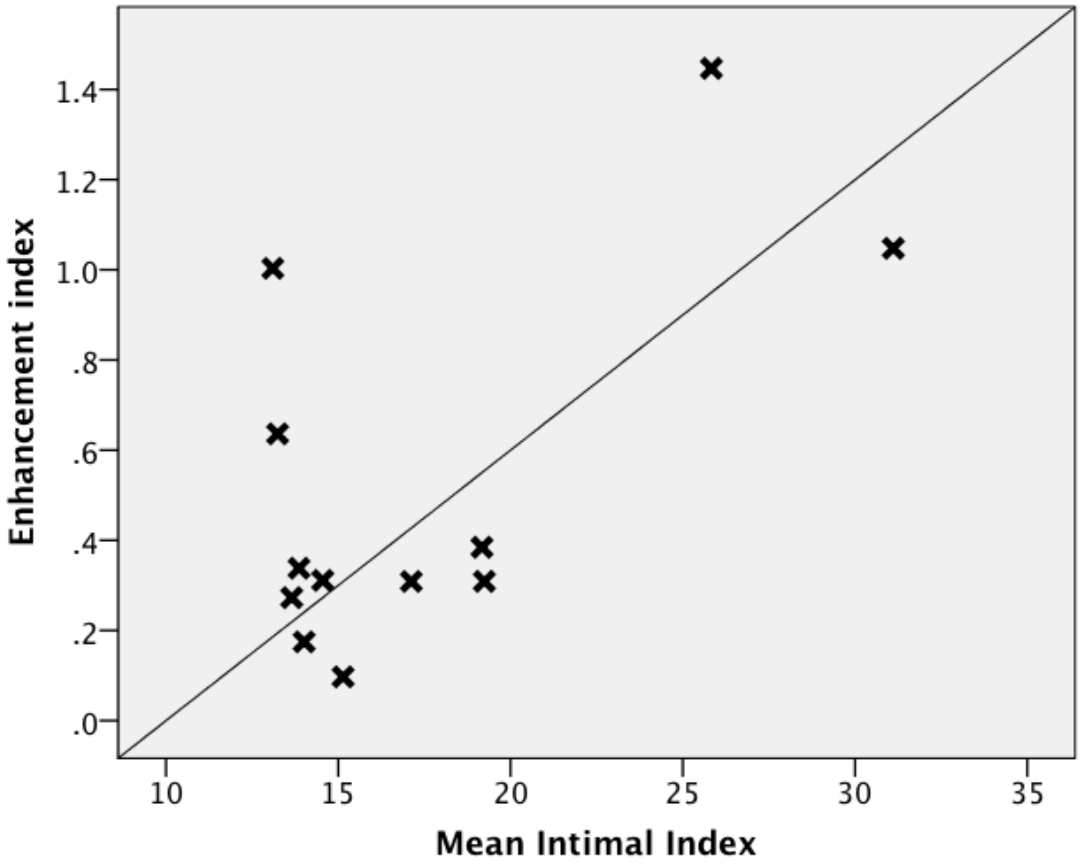

Figure 28. Scatter plot for Correlation of Enhancement Diameter on MRI against Mean Intimal Index on IVUS.

It shows individual values and regression line. Pearson's Correlation coefficient 0.62, p=0.03

No patient had angiographic evidence of disease. Two patients had Stanford grade 4 Coronary Allograft Vasculopathy on IVUS. If disease on MRI was defined as enhancement diameter > 7.5mm, sensitivity and specificity values of 100% are obtained for the detection of CAV as defined by IVUS & angiography. Similarly, an enhancement index of >1 again gives identical sensitivity and specificity values (Figure 29 shows example cases).

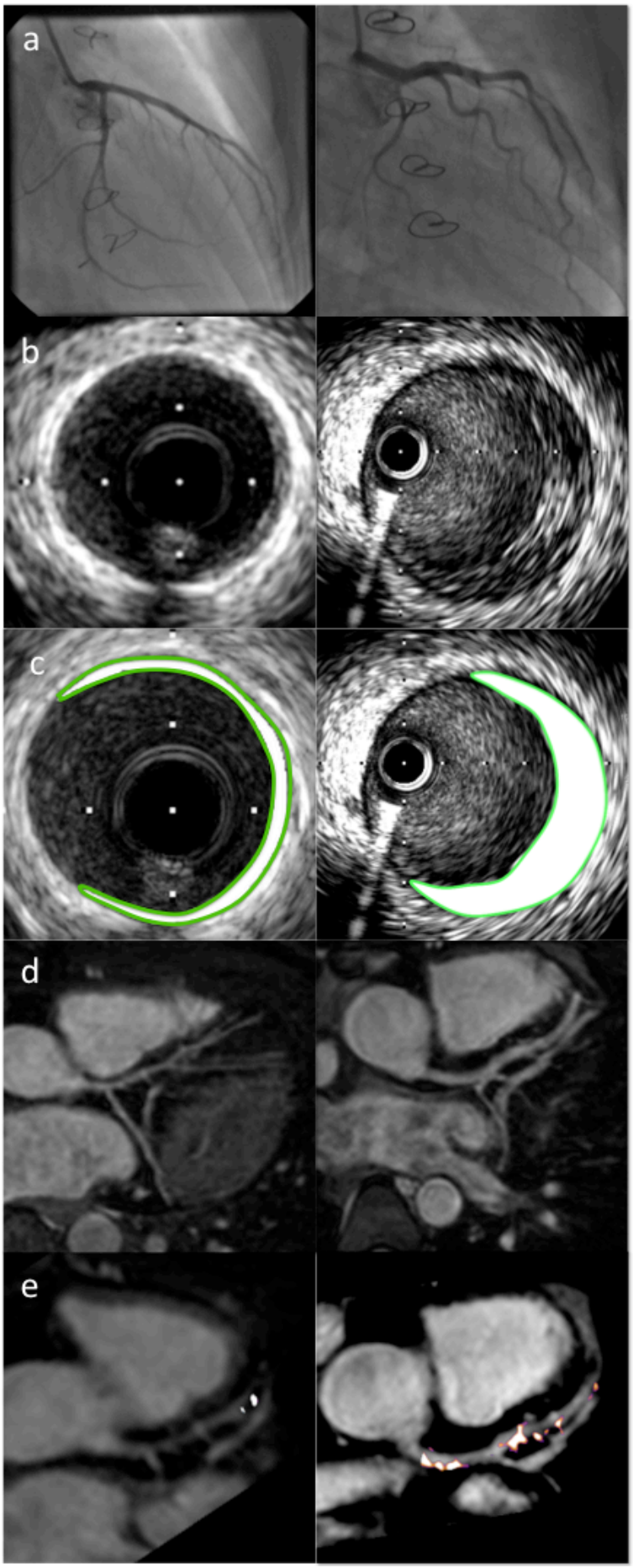
a
b
c
d
e

Figure 29. Coronary Allograft Vasculopathy MR Image

Two cases are shown for comparison. The first, left-hand, column shows images from a patient with mild (Stanford Grade 2) CAV. The second, right hand, column shows a patient with severe (Grade 4) CAV. Row (a) demonstrates that both patients have normal conventional angiography showing how poorly angiography detects CAV. Row (b) shows the IVUS images showing a small rim of intimal thickening in the first patient compared to severe intimal thickening in the second patient. Row (c) shows the segmentation of the intimal layer on the IVUS picture for clarification (bright white rendered area). Row (d) shows the quality of coronary MRA routinely achieved (Soapbubble reformat). Row (e) shows overlay of LGE (arrows) on a multiplanar reformat of the coronary artery. A much greater volume of LGE (arrows) is seen in the second patient (140mm3/cm vessel imaged) than the first patient (20mm3/cm vessel imaged).

4.1.4.3. Inter-observer and Intra-observer variability

All enhancement measures were measured twice in a blinded and random order by the first observer and once independently by the second observer in order to calculate inter-observer and intra-observer variability in scoring LGE. For presentation of results, the observation set with the worst correlation was chosen. For example, this study quotes a correlation coefficient of 0.81 ($p=0.001$) for MIT against enhancement diameter, whereas observation set 2 and observer 2 had coefficients of 0.88 ($p<0.001$) and 0.87 ($p<0.001$) respectively.

The Bland–Altman analyses indicate that there was no significant bias between the two sets of repeated enhancement diameter measurements (+0.1 mm for intra-observer error (p=0.83) and -1.3 mm for inter-observer error (p=0.13)). However, although intra-observer agreement was acceptable with 95% limits of agreement ranging from +2.8 to -2.6 mm (Figure 30), inter-observer agreement was less acceptable at +4.0 to −6.5 mm (Figure 31).

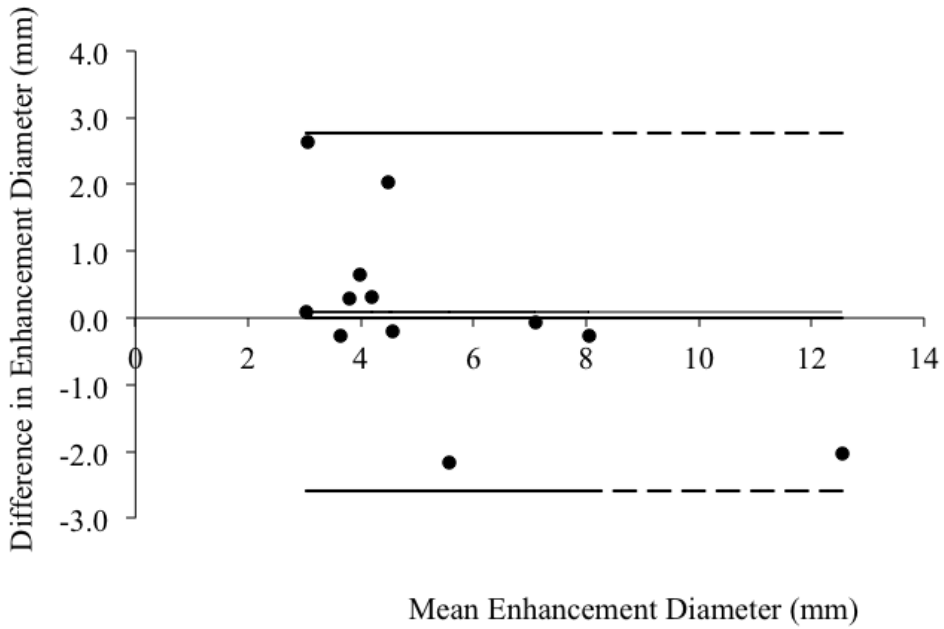

Figure 30. Bland-Altman Plots for intra-observer agreement for Late Gadolinium Enhancement scoring.

Half-dashed line represents 95% level of agreement and solid line centre-line represents the mean bias.

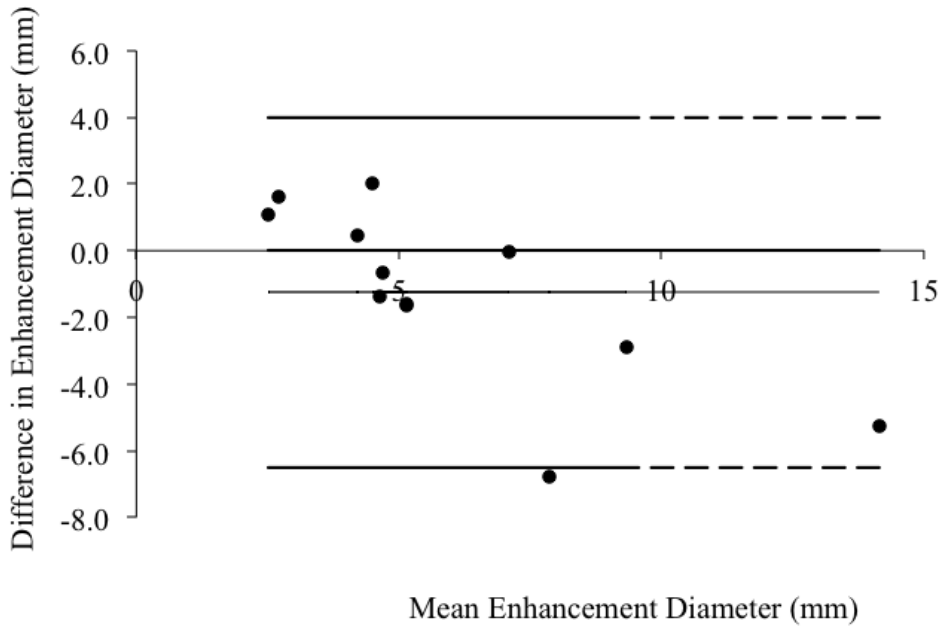

Figure 31. Bland-Altman Plots for inter-observer agreement for Late Gadolinium Enhancement Scoring.

Half-dashed line represents 95% level of agreement and solid line in-between represents the mean bias.

4.1.4.4. Control Group

The control group consisted of ten volunteers (6 male) with a mean age of 23yrs and 11 months. They were significantly older than the transplant patients (p=0.007 by independent samples t-test). However, they were of a similar age to the donor heart age (mean donor age 23yrs and 3months, p=0.88 by independent samples t-test). In general terms, the volunteers had very little coronary late enhancement. Four volunteers had no discernible late enhancement. The mean enhancement diameter was 0.27 mm ± 0.09mm. This was significantly lower than

the transplant recipients, who had a mean enhancement diameter of 5.38 ± 2.39 mm ($p<0.001$). Similarly, enhancement index of the volunteers (0.02 ± 0.03) was significantly lower than the transplant patients (0.53 ± 0.42) ($p=0.002$).

4.1.5. Discussion

In this study, we have demonstrated the possibility of direct non-invasive imaging for CAV. Late gadolinium enhancement scores appear to correlate well with traditional IVUS measures of MIT and MII (Pearson's coefficient respectively 0.81, $p=0.001$ and 0.62 $p=0.03$). The sensitivity and specificity of MRI to detect significant disease appears promising. An enhancement diameter > 7.5mm, gave sensitivity and specificity values of 100% for the detection of significant CAV.

There was very little late enhancement in the controls and although they were older than the transplant patients, the age was almost identical to the donor heart age for our patients. The non-invasive nature of MRI, would allow closer follow-up for CAV than has been previously possible, especially in children. Earlier detection may therefore result in better prevention.

There are several issues that need to be raised, however. The study is small and we must remain circumspect regarding its conclusions. Although the feasibility of LGE to directly image and grade CAV in children has been shown here, a larger study would confirm the utility of this technique.

Quantitative assessment was encouraging. If disease on MRI was defined as enhancement diameter > 7.5mm, sensitivity and specificity values of 100% are obtained for the detection of CAV as defined by IVUS & angiography. Similarly, an enhancement index of >1 again gives identical sensitivity and specificity values.

In addition to the quantitative assessment, the majority of cases also demonstrated good anatomical correlation between areas of enhancement on MRI and thickening on IVUS, (to within 1mm for location from a major branch-point). However, there were a significant number (6/17) of areas showing enhancement on MRI that were not markedly thickened on IVUS. This finding may be congruent with an earlier study into atherosclerosis,[135] which suggested that it is not the plaque itself that is imaged by Gadolinium deposition, but it is particular plaque compositions that result in a predilection to Gadolinium deposition. Previous studies note that arterial inflammation (both acute and chronic) and fibrosis enhance on late Gadolinium images.[170-172] One possible explanation for our anatomical correlate findings, therefore, is that only areas of CAV with a greater inflammatory or fibrous component will enhance on LGE imaging. Therefore, acute inflammation without the same degree of intimal thickening, may also be imaged on LGE. Conversely, some areas of intimal thickening (especially, for example, donor atherosclerosis), may not have the same degree of inflammation or fibrosis to give enhancement on LGE images. If this is the case, then there may be even greater potential prognostic significance of coronary enhancement on LGE MRI. If coronary inflammation can be imaged before intimal proliferation occurs, then the potential for tailoring preventative therapy (antiviral or immunosuppressive therapy)[173, 174] may be realised.

Currently, the inter-observer variability for measuring coronary LGE remains high and future work should concentrate on improvements in image quality, analysis and observer experience. It should be noted, however, that this is a new technique and that there will be a learning curve for acquisition, analysis and interpretation. Interestingly, (Figure 26) also shows enhancement in the area of one of the

pulmonary veins as it enters the left atrium. This was a relatively common finding. This may represent scarring near the pulmonary vein ostia in the left atrium from the transplantation suture line. Alternatively, it may represent labeling of the venous blood from the navigator, as has been previously described.[175] Despite this, overlaying the LGE and CMRA images, as shown in (Figure 26) can differentiate this enhancement from coronary vessel wall enhancement.

LGE has previously been shown to be useful for risk stratification in carotid vessel wall disease.[176] Gadolinium has also been shown to accumulate in the coronary vessel wall in the setting of damaged endothelium after myocardial infarction.[136] Recently, an elastin-specific magnetic resonance contrast agent has been identified.[177] Such specific magnetic resonance binding agents would be much more suitable for the purposes of imaging and grading CAV. However, it will take time before these contrast agents can be used clinically in children.

Finally, there are implications from this study for conventional atherosclerosis imaging. CAV is thought to be a largely autoimmune-mediated vasculopathy with a clear inflammatory component.[3] As such, the strong correlation in this study between disease severity, as demonstrated by IVUS, and LGE measures adds weight to the argument that late gadolinium enhancement may be able to identify atherosclerotic plaque with an inflammatory component.

4.1.6. Conclusion

This study has shown that imaging CAV with MRI is possible in paediatric transplant recipients. The late gadolinium enhancement scores correlate well with traditional IVUS measures. Non-invasive coronary imaging is highly desirable in

children, but the greatest potential of this technique may be in the identification of areas of inflammation and targeted therapy.

4.2. Diagnosis of Post-Transplant Coronary Artery Disease using Contrast-Enhanced Coronary Vessel Wall imaging at 3.0 Tesla.

4.2.1. Abstract

Coronary plaque characterisation at 3.0 Tesla holds great potential for clinical benefit. Coronary allograft vasculopathy (CAV) occurs after heart transplantation and is an immune-mediated diffuse coronary intimal disease. We demonstrate the use of contrast-enhanced inversion-recovery prepared coronary vessel wall MRI at 3T for diagnosis. We further validate the technique in 23 patients with intravascular ultrasound (IVUS), showing an accuracy of 91%. Direct non-invasive imaging has great potential benefit for screening and prevention in these patients. The study has further significant implications for conventional coronary atherosclerosis.

4.2.2. Introduction

Coronary Allograft Vasculopathy (CAV) remains the leading cause of late death after heart transplantation in children[6] but is poorly detected by X-ray angiography.[8] Intravascular ultrasound (IVUS) has been proven to be able to detect rapid early progression of CAV and this has proven prognostic significance.[25] However, it is invasive and costly. This precludes close follow-up, especially in children. We have previously demonstrated the feasibility of MRI late gadolinium enhancement (LGE) in the coronary vessel wall to detect and grade

CAV.[178] This previous study, performed at 1.5 Tesla field strength showed a promising correlation between IVUS measures and LGE scores. However, concerns remained regarding the anatomical correlation between location of enhancement on MRI and location of disease on IVUS.[178] One potential explanation for this is that the signal-to-noise (SNR) ratio at 1.5T is inadequate for accurate and reproducible image analysis. Since SNR is proportional to the static magnetic field (B0), imaging at 3 T should theoretically increase SNR. In this regard, feasibility studies for coronary atherosclerotic plaque and thrombus characterisation at 3.0 Tesla have already been demonstrated.[134, 137] Furthermore, there were previous concerns about image quality at 3.0 Tesla due to off-resonance artefact levels but recent advances in parallel transmission have reduced such artefacts.[144] Therefore it was hypothesized that the increase in SNR at 3.0 Tesla may improve image quality and make image analysis more reproducible.

The purpose of this study was to evaluate the clinical utility of LGE coronary vessel wall imaging for CAV and to see if it could be improved by imaging at 3.0 Tesla with parallel transmit technology.

4.2.3. Methods

4.2.3.1. Subjects

Patients older than 10 years undergoing annual review after orthotopic heart transplantation were invited to take part in the study. Written, informed consent was obtained from the patient and/or parent accordingly. This study has appropriate Institutional Review Board approval (Research Ethics Committee

reference number 09/H0713/53). Participants underwent cardiac MRI followed by their routine conventional X-ray angiography and IVUS, one day later.

4.2.3.2. MRI

Cardiac Magnetic Resonance was performed using a 3.0 Tesla Achieva clinical MR scanner with parallel transmit technology (Philips Healthcare, Best, NL gradient amplitude 30 mT/m and slew rate 200 mT/m/sec). Images were obtained using a 32-element cardiac phased-array receiver coil. Prior to entering the scan room, 0.2 mmol/kg body weight of a Gadolinium-based contrast medium (Gadovist, Bayer Schering, Berlin, Germany) was administered intravenously. Subsequently, an initial survey and reference scan were acquired to obtain coil sensitivity maps. An additional B1 calibration scan was performed between the survey and reference scans in order to calculate the patient-specific absorption rate and allow for B1 volume shimming by utilising parallel transmit technology. Following this, the cardiac rest period was ascertained using a high temporal resolution, balanced-SSFP, two-dimensional cine MR sequence in a four-chamber view orientation. (Imaging parameters included: repetition time = 2.4 ms, echo time = 1.2 ms, flip angle = 60° at 1.5T and 40° at 3T, slice thickness = 10mm, FOV = 300-350 mm, 80 cardiac phases, echo train length = 11 at 1.5T and 22 at 3.0T, temporal resolution = 10 to 16 ms/ frame). The mid-diastolic rest period, ascertained from the cine images, was used to define the acquisition window for the subsequent coronary lumen and vessel wall scans.

First, a rapid whole-heart cardiac magnetic resonance angiogram (CMRA) was performed as a roadmap for a subsequent 3-point plan-scan for a targeted double-oblique CMRA parallel to the native left coronary artery system.[145] Targeted CMRA

was performed with a previously described navigator-gated free-breathing and cardiac-triggered T2-prepared three-dimensional (3D) balanced steady-state free-precession (SSFP) sequence allowing visualisation of the anatomy of the coronary artery lumen.[146] A volume B1 shim was applied utilising the parallel transmit technology. Imaging parameters included the following: FOV = 320x320 mm, matrix = 320x320, acquired in-plane resolution = 1x1 mm (reconstructed 0.5x0.5 mm), reconstructed slice thickness = 1.5 mm (acquired thickness = 3 mm overcontiguous slices), acquisition window = 80 to 100 ms, repetition time (TR) /echo time (TE) = 5.2 ms/2.6 ms, flip angle = 70°; start-up cycles = 5, and number of slices = 20.

Finally, using an identical imaging plane and spatial resolution as the targeted CMRA, a coronary late gadolinium enhancement (LGE) sequence was performed. This was performed 30-40 minutes after the administration of gadolinium. This time delay is longer than that used for clinical myocardial late enhancement. This approach ensures that most of the contrast medium had been cleared renally and that most of the physiologic uptake of contrast medium in healthy tissues had been washed out. This allows for greater contrast between diseased and healthy tissues. This approach is less favourable for clinical myocardial imaging as residual blood-pool contrast agent enables distinction of the physiological blood-pool to myocardial boundary and makes image analysis for myocardial gadolinium uptake easier. In contrast, for coronary LGE, it is helpful to null signal from both myocardium and blood-pool. This delayed imaging approach has been previously used for the depiction of coronary atherosclerosis.[135] This sequence is a navigator-gated, vector ECG-triggered, fat-suppressed T1-weighted 3D gradient-echo inversion-recovery sequence.[135, 166, 167] Again, a volume B1 shim was applied

utilising the parallel RF transmit technology. Imaging parameters included the following: field of view = 320x320 mm, matrix = 320x320, acquired in-plane resolution = 1x1 mm, reconstructed slice thickness = 1.5 mm (acquired thickness = 3 mm), acquisition window = 80 to 100 ms, repetition time/echo time = 5.7 ms/1.7 ms, flip angle = 30°; start-up cycles = 5, and number of slices = 20. The patient-specific inversion time was adjusted to null blood signal with a preceding Look Locker sequence.[168] Typical inversion times were 180 to 240ms.

Data from the previous feasibility study at 1.5 Tesla was used for comparison of imaging and to calculate overall sensitivity and specificity of the technique.[178]

4.2.3.3. Conventional Angiography and IVUS

Cardiac catheterisation was performed under general anesthesia for children and adolescents, according to institutional protocol, but for older adolescents or young adults, performance under local anesthesia is encouraged. Catheterisation and IVUS were only performed as clinically indicated for annual review. CAV on angiography is defined as mild, moderate or severe according to published criteria.[7] A single experienced observer reported angiograms but a second experienced observer confirmed any abnormalities.

IVUS was performed in the left anterior descending coronary artery with automated pullback at 0.5mm/s. This imaging has a temporal resolution of 30 frames/second. A suitable length of vessel was imaged to allow analysis of at least 30 cross-sectional images evenly spaced (at approximately 1.5mm intervals) over the same segment of left anterior descending artery that was analysed at the previous annual review (identified by branch points). Additionally, the images analysed were always taken during the mid-diastolic rest period for consistency.

Maximal intimal thickness (MIT), mean intimal index, (MII) and Stanford Grading score were recorded.[10] Mean intimal index is defined as the ratio of the mean intimal area to the sum of the mean intimal and luminal areas. In addition, a semi-automatic interactive edge-detection software was used (QIVUS Clinical Edition, Medis medical imaging systems) to improve reproducibility of measurements.[27] Finally, the position of the most affected regions (regions with thickness greater than twice the mean intimal thickness for that patient) of the left main and anterior descending coronary artery were recorded, using distance from major side branches.

4.2.3.4. MR Image analysis

Magnetic resonance LGE images were scored as previously described. Briefly, LGE was defined as areas in the vessel wall with a signal intensity that is significantly (>2 standard deviations (SD)) higher than normal non-enhancing vessel wall. The ascending aorta (distal to anastomosis site) or the descending aorta was used as the reference for normal vessel wall. Using the coronary MRA as an overlay roadmap, the volume of coronary vessel wall enhancement was then measured. Using this volume and quantitative coronary lumen measurements, mean enhancement area (=volume/length imaged), enhancement diameter (ED) and mean enhancement index (Ei =enhancement area/coronary lumen mean cross sectional area) were derived and recorded. Location of areas of coronary wall LGE on MRI was also recorded for comparison.

Finally, a qualitative analysis was undertaken by means of a consensus reading for image quality scoring on all the LGE images in a blinded and random order by two readers (T.H. and G.F.G. (>3 years and >10 years respectively of CMRA

experience)). The two readers first reviewed the images independently and any disagreement was then discussed before the final grade was given. The following scoring system was used: 0 indicates that the coronary vessel wall was not visible; 1 visible but with markedly blurred borders; 2 visible with moderately blurred borders; 3 visible with mildly blurred borders and 4 visible with sharply defined borders.[111]

4.2.3.5. Statistical Methods

First an anatomical comparison was made between the location of areas of enhancement on MRI and the location of prominent thickening on IVUS using distance (mm) from the nearest major side-branch. Variables are then formally assessed for normality of distribution using the Kolmogorov-Smirnov test. Then specific bivariate correlation was performed between enhancement index (MRI) and intimal index (IVUS). Further bivariate correlation was made between enhancement diameter and maximal intimal thickness.

A receiver-operating characteristic (ROC) curve is constructed to choose the optimal cut-off for the sensitivity and specificity of LGE for the detection of significant CAV. Significant CAV is defined as that present on X-ray angiogram or scored as Stanford grade IV on IVUS.

Associations with known risk factors were further explored by forward stepwise multivariate linear regression. Donor age, cytomegalovirus (CMV) infection, time post-transplant, occurrence of severe or recurrent rejection and blood pressure are the risk factors that were assessed.[6, 173, 179] Included variables were only kept in the analysis if they improved model fit.

Image Quality was compared between 1.5 and 3T using a Mann-Whitney test. Statistical analyses were performed on SPSS version 19 (Release 19.0.0, IBM Software Group, New York, USA).

4.2.4. Results

24 adolescents participated in the study in total (patient characteristics (Table 13)). This included 12 at 1.5T and 12 at 3.0T. One MRI at 3.0T failed due to patient discomfort. Overall, there was excellent correlation of MRI with IVUS. Pearson's correlation for ED with MIT was 0.80 ($p<0.001$) and for Ei with MII was 0.92 ($p<0.001$). Correlation coefficients at 3T were comparable to 1.5T (0.77 & 0.96 versus 0.81 & 0.62 respectively (all $p<0.05$)).

Table 13. Descriptive Summary of Heart Transplant Patient Characteristics. Variables are reported separately for 3.0T and 1.5T

	1.5 TESLA	3.0 TESLA
Number of Patients	12	11
Male (n=)	5	5
Age (years)	15.1 ± 2.2 years	15.8 ± 1.7 years
Weight (kg)	58.9 ± 20.9	57.7 ± 10.9
Height (cm)	162 ± 9	164 ± 11
HR (bpm)	81 ± 8	88 ± 8
MIT (mm)	0.50 ± 0.29	0.98 ± 0.56
MII (%)	17.5 ± 5.7	24.7 ± 13.5
ED (mm)	5.38 ± 2.39	7.86 ± 6.57
Ei	0.53 ± 0.42	1.72 ± 2.35
Stanford Grade 4 disease (n=)	2	5
Previous CMV infection (n=)	2	1
Hypertension (n=)	10	7
Donor Age (years)	23.3 ± 11.9	25.1 ± 16.1

At 1.5T, although intra-observer agreement was acceptable with 95% limits of agreement ranging from +2.8 to -2.6, inter-observer agreement was less acceptable at +4.0 to −6.5 mm. However, this was improved at 3.0T, with 95% limits of agreement for intra-observer agreement ranging from +1.7 to -2.3 and for inter-observer from +3.5 to −2.5 mm. This improvement in repeatability was likely due to an increase in LGE image quality at 3.0T (median=3) compared to 1.5T (median=2; p=0.019 by Mann-Whitney test). Furthermore, at 1.5T only 11 out of 17 areas of enhancement on MRI were associated with corresponding significant disease on IVUS (i.e. location match to within 1mm from a major branch-point). At 3T, however, 11 of 13 enhancing lesions had exact and anatomical match (Figure 32).

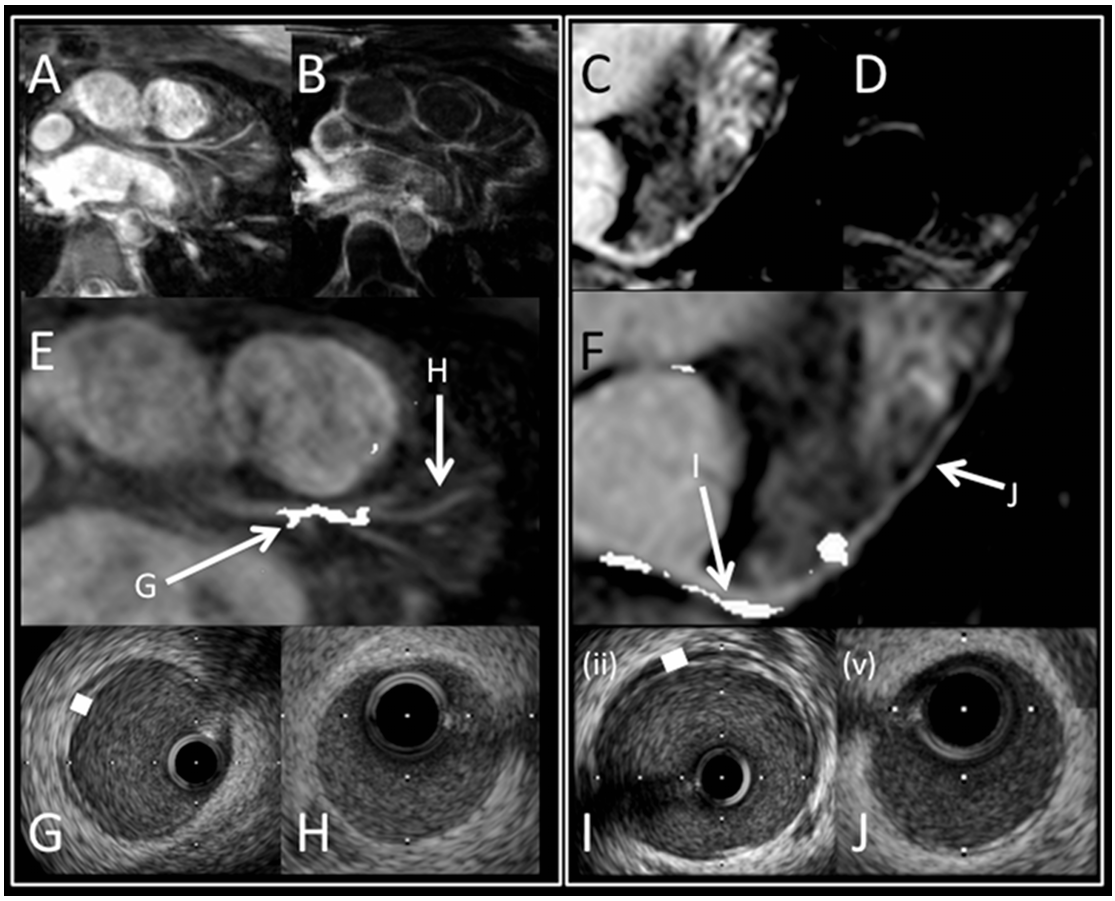

Figure 32. 3.0 vs. 1.5 Tesla imaging for CAV.

A) Patient 1 Left Coronary system CMRA at 3T.

B) Patient 1 LGE at 3T.

C) Patient 2 Left coronary CMRA at 1.5T.

D) Patient 2 LGE at 1.5T

E) Overlay of Patient 1 LGE on CMRA at 3T. Arrows show corresponding positions for IVUS pictures G & H.

F) Overlay of Patient 2 LGE on CMRA at 1.5T. Arrows show corresponding positions for IVUS pictures I & J.

G & I) IVUS images. White box illustrates intimal thickening corresponding to enhancement on overlay picture above

J & H) IVUS images. No significant intimal thickening corresponding to areas without enhancement on overlay picture above

Overall, the receiver operating characteristics curve demonstrates that a cut-off of 7.5 mm ED on MRI has 86% sensitivity and 94% specificity for the detection of significant (Stanford grade 4 on IVUS) CAV. This gives a positive predictive value of 86%, negative predictive value of 94% and accuracy of 91%.

In the multivariate analysis, donor age, length of time post transplant and MRI (ED) were the only significant independent predictors of maximum intimal thickness on IVUS (model R^2= 0.79; $p<0.001$). Standardised correlation coefficients were 0.69 for ED ($p<0.001$); 0.65 for donor age ($p=0.002$) and 0.42 for time post-transplant ($p=0.048$). There were no significant correlations between ED and donor age or between ED and time post-transplant.

4.2.5. Discussion

We have demonstrated that coronary vessel wall late gadolinium enhancement has 91% accuracy in the detection of significant coronary allograft vasculopathy as defined by intravascular ultrasound. We have further demonstrated improved coronary vessel wall LGE image quality at 3.0 Tesla. This is likely to be responsible for the improved anatomical correlation with IVUS at 3.0 Tesla in comparison to 1.5 Tesla imaging.

Due to time constraints, we did not perform LGE imaging at 3.0 Tesla without the use of parallel transmit technology for comparison and so it is difficult to infer specific benefits from its use. It is known that, at higher field strengths, there is difficulty in achieving uniform radiofrequency (RF) excitation over the entire field of view (FOV). This results in a reduction of image quality (e.g. B1 attenuation artefacts). Parallel radiofrequency transmission can be used to improve the radiofrequency (B1 field) homogeneity in high-field MRI.[142] More accurate knowledge of the local B1 field also allows for improved management of the local specific absorption rate (SAR), thereby enabling shorter repetition times (TR) to be employed.[143] This may be responsible for the overall improvement in image quality by reducing artefact levels, as demonstrated recently in a small study comparing cine images with and without the use of parallel transmission.[144]

In this study, we demonstrate a non-invasive but direct means by which to image CAV. In order to do this reliably, we have made use of recently applied technology including parallel radiofrequency transmission at 3.0 Tesla. Non-invasive follow-up with MRI would allow more frequent screening for CAV; would limit the number of invasive procedures; would reduce exposure to ionising radiation; may allow earlier detection and allow earlier therapeutic intervention. Future study

should focus on the prognostic significance of LGE in the setting of CAV and on the implementation of MRI into a clinical trial to prevent CAV.

4.2.6. Conclusion

Coronary vessel wall delayed enhancement MRI is a valuable and accurate non-invasive method to quantify CAV. Improved image quality at 3.0 Tesla further ameliorates the accuracy of this technique.

4.3. Contrast-Enhanced Inversion Prepared Coronary Vessel Wall Imaging for Kawasaki Disease

4.3.1. Introduction

Aside from CAV, Kawasaki Disease is the other main coronary vasculopathy encountered in childhood. Hence, the technique of contrast-enhanced vessel wall imaging described for CAV may have important implications for Kawasaki Disease. Indeed, 2d cross-sectional Dual-Inversion-Recovery (DIR) black-blood imaging of the coronary arteries has been previously used to assess Kawasaki Disease (KD).[180] Hence, in this thesis the utility of a 3d coronary black-blood approach is examined. This 3d black-blood approach has been shown to give better coverage of the coronary tree.[97] Furthermore, uptake of gadolinium contrast agent has been shown to indicate inflammation (both acute and chronic) or fibrosis in other pathological processes. [170-172] Therefore, we also sought to investigate coronary vessel wall uptake of gadolinium after Kawasaki Disease to see if any inference can be drawn regarding the pathological processes involved.

4.3.2. Aim

To investigate whether in-plane 3d coronary vessel wall imaging utilising a local-inversion technique and spiral image acquisition, in combination with contrast-enhanced inversion-recovery (IR) imaging allows more comprehensive assessment of KD.

4.3.3. Method

Patients with previous coronary aneurysms due to KD undergoing routine CMR evaluation had additional vessel wall imaging before and after contrast administration (0.2 mmol/kg gadopentetate dimeglumine). All examinations were performed on a 1.5T MR-system and the coil was selected according to patient size (two-element/five-element). Coronary MRA was followed by a targeted, free-breathing, ECG-triggered 3d vessel wall sequence using local inversion and spiral image acquisition (spatial resolution=0.76x0.76x2mm; TE/TR=2/29ms, FA=90°). Areas of vessel wall thickening on in-plane imaging were then further evaluated with through-plane 2d DIR technique.

Post-contrast imaging was performed using a free-breathing, ECG-triggered, 3d-IR segmented gradient-echo sequence (spatial resolution=1.25x1.25x3mm, TE/TR=1.4/3.5ms, FA=30° & TI chosen to null blood using Look-Locker).

4.3.4. Results

13 CMR examinations were performed in 12 children (7 male, age=2-19yrs; HR=60-110bpm; 6 weeks-18 years post-acute KD). 6 cases showed persistent aneurysms; 4 cases had coronary ectasia and the remaining resolved aneurysms had a normal lumen. One case showed a mild LAD stenosis shown on CMRA and

confirmed on conventional angiography. Complete black blood coverage of the affected portions of the coronary arteries was achieved using the new 3d in-plane local-inversion technique. Targeted 2d cross-sectional imaging showed that aneurismal segments had greater wall thickness (mean 0.87mm) than ectatic segments (0.42mm) or resolved aneurysms (0.31mm). Delayed enhancement of the coronary vessel wall was only present in three cases (all of whom had recent KD <2yrs ago).

4.3.5. Conclusion

Our data suggests that late gadolinium enhancement of the coronary vessel wall in Kawasaki Disease may persist for up to 2 years post-acute insult. This may represent inflammation and subsequent resolution. This type of imaging may therefore be helpful for confirmatory evidence of disease in atypical cases or for follow-up purposes to show resolution of pathology.

We have further shown that vessel wall remodeling seems to have occurred effectively in the resolved aneurysms studied here. 3d in-plane local-inversion black-blood imaging gives more complete coverage of affected segments and allows targeting of cross-sectional imaging on thickened portions. This type of vessel wall imaging has the potential to allow pathophysiological insights into disease or to be an imaging biomarker for future therapeutic trials.

Chapter 5: Aortic Imaging and Correlates with Cardiovascular Disease

5. Aortic Imaging and Correlates with Cardiovascular Disease

5.1. Aortic Pulse Wave Velocity as a marker for coronary allograft vasculopathy

5.1.1. Abstract

Background: Pulse wave velocity (PWV), a marker for intrinsic stiffness of the aortic wall, has been shown to be highly predictive for cardiovascular events in the setting of atherosclerosis. The purpose of this study is to investigate whether central arterial stiffness in children relates to the degree of coronary intimal disease after heart transplantation.

Method: 10 children (5 male) underwent cardiac magnetic resonance (CMR) followed by X-ray angiography and intravascular ultrasound (IVUS). Published normal values were taken for age-matched controls. PWV was measured using a VCG-gated gradient-echo pulse sequence with velocity encoding (temporal resolution 5 to 7ms). Magnitude images were used to give an image-based assessment of central aortic stiffness (β index). Total peripheral vascular resistance (TPR) was calculated, using ascending aorta flux as cardiac output.

IVUS was performed in the left anterior descending coronary artery. Maximal and mean intimal thicknesses were recorded as measures of CAV burden.

Results: PWV in transplant patients was significantly higher than normal volunteers (4.5 vs. 3.3 m/s; p=0.002). β index was not raised significantly (3.2 vs. 2.5 in normal volunteers; p=0.17) and neither was TPR (1245 vs. 1144 dyn.sec.cm^{-5} in normal volunteers; p=0.08).

PWV was significantly positively correlated with CAV burden as measured by maximal intimal thickness (Pearson's Coefficient = 0.66; p=0.036) and by mean intimal thickness (Pearson's Coefficient = 0.71; p=0.02). β index was also positively correlated with these indices of CAV burden (Coefficient = 0.74 and 0.78; p=0.014 and 0.008 respectively). TPR does not, however, correlate with these measures of CAV (Coefficients = -0.015 and -0.001; p>0.9).

BP parameters; age; time post-transplant; and PWV were added into the multivariate linear regression model for mean intimal thickness prediction. Only PWV remained in the model after forward stepwise exclusions. PWV was the only independent predictor of CAV burden (model R^2=0.51; p=0.02).

Conclusions: In this study we demonstrate that central arterial stiffness, measured by pulse wave velocity correlates with coronary allograft vasculopathy independently of closely related parameters such as blood pressure. PWV may be a potential surrogate marker for adverse vascular modeling after heart transplantation.

5.1.2. Introduction

Pulse wave velocity (PWV) is a marker for the intrinsic stiffness of the aortic wall, which has been shown to be highly predictive for cardiovascular events in the setting of atherosclerosis.[69-74] The precise relationship between PWV and CV disease is unknown but one explanation is that PWV is a marker of advanced plaque burden.[75] Furthermore, increased aortic stiffness signifies adverse myocardial haemodynamic conditions including an increase in systolic blood pressure and pulse pressure with increased systolic load and decreased myocardial perfusion pressure.[76-78] Coronary Allograft Vasculopathy (CAV) is the

leading cause of late death or graft loss after heart transplantation in children [6]. A small study performed in children above 5 years of age showed a significant correlation between length of time since transplantation and PWV. However, this study fell short of correlating PWV with direct measurements of CAV. The relative ease of measurement would make it an attractive adjunct to the clinic if its utility can be shown in the setting of CAV. It would be particularly beneficial in children for whom quick non-invasive markers are more acceptable.

The purpose of this study is to see if central arterial stiffness in children is related to the degree of coronary intimal disease after heart transplantation. Cardiac Magnetic Resonance (CMR) is used in this exploratory study as it affords the ability to image aortic vessel changes through the cardiac cycle, measure PWV, and calculate cardiac output within a single imaging modality.

5.1.3. Method

5.1.3.1. Subjects

Children over 10 years of age attending for routine annual review for heart transplantation were invited to participate in this study. Ten children (5 male) participated in the study. Institutional Review Board approval was obtained prior to commencing the study (Research Ethics Committee reference number 09/H0713/53). Written, informed consent was obtained from the patient and/or parent accordingly. Participants underwent cardiac MRI followed by their routine conventional X-ray angiography and IVUS, one day later. Normal values for arterial stiffness were taken from published literature for age-matched controls.[181, 182]

5.1.3.2. Blood Pressure Recordings

In clinic, routine blood pressure recordings are taken with the child seated and for five minutes before conventional BP measurement. Measurements are taken in the right arm with an appropriate-sized cuff. The mean of 3 sphygmomanometer readings is taken as the conventional (clinical) BP measurement. Hypertension is classified as recordings on three separate occasions being higher than the 95th centile for height and age.[183-185] Prior to commencement of therapy, hypertension is further classified and confirmed according to 24-hour ambulatory blood pressure measurements. Classification of hypertension and antihypertensive medications were recorded from the clinical records. Finally, a blood pressure is also taken at the time of the MRI using an automated cuff (Datex Ohmeda oscillometric blood pressure device, GE Healthcare, WI, USA) with an appropriately sized cuff. This blood pressure is used for reference of indices of arterial stiffness.

5.1.3.3. MRI & Arterial Stiffness Indices

Cardiac Magnetic Resonance was performed using a 1.5 Tesla Achieva clinical MR scanner (Philips Healthcare, Best, NL). Images were obtained using a 32-element cardiac phased-array receiver coil. Pulse-wave velocity is recorded according to a previously validated method.[186] In this study, PWV was measured between the ascending aorta and the descending aorta at the level of the diaphragm. A retrospectively VCG-gated gradient-echo pulse sequence with velocity encoding was applied at these levels to measure through-plane flow. This sequence was performed free-breathing and imaging parameters included: Echo Time 2.9ms,

Repetition Time 5 ms, Slice Thickness 8 mm; Acquired resolution 2.2x2.2 mm; 2 to 3 signal averages; 125 cardiac phases and temporal resolution 5.1 to 6.9 ms.

PWV was subsequently calculated as $\Delta x/\Delta t$ (expressed in m/s), where Δx is the aortic path length between 2 imaging levels and Δt is the time delay between the arrival of the foot of the pulse wave at these levels. Flow analysis was performed using commercially available analysis software (View Forum; Philips Healthcare, Best, The Netherlands). Arrival of the foot of the pulse wave was calculated using the method of intersecting tangents. Matlab Release 2009b (version 7.9) is used to identify the inflection point (using change of sign of the second derivative) to centre the first tangent. The intersection this tangent and the second line drawn horizontal to the minimum diastolic flow, identified the foot of the wave (Figure 33).

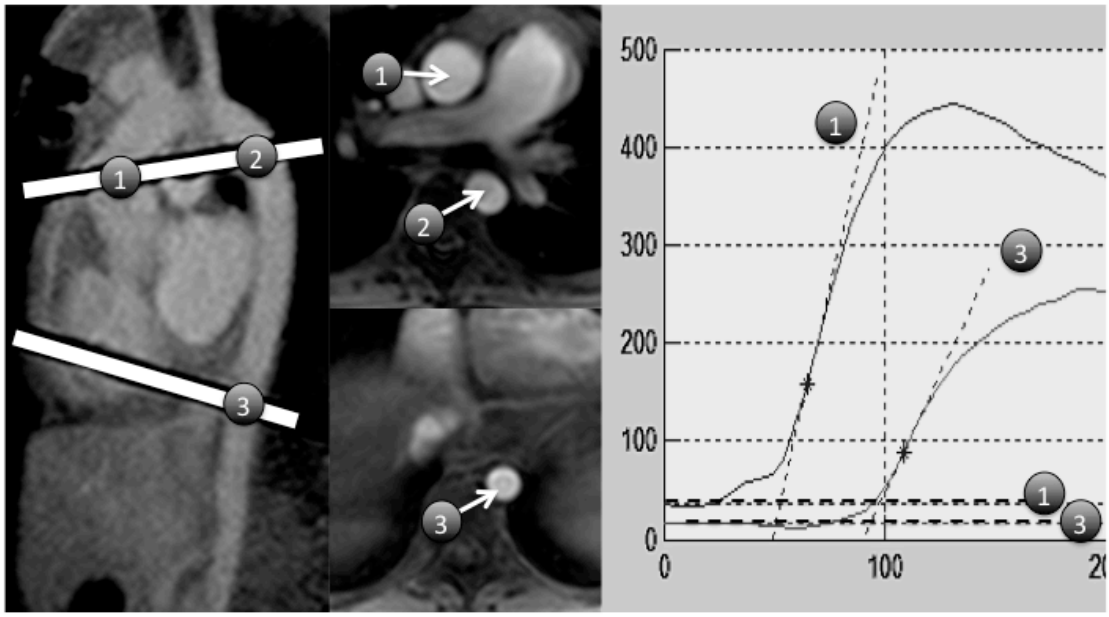

Figure 33. Pulse Wave Velocity Calculation

a) Shows sagittal view of the ascending aorta, aortic arch and descending aorta. Δx is calculated using a centre-line plot from point (1) to point (3). White lines represent location of cross-sectional axial views b) and c) for flow measurements. Position (1) in the ascending aorta; position (2) in the

proximal descending aorta and position (3) in the descending aorta at the level of the diaphragm. Position (2) is taken for image-based assessment of diastolic and systolic diameters. d) shows offline analysis of flow to calculate Δt, the time delay between the pulse wave arrival at different levels ("foot" method). Arrival of the foot of the pulse wave was calculated using the method of intersecting tangents. Matlab Release 2009b (version 7.9) is used to identify the inflection point (using change of sign of the second derivative) to centre the first tangent. The intersection this tangent and the second line drawn horizontal to the minimum diastolic flow, identified the foot of the wave. Tangents for positions (1) and (3) are labeled. Pulse wave velocity = Δx/Δt.

Magnitude images of the velocity-encoded cine of the proximal descending aorta were used to give image-based traditional assessment of central aortic stiffness. Diameter changes were quantified using a semi-automatic tool (View Forum; Philips Healthcare, Best, The Netherlands) taking values to the nearest mm^2. Maximum and minimum diameters were taken as an average of three readings and all values were confirmed manually. The Aortic stiffness β index was given as:

$$\beta = \ln (SBP/DBP) / [(As-Ad)/Ad]$$

Where ln = natural logarithm; SBP = systolic blood pressure (mmHg); DBP = diastolic blood pressure (mmHg); As = maximum systolic aortic area (mm^2) and

Ad = minimum diastolic area (mm^2).[182]

Finally, total peripheral vascular resistance (TPR) was calculated, using net flux in the ascending aorta as the cardiac output, as:

$$TPR = (MBP/CO) \times 80$$

Where TPR is measured in $dyn.sec.cm^{-5}$; MBP = mean blood pressure (mmHg); CO is cardiac output (l/min).[181]

5.1.3.4. Intravascular Ultrasound

Intravascular Ultrasound (IVUS) was undertaken on the day following the MRI scan. Catheterisation is performed under general anaesthesia for children and adolescents, according to institutional protocol, but for older adolescents or young adults, performance under local anaesthesia is encouraged. Catheterisation and IVUS were only performed as clinically indicated for annual review. IVUS was performed in the left anterior descending coronary artery with automated pullback at 0.5mm/s. Typically, the imaging has a temporal resolution of 30 frames/second. A suitable length of vessel was imaged to allow analysis of at least 30 evenly spaced cross-sectional images (at approximately 1.5mm intervals). Maximal and mean intimal thicknesses were recorded as measures of CAV burden.[23, 25] In addition, a semi-automatic interactive edge-detection software was used (QIVUS Clinical Edition, Medis medical imaging systems, Leiden, Netherlands) to improve reproducibility of measurements.[27]

5.1.3.5. Data analysis

First, measures of central arterial stiffness and TPR were tested using single sample t-test against known normal mean values for adolescents (β index of 2.5; PWV of 3.3 m/s and TPR of 1144 dyn.sec.cm^{-5}).[181, 182] Then, bivariate correlation between indices of coronary intimal disease on IVUS and measures of central arterial stiffness or TPR was performed.

PWV associations were further explored by multivariate linear regressions and forward stepwise addition of blood pressure indices, age and time since transplant. These variables were chosen due to the known interdependence of stiffness, blood pressure and age. Furthermore, a previous study in children after

heart transplantation identified time since transplantation as a predictor of PWV.[187] Only these important variables were included, as the study size would not allow more variables. Furthermore, included variables were only kept in the analysis if they improved model fit.

Statistical analysis was performed on SPSS version 19 (Release 19.0.0, IBM Software Group, New York, USA). Results are quoted as mean ± standard deviation and a p value of <0.05 was considered significant.

5.1.4. Results

5.1.4.1. Subjects

Ten children (5 male) participated in this study. Mean age was 16 ± 2 years (range 12 to 17 years) and mean time since transplant was 4 ± 4 years (range 0.3 to 13 years). Mean intimal thickness was 0.22 ± 0.12 mm and maximum intimal thickness was 0.66 ± 0.42 mm.

Seven children were diagnosed as hypertensive and were on treatment. Of these, four were diagnosed with isolated systolic hypertension. All seven children were on calcium channel antagonists and two were additionally taking angiotensin converting enzyme inhibitors for blood pressure control. During MRI, diastolic blood pressures were normal (i.e. below 95th centile for age and height; mean 72 ± 10 mmHg; range 50 to 82 mmHg) whereas three systolic blood pressures were raised (mean 123 ± 11 mmHg; range 101 to 137 mmHg). A descriptive summary of variables is given in (Table 14).

	Minimum	Maximum	Mean	Standard Deviation
Age (years)	12.50	17.63	16.05	1.56
Weight (kg)	33.30	102.00	61.95	22.43
Height (cm)	140.70	176.00	163.42	9.97
Time Post-transplant (years)	0.27	12.94	4.24	4.48
Mean Intimal Thickness (mm)	0.08	0.47	0.22	0.12
Max Intimal Thickness (mm)	0.29	1.50	0.66	0.42
Systolic Blood Pressure (mmHg)	101.00	137.00	122.60	10.91
Mean Blood Pressure (mmHg)	70.00	100.00	89.00	9.79
Diastolic Blood Pressure (mmHg)	50.00	82.00	72.00	9.90
Cardiac Output (l/min)	4.99	7.38	5.85	0.73
Heart Rate (bpm)	70.00	95.00	82.20	7.89
PWV	3.20	6.63	4.49	0.86
β index	1.41	5.82	3.18	1.45
TPR (dyn.sec.cm^{-5})	1039.76	1435.44	1244.54	147.55

Table 14. Descriptive summary of variables for pulse wave velocity study

5.1.4.2. Comparisons

Pulse wave velocity was significantly higher when compared to previously published reference population of similar age (4.5 vs. 3.3 m/s; p=0.002). Beta index was not raised significantly (3.2 vs. 2.5 in normal volunteers; p=0.17) and neither was TPR significantly raised (1245 vs. 1144 dyn.sec.cm^{-5} in normal volunteers; p=0.08)

Bivariate Correlation: PWV was significantly positively correlated with CAV burden as measured by maximal intimal thickness (Pearson's Coefficient = 0.66; p=0.036) and by mean intimal thickness (Pearson's Coefficient = 0.71; p=0.02). Arterial stiffness β index also has significant positive correlations with these indices of CAV burden (Coefficient = 0.74 and 0.78; p=0.014 and 0.008

respectively). TPR does not, however, correlate with these measures of CAV (Coefficients = -0.015 and -0.001; p=0.97 and 0.98 respectively).

5.1.4.3. Multivariate regression

As explained above, blood pressure parameters at the time of imaging, age, time post-transplant and PWV were added into the linear model for mean intimal thickness prediction in a forward stepwise manner. Only PWV remained in the model after exclusions of variables not improving model fit. PWV was the only independent predictor of CAV burden (R^2=0.51; p=0.02). The result is not changed if previous clinic blood pressures are used for the model (prior to initiation of antihypertensives).

5.1.5. Discussion

We have demonstrated in this study that central arterial stiffness is increased in patients after heart transplantation. Furthermore, PWV correlates with CAV in the multivariate analysis independently of closely related variables such as age, time post-transplant and blood pressure. TPR is a measure of arteriolar constriction or disease and does not have a direct relationship with central aortic stiffness.[188] Congruent with this fact, we did not demonstrate a significant increase in TPR in these patients, nor did we find a relationship between TPR and CAV. The implications and insights from these findings deserve attention.

Arterial stiffness, as measured by PWV, is a well-documented predictor of cardiovascular events in the setting of conventional atherosclerosis.[69-74] The use of PWV as a predictor for coronary allograft vasculopathy has been suggested but not well investigated.[189] Our study demonstrates PWV does have a moderate

correlation with extent of CAV. However, we cannot extrapolate whether central arterial stiffness is a cause or effect of CAV.

We know that, in adults, hypertension has been significantly associated with angiographic onset of CAV.[179] Furthermore, Calcium channel antagonists have been shown to prevent CAV.[190] If taken in combination with our findings regarding central arterial stiffness, we may be lead to believe that stiffness is a modifiable risk factor in the pathogenesis of CAV.

However, we should also note that certain insults such as cytomegalovirus infection result in coronary endothelial insult[191] and, in children, could cause chronic systemic inflammatory endothelial insult.[192] It may be that increased arterial stiffness results from these types of systemic inflammatory insults that are also related to CAV. In support of this, systemic inflammation in the general population is associated with increased arterial stiffness.[193] Furthermore, our results may not be due to any direct relationship between CAV and arterial but rather because another risk factor such as rejection or CMV influences both PWV and CAV. A wider study may help answer such questions.

Isolated systolic hypertension is usually found in elderly patients and is the typical pattern of blood pressure increase seen with increased arterial stiffness.[194, 195] In our study, 4 out of 7 of the patients with hypertension did in fact show isolated systolic hypertension. In comparison, a previous study in children showed that diastolic blood pressure increase after heart transplantation was more common in children whereas isolated systolic hypertension was relatively uncommon.[79] However, the cohort described in our study is older (median 16.5 years vs. 6.3 years in previous study) and this may explain the difference. Indeed older recipient age has been previously found to be the major recipient risk factor for

the development of CAV in children.[6] If isolated systolic hypertension is indeed more common in older recipients, this may be one factor related to the earlier development of CAV. There is some support for that theory from another PWV study in children, by *Klinge et al*, which showed that children after heart transplantation had increased arterial stiffness which was associated with both age and length of time since transplant.[187]

Another important point to note from the multivariate analysis was that PWV had an independent and even more important relationship to CAV than blood pressure. Indeed, a recent study in healthy volunteers showed that increased PWV in volunteers could predict an increase in blood pressure over time and the onset of future hypertension.[196] Hence, another potential future study would be to trial the treatment of raised arterial stiffness to prevent the onset of both hypertension and CAV.

However, in this study, TPR was not significantly raised in children after heart transplantation compared to previously published reference population. Raised TPR is often found in young adult hypertensives causing upstream increase in transmural pressure resulting in stretching and stiffening of large central arteries and typically presents with elevated diastolic BP.[194] This type of hypertension may better explain the rise in arterial stiffness and diastolic blood pressure seen in the younger heart transplant recipients described by *Klinge et al*.[187]

Our study was an exploratory study to investigate the relationship between arterial stiffness and CAV. The use of MRI in this regard is invaluable offering rapid assessment of numerous physiological variables. PWV is now regarded as the gold-standard measure of arterial stiffness.[197] In the clinic setting, it can be rapidly acquired in a non-invasive & child-friendly manner using carotid-femoral

tonometry. Given the ease of acquisition, this study clearly demonstrates the need for further investigation of the utility of PWV in heart-transplant medicine.

We took care in the acquisition and analysis of this data. This was the reason behind adding a traditional independent image-based method to assess arterial stiffness, the β index. Analyses using this variable may lend support to our findings further because the β index was higher in our study patients compared to normal volunteers (although not significantly perhaps due to study size) and because the β index also showed significant positive correlation with CAV disease burden on IVUS. Further care was taken to limit the multivariate analysis to specific important variables in a stepwise approach. Nevertheless, this study remains an exploratory one demonstrating only moderate correlation. Further study is warranted to confirm this observation. In addition, it is difficult to draw conclusions from our study regarding resistance at the arteriolar level due to concomitant use of vasodilators.

Potentially, PWV is not only a biomarker but also a means by which to better understand the contribution of hypertension to CAV. The methodology described here helps us to non-invasively classify hypertension and arterial stiffness using MRI. This will not only help to tailor therapy but will give us a better understanding of the pathophysiology of endothelial damage in CAV.

Conclusion: In this study we observe that central arterial stiffness, measured by pulse wave velocity, correlates with coronary allograft vasculopathy independently of age, blood pressure or length of time since transplant. We believe that central PWV may have potential as an early biomarker or as a modifiable risk factor in the setting of coronary allograft vasculopathy.

5.2. Zoom Imaging for Rapid Aortic Vessel Wall Imaging and Cardiovascular Risk Assessment

In sub-chapter 5.1, we discussed the potential value of measuring central arterial stiffness as a marker for CAV. For future study of central arterial stiffness, it is important to investigate the mechanism of the increase in this stiffness that occurs in these patients. In order to this this, rapid anatomical aortic vessel wall imaging is required to assess vessel wall thickness and plaque formation is desirable. In this sub-chapter, we consider the use of 'zoom imaging' to accelerate anatomical black-blood imaging of the aorta. The further potential implication for this sequence in the wider setting of atherosclerosis is discussed in detail.

5.2.1. ABSTRACT

Purpose: To demonstrate the utility of a 'reduced field-of-view' (zoom imaging) technique to accelerate free-breathing, ECG-triggered, turbo-spin-echo black-blood sequences, which have been previously described to detect subclinical aortic atherosclerosis. *Materials and Methods:* Fifteen healthy volunteers underwent MRI of the thoracic and abdominal aorta. Imaging with the conventional full field-of-view sequence was compared to zoom imaging. Total scan time, image quality (i.e. contrast-to-noise ratio and vessel wall sharpness) and vessel wall thickness were analysed. A subgroup of ten volunteers also underwent acceleration of imaging using sensitivity encoding (SENSE) for comparison. *Results:* Zoom imaging significantly reduced imaging time from a mean of 41±9 minutes (conventional imaging) to 15±0.5 minutes ($p<0.01$). There was no difference in image quality between conventional and zoom imaging with respect to CNR (10.1±6 vs. 10.1±6)

or vessel wall sharpness (38±4% vs. 39±4%). Furthermore, Bland Altman plots showed excellent agreement in vessel wall thickness measurements using the two methods. In comparison, SENSE not only reduced CNR but also resulted in underestimation of vessel wall thickness compared to the conventional sequence. *Conclusion:* Zoom imaging allows accurate and time-efficient imaging of the abdominal and thoracic aorta for cardiovascular risk prediction. In this application, it is preferable to SENSE.

5.2.2. INTRODUCTION

Atherosclerosis remains the leading cause of mortality and morbidity in developed countries.[127, 128] Appropriate therapy in asymptomatic individuals has the potential to reduce risk at the population level but there remains significant concerns about the applicability of currently available risk scores to guide such therapy.[198] A more acceptable approach would be to identify individuals with an appreciable atherosclerotic burden at an asymptomatic stage and to target them for treatment. Thoracic aortic plaque burden correlates closely with the coronary arterial plaque burden.[199] The extent of thoracic atherosclerosis may be a stronger predictor of coronary artery disease than conventional risk factors [200] and may be a stronger predictor than even carotid or femoral artery plaque burden as detected by ultrasound.[201] For this reason, a free-breathing ECG triggered, turbo-spin-echo (TSE) black-blood sequence has been described to detect subclinical aortic atherosclerosis and the value of this sequence to stratify cardiovascular risk has been demonstrated in more than 2000 participants recruited from the Framingham population.[202-204] Routine use of this sequence for aortic plaque screening is challenging due to the relatively long imaging time.

Oyama et al described this aortic wall cardiovascular magnetic resonance (CMR) imaging sequence encompassing the aorta from the arch to the aortoiliac bifurcation using 5mm slices imaged in the transverse plane. Total aortic imaging time is stated as less than twenty minutes.[204] In order to achieve this, however, 24 slices were obtained with a slice gap of 10mm. It is acknowledged that denser sampling of the aorta was not possible due to time constraints.

Previous studies have demonstrated how zoom imaging can be used for rapid small field of view (FOV) imaging during percutaneous interventions.[205] Zoom imaging is implemented for TSE techniques by having the slice-selection and refocusing gradients perpendicular to each other. By doing this, refocusing of spins only occurs in the section that is crossed by both gradients and so, a narrow field of view can be imaged without wraparound artefacts. Hence, imaging time is substantially reduced (Figure 34). This study seeks to demonstrate the use of the 'reduced FOV' or more recently renamed 'zoom imaging', technique for accelerating aortic vessel wall imaging. This would allow denser sampling of the aorta with a reduced imaging time. In this study, we sought to investigate how the use of zoom imaging compares with the standard non-accelerated black blood TSE technique with respect to image quality and image analysis and how it compares with rapid black blood imaging with SENSE reconstruction.

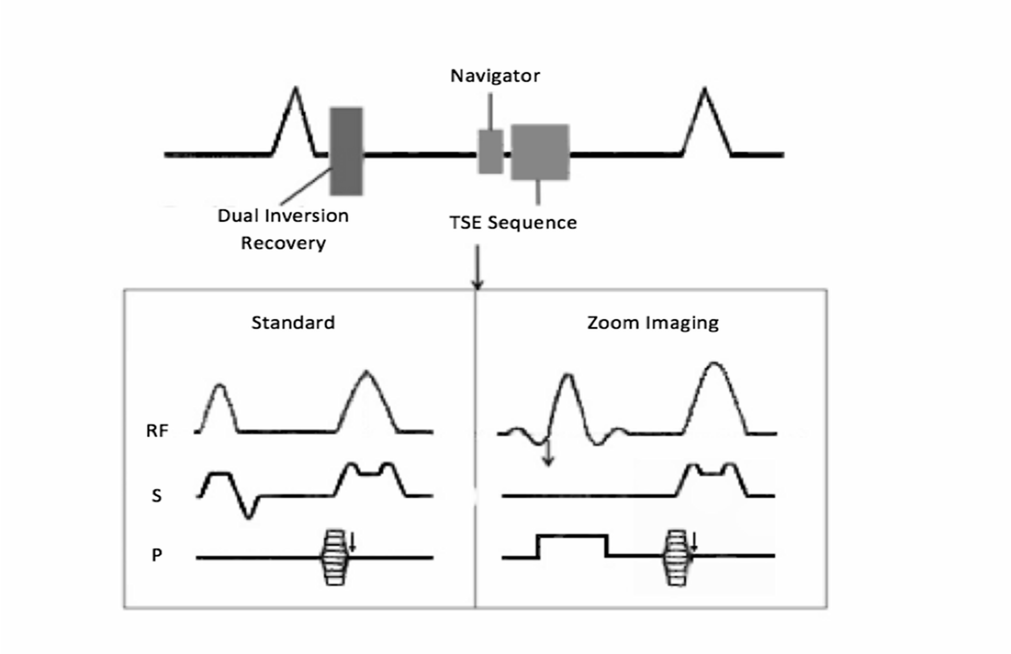

Figure 34. Zoom Pulse Sequence

At the top of this diagram, the zoom TSE pulse sequence timing to the ECG is shown. The bottom panel in the figure shows more detail of the TSE block for zoom imaging. In the zoom TSE sequence, the excitation and refocusing pulses are in orthogonal planes, allowing a small FOV without wrap-around artifact. This bottom TSE panel only shows the first 90-degree and 180-degree pulse: Subsequent 180-degree pulses are not shown but are just a copy of the first 180-degree pulse. (RF = radiofrequency pulse; S = slice selection; P = phase encoding).

5.2.3. MATERIALS AND METHODS

Institutional Review Board Approval was obtained prior to commencing this study (Local Research Ethics Committee Ref EC04/015).

5.2.3.1. MR Imaging

Fifteen healthy volunteers underwent CMR of the thoracic and abdominal aorta using a 1.5T Achieva clinical MR scanner (Philips Healthcare, Best, NL). Aortic vessel wall images were obtained using a five-element cardiac phased-array receiver coil. An initial survey and reference scan were acquired to obtain coil sensitivity maps. Subsequently, sixty-six transverse slices encompassing the thoracic and abdominal aorta down to the aorto-iliac bifurcation were obtained using a free-breathing ECG-triggered, black-blood 2D TSE sequence. The 66 slices were acquired in 2 slabs consisting of 33 slices. The echo-train length was 12 and the acquired matrix was 224 x 208 (acquired resolution 0.98 x 1.06mm). Thoracic imaging was respiratory navigator-gated using an 8mm navigator window whereas, for abdominal aorta imaging, respiratory motion correction was not used. The receiver coil was repositioned after the thoracic aorta was imaged to allow abdominal aorta imaging. A 5mm slice-thickness was used and partial Fourier imaging (factor = 0.75) was used to further shorten scan time. Other imaging parameters included: pixel bandwidth 416, repetition time of two heart beats, one signal average, shortest trigger delay (~500 ms), echo time of 5.0 ms and 60ms acquisition window. Imaging was performed with zoom imaging (FOV = 220mm x 67mm). The five central abdominal and thoracic slices within each of the respective two slabs of 33 slices were then repeated without zoom imaging (FOV = 220mm x 220mm) for comparison.

Use of sensitivity-encoding (SENSE) acceleration would be an alternative method to shorten imaging time. Hence, ten of the fifteen volunteers also underwent repeat TSE black blood imaging of the same 5 central abdominal and thoracic

slices using undersampled data acquisition and SENSE reconstruction with an acceleration factor of 2.

5.2.3.2. Image Analysis

Scan times, signal-to-noise ratios (SNR) and contrast-to-noise ratios (CNR) were analysed for conventional non-accelerated TSE black blood imaging and for the zoom imaging sequence. For accelerated TSE black blood imaging using SENSE reconstruction, only scan times and CNR were analysed. The full sixty-six slices were acquired for the zoom imaging sequence whilst only central slices were acquired for the non- and SENSE accelerated full FOV sequences. Hence, the corresponding respective central imaging slices were identified and used for image quality analyses. Additionally, image analysis of aortic vessel wall sharpness and vessel wall thickness was compared between the conventional and accelerated (zoom imaging and SENSE) imaging techniques using the 'SoapBubble' software analysis tool.[147] Using this tool, the local vessel wall sharpness can be calculated in percent by normalising the magnitude of the local change in signal intensity (using a Deriche filter) at the selected vessel wall border to the average signal intensity of the centerline of the selected vessel wall.[147, 148] In brief, this algorithm calculates an edge image using a first-order derivative of the input image. A vessel sharpness of 100% refers to a maximum signal intensity change at the vessel wall border. Sharpness, as a measure of edge detection, is useful as it gives a measure of the ability to quantify vessel wall parameters such as plaque volume. The "Soapbubble" software permits application of automated algorithms for sharpness with standardised comparisons of different imaging sequences.[105] Time for imaging without zoom was calculated by taking the nominal time from

the scanner console for all sixty-six slices whilst planning and allowing for exactly the same navigator efficiency as the zoom sequence.

SNR was defined according to the difference in repeated images. This SNR_{diff} in an ROI (region of interest in the aortic vessel wall) is calculated as the quotient of the mean value (with respect to the ROI) of the signal in the sum image and the SD (evaluated in the same ROI) of the signal in the difference image, divided by the factor $\sqrt{2}$.[206]

CNR was defined according to the following formula:

$$CNR = \frac{Signal\ Mean\ (aortic\ vessel\ wall) - Signal\ Mean\ paraspinal\ muscle}{0.5*(SDEV aortic\ vessel\ wall\ signal + SDEV paraspinal\ muscle\ signal)}$$

5.2.3.3. Statistical Analyses

Statistical analyses were performed using *SPSS version 18* (IBM, Chicago, USA). SNR, CNR and Vessel wall sharpness were compared between conventional and zoom imaging techniques using paired t-tests. CNR and vessel wall sharpness were compared between conventional and SENSE imaging techniques using paired t-tests.

Agreement between conventional and accelerated imaging techniques for vessel wall thickness analysis was investigated by the use of a Bland-Altman plot. Reproducibility of vessel wall thickness measurements between techniques was further assessed using intra-class correlation.

5.2.4. RESULTS

15 healthy volunteers (4 male) were recruited for this study with a mean age of 33 years (range 25 to 75 years) and a mean heart rate of 72bpm (range 54 to 95). In-

plane spatial image resolution was 0.98 x 1.06mm (0.31 x 0.30mm reconstructed). Mean navigator efficiency was 55±9% (range 40 to 70%). All CNR, SNR, sharpness and time parameters for the different groups were normally distributed (as confirmed by the One-Sample Kolmogorov-Smirnov Test for normality).

5.2.4.1. Zoom Imaging

Zoom imaging significantly reduced total (abdomen and thorax) imaging time from a mean of 41±9 minutes with conventional non-accelerated full FOV imaging to a mean of 15±0.5 minutes ($p<0.01$). There was a trend towards higher SNR without zoom imaging (11.8±5.7 vs. 14.0±3.7; $p=0.1$). However, CNR was comparable at a mean of 10.1±6 with zoom imaging and 10.1±6 without ($p=0.99$). More importantly, aortic vessel wall sharpness was also comparable at a mean of 39±4% with zoom imaging and 38±4% at full FOV ($p=0.21$).

Furthermore, there was no difference in aortic vessel wall thickness (mean 1.70±0.14mm with zoom and 1.72±0.14mm at full FOV; $p=0.2$). Aortic wall thickness measures showed excellent agreement on Bland-Altman analysis with a negligible mean bias of 0.02 mm (Figure 35) and the 95% limits of agreement between the two methods ranged from -0.09 (95% CI -0.31, 0.14) to 0.13 (95% CI -0.10, 0.35) mm. Good reproducibility of measurements between the two techniques is shown by the Intraclass Correlation (ICC = 0.91, 95% CI (0.82, 0.96)).

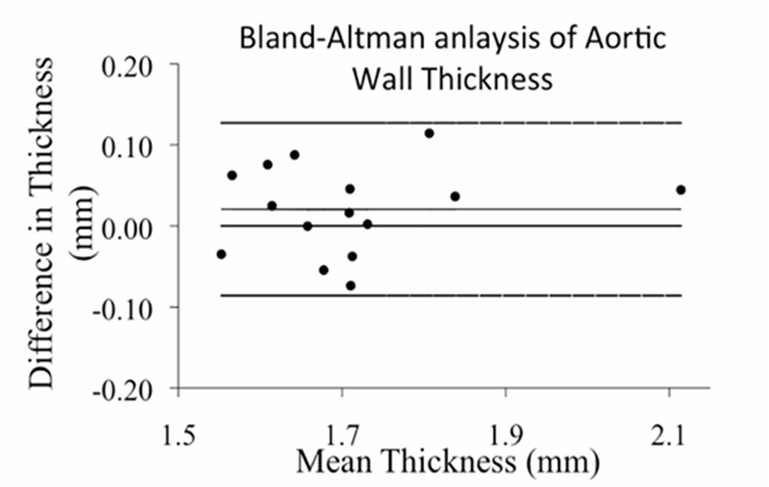

Figure 35. Bland-Altman plot (zoom)

Aortic wall thickness using standard TSE imaging minus thickness using Zoom TSE imaging. Image slice thickness used was 5 mm and the in- plane resolution was 0.98 x 1.06 mm.

5.2.4.2. SENSE acceleration

Parallel imaging with SENSE reconstruction and a reduction factor of 2 in the phase encoding direction was used for ten of the volunteers. This technique also significantly reduced imaging time (26 ± 7 minutes vs. 39 ± 10 minutes for conventional full FOV; $p<0.01$), although this was still substantially longer than with the zoom imaging sequence. Furthermore, CNR using SENSE (5.4 ± 3.5) was also significantly lower than for conventional full FOV imaging (9.8±3.5) ($p=0.007$). Vessel wall sharpness was comparable between the two techniques (39±5% using SENSE and 38±5% for conventional). However, Bland-Altman plots for vessel wall thickness showed a significant mean bias of 0.06mm (mean vessel wall thickness using SENSE: 1.68 ± 0.14mm vs. 1.74 ± 0.16mm for standard full FOV, $p=0.02$). 95% limits of agreement are also wider than for zoom imaging (-0.08

(95% CI -0.4, 0.25) to 0.20 (95% CI -0.13, 0.52) mm) (Figure 36). Reproducibility of measurements between the two techniques is shown by the Intraclass Correlation (ICC = 0.82, 95% CI (0.59, 0.93)), which was not as good as for zoom imaging.

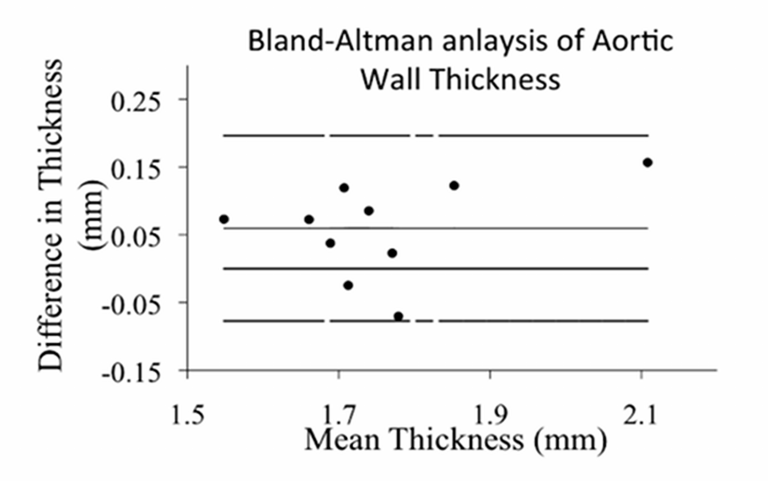

Figure 36. Bland-Altman plot (traditional)

Aortic wall thickness using standard TSE imaging minus thickness using TSE imaging with SENSE. Image slice thickness used was 5 mm and the in-plane resolution was 0.98x1.06 mm

Wraparound artefact was intermittently problematic for both conventional full FOV TSE and TSE with SENSE. Foldover suppression using saturation bands or, in the case of SENSE imaging, increase of the oversampling factor in the phase encoding direction during reconstruction was used to overcome this artefact. A sample of images is given in (Figure 37) to show how lack of wraparound artefact with zoom imaging is a particular advantage of the technique.

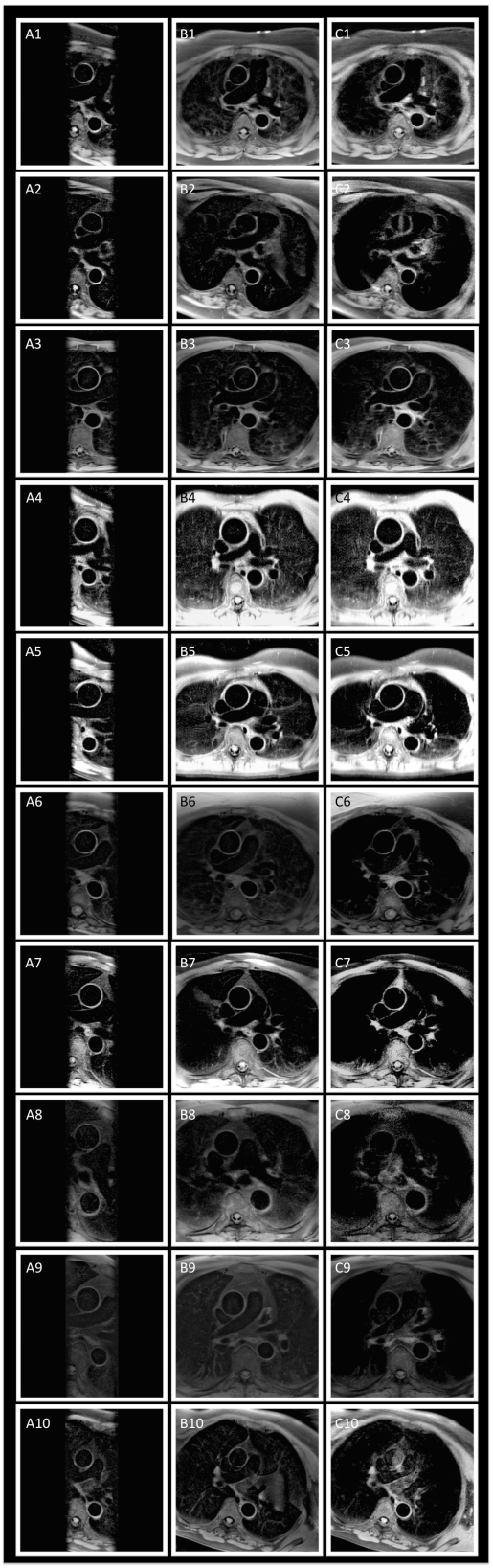

Figure 37. Sample Images

Column A shows TSE black blood images using zoom. Column B Shows conventional TSE Black Blood Images. Column C shows equivalent using

SENSE acceleration. Row 10 displays one of the advantages of Zoom imaging, i.e., lack of problems associated with wrap-around artifact. This is more problematic with SENSE acceleration, as is shown in C10. FOV = field of view; TSE = turbo spin echo.

5.2.5. DISCUSSION

It has previously been demonstrated that zoom imaging can be used for rapid small field of view imaging during percutaneous interventions.[205] This study demonstrates the use of zoom imaging to reduce imaging time for diagnostic cardiovascular aortic vessel wall imaging. We were able to reduce imaging time by 63% with zoom imaging without loss of contrast-to-noise ratio (CNR) or vessel sharpness compared to previously used full FOV TSE imaging techniques.[202-204] There was a trend towards lower SNR without affecting image quality or image analysis (in particular in the assessment of vessel wall thickness).

In comparison to SENSE data acquisition acceleration, zoom imaging reduced imaging time more effectively and did not reduce CNR. However, most importantly, SENSE not only reduced CNR but also resulted in a small but significant underestimation of vessel wall thickness compared to the conventional non-accelerated full FOV technique.[202-204]

The technique of zoom imaging, as described, achieves a reduction in the field of view by implementing excitation and refocusing pulses in orthogonal planes. As a result signal is produced only from the volume at the intersection of these pulses. Hence, a narrow field of view can be achieved without concerns regarding image aliasing. The acceleration achieved can be used to improve image resolution or acquire more slices. This technique, also known as 'inner volume imaging', was

first described by *Feinberg et al*.[207] The theory has also been applied for other sequence designs, including echo-planar imaging and 3D fast spin echo imaging.[208-210] The study described here, is therefore a novel application of this well described imaging approach. Another theoretical approach would have been to use a local excitation pulse, hence giving an alternative way of minimizing signal from outside the region of interest. This technique would also achieve an effective reduction of the field of view without concerns regarding image aliasing. This alternative approach has also been well-described.[211-213] The main concern about using a selective excitation pulse approach is the relatively long duration of the RF waveform and the resulting prolonged acquisition window duration.

It is acknowledged that there was a low aortic plaque burden in our cases due to mostly healthy volunteers with a low cardiovascular risk profile. However, (Figure 38) shows an area of abdominal aortic plaque in a 66 year-old volunteer demonstrating the ability of this technique for plaque quantification, as demonstrated with the conventional technique previously in more than 2000 cases.[202-204] Zoom imaging enables comparable data quality in shorter time compared to the conventional technique. This time saving can be used to improve coverage of the anatomic region of interest. It should also be noted that this study used a relatively narrow acquisition window of 60ms to reduce motion artefact but, in clinical practice, acquisition times of 120 to 150ms are routinely used in aortic imaging. Therefore the whole aorta can be imaged in less than 10 minutes and cardiovascular risk prediction using just the thoracic aorta could be completed within 5 minutes. Previously gaps of 10 mm were accepted but, in doing so, plaque burden was probably underestimated. It is likely that future

studies using complete coverage, as in this study, will give more accurate cardiovascular risk prediction.

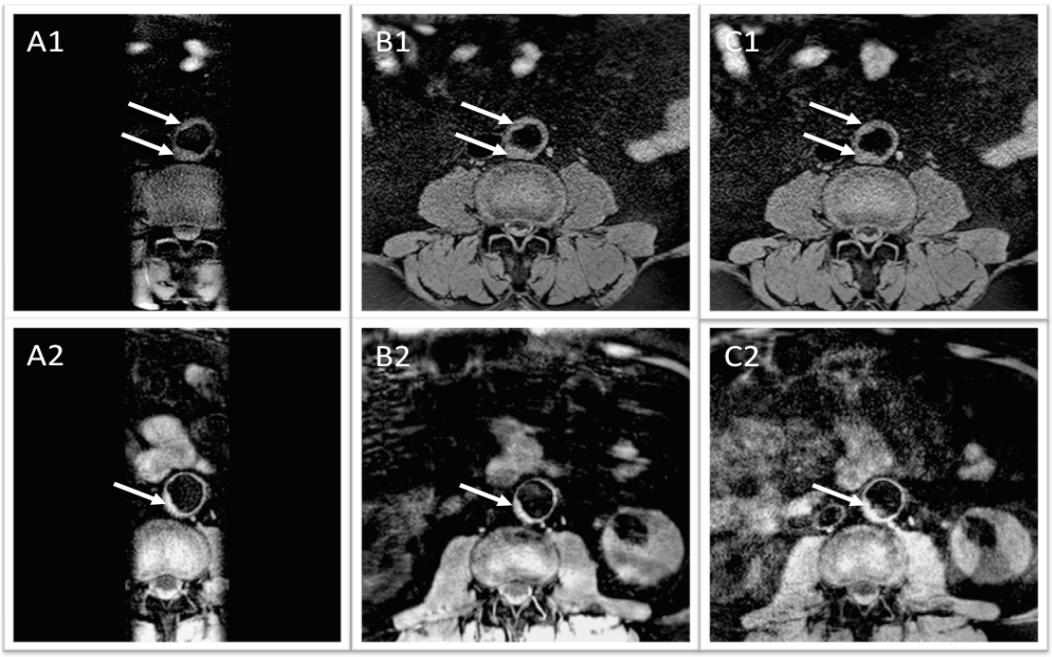

Figure 38. Sample Plaque Images

Among the healthy volunteers, the plaque burden was low but these images indicate the presence of aortic plaque (arrows). Zoom imaging depicts this well. Again, column A shows TSE black blood images using zoom imaging; column B shows conventional TSE black blood images, and column C shows equivalent full FOV images using SENSE acceleration. FOV = field of view; TSE = turbo spin echo.

Aortic plaque burden has been shown in autopsy studies to predict the amount of coronary atherosclerosis.[199] Furthermore, measurement of thoracic aortic plaque burden by MRI has been shown to be an independent risk factor for the severity of coronary atherosclerosis demonstrated by coronary angiography.[214] This evidence forms the basis of recommendations for screening atherosclerotic disease by imaging the aorta.[203] Currently, this approach is simpler and less time-consuming than direct non-invasive imaging for coronary atherosclerotic burden using high-resolution MR coronary vessel wall imaging.[97, 99, 215] It also offers advantages for screening in terms of lack of ionising radiation exposure when compared to Computed Tomography screening for cardiovascular disease by imaging of the aorta[216] or coronary arteries.[217] Furthermore, using ultrasound, thoracic aortic atherosclerosis has been shown to be a stronger correlate of cardiovascular disease than screening of carotid arteries or femoral arteries.[218]

The use of aortic imaging to guide primary prevention would obviate the concerns regarding the applicability, accuracy and ethical dilemmas surrounding use of currently available risk scoring alone to guide such therapy.[198] Furthermore, it provides patients with a goal-directed prevention therapy with the ability to monitor disease progress and should therefore improve compliance and acceptability of therapy.

In the clinical setting, carotid-femoral pulse wave velocity is much easier to perform than aortic imaging and has been shown to be predictive of cardiovascular events, although the incremental value for risk prediction still needs to be ascertained.[219] Undoubtedly, aortic atherosclerosis is a determinant of arterial stiffness but the lack of consistent association between pulse wave

velocity and many conventional atherosclerotic risk factors warrants further evaluation.[220] In this respect, the zoom TSE black blood imaging sequence described here would also allow better evaluation of the determinants of aortic stiffness.

In conclusion, we propose that use of the zoom imaging sequence will allow accurate and more time-efficient imaging of the abdominal and thoracic aorta for cardiovascular risk prediction. By reducing imaging time, the sequence becomes more applicable for future studies of cardiovascular risk stratification and monitoring of treatment effects in those individuals.

Chapter 6: Overall Discussion

"A discipline that increases the efficiency of determining the relevance of novel discoveries in the biological sciences to human disease and helps clinical researchers identify, through direct human observation, alternative hypotheses relevant to human disease. A further goal is to accelerate the rational transfer of new insights and knowledge into clinical practice for improving patients' outcomes and public health."[1]

Referring once more to Littman's original definition of translational research,[1] this thesis has succeeded in determining ***'the relevance of novel discoveries'*** including contrast-enhanced vessel wall imaging, dual phase imaging, parallel transmit technology at 3.0 Tesla, i-T2 prep and 'zoom imaging'. In attempting to address the pressing need for non-invasive imaging for Coronary Allograft Vasculopathy (CAV), this thesis has not only accelerated ***'the rational transfer of new insights and knowledge'*** into imaging for CAV but also for Congenital Heart Disease, Kawasaki Disease and Atherosclerosis.

Chapter 2 describes optimisation of the whole-heart sequence for coronary artery lumen imaging using dual phase approach. It further describes the use of this approach in children to develop of normal reference values for coronary magnetic resonance angiography (CMRA). This development enables the use of CMRA for follow-up of both CAV and Kawasaki disease.

Use of the dual phase technique for this thesis, allowed formation and subsequent proof of an ***'alternative hypothesis relevant to'*** Congenital Heart Disease. That is to say that this dual phase approach is not only relevant to coronary imaging but

that it is shown to improve the overall success rate in achieving diagnostic image quality, and is further shown to be particularly useful for interventional planning. Despite the advance of dual phase imaging, CMRA remains challenging. Chapter 3 goes on to investigate the relevance to CMRA of the novel discoveries of i-T2 prep and parallel transmit technology at 3.0 Tesla. i-T2prep, has great potential for future use in patients to image coronary lumen and vessel wall using a single sequence. Image quality from the volunteers in Chapter 3 demonstrates this potential. In this study, it is shown that an approach using sublingual nitroglycerin (NTG) prior to imaging would improve image quality. This may therefore allow a non-invasive evaluation of the influence of CAV, atherosclerotic plaque or calcification on endothelium-independent vasodilatation. Chapter 3 also demonstrates that lumen imaging is still preferable at 1.5 Tesla field strength. However, the use of novel parallel transmission technology at 3.0 Tesla gave acceptable image quality.

The central study of this thesis was the demonstration and grading of CAV in children using LGE MRI. An accuracy of 91% is shown for the detection of significant CAV as corroborated by invasive coronary intravascular ultrasound (IVUS). The advantage of 3.0 Tesla field strength for the detection of CAV was also shown. It is unclear whether LGE MRI images acute inflammation or chronic fibrosis. However, the strong correlation with IVUS suggests that it may be a combination of both. Further longitudinal studies may help to elucidate this. If acute inflammation can be imaged, the potential for tailoring therapy to prevent CAV may be realised. Ideally, a randomised control trial using LGE MRI to direct changes in therapy and using intravascular ultrasound to assess response would

be the future direction of this research. Such a study would hopefully demonstrate how these novel technologies could directly become responsible '***for improving patients' outcomes'***.

Chapter 5 demonstrates that pulse wave velocity, a marker for central aortic stiffness, is increased in children after heart transplantation. The mechanism for this is unclear. Chapter 5 goes on to describe a rapid aortic vessel wall assessment, which can be performed using 'zoom imaging'. This sequence could be used in future studies to see if the increase in aortic stiffness associated with CAV is actually due to an increase in aortic vessel wall thickness. Indeed, if a causal mechanism is proven, then applanation tonometry, a rapid method to quantify pulse wave velocity, could be performed in the clinic to routinely screen for CAV.

In summary, this thesis has indeed generated a myriad of ***'alternative hypotheses relevant to human disease"***. In the setting of CAV, we could hypothesise that LGE MRI can be used to direct therapy in clinical trials aiming to improve outcome. In the setting of Kawasaki Disease, we could hypothesise that LGE MRI is a marker for outcome, including death or infarction. In the setting of CAV or traditional atherosclerosis, we could hypothesise that native vessel wall imaging with i-T2prep could reveal the disease-specific relevance of impaired endothelium-independent vasodilatation. Regarding the observation of raised central arterial stiffness after heart transplantation, we could hypothesise that aortic thickness is increased due to systemic inflammatory insults and this could be investigated using 'zoom imaging'. The methods required to investigate these hypotheses are detailed in this thesis. The future direction of this work will be to establish

coronary vessel wall imaging into routine practice in the follow-up of paediatric heart transplantation. The first step would be to conduct larger multi-centre trials to confirm the diagnostic ability of the technique and ensure that the technique is robust from centre to centre and across imaging platforms. Once this is achieved, the technique should be implemented into a clinical trial looking to direct therapy using this imaging as a biomarker of disease. The endpoint of the research would be to reduce the incidence of clinically significant CAV by instituting a programme of increased imaging surveillance.

The objectives as set out in the introduction to this thesis have been fulfilled: The thesis demonstrates improvements in coronary lumen imaging; describes the clinical relevance of contrast-enhanced vessel wall imaging to paediatric coronary vasculopathies and explores aortic imaging as a correlate for coronary disease. The structure of this thesis has been guided by the discipline of translational research.

References

1. Littman BH, Di Mario L, Plebani M, Marincola FM. What's next in translational medicine? *Clin Sci (Lond)*. 2007;112:217-227
2. Lord GM, Trembath RC. A strategy for translation. *Lancet*. 2007;369:1771-1773
3. Schmauss D, Weis M. Cardiac allograft vasculopathy: Recent developments. *Circulation*. 2008;117:2131-2141
4. van Loosdregt J, van Oosterhout MF, Bruggink AH, van Wichen DF, van Kuik J, de Koning E, Baan CC, de Jonge N, Gmelig-Meyling FH, de Weger RA. The chemokine and chemokine receptor profile of infiltrating cells in the wall of arteries with cardiac allograft vasculopathy is indicative of a memory t-helper 1 response. *Circulation*. 2006;114:1599-1607
5. Taylor DO, Edwards LB, Boucek MM, Trulock EP, Waltz DA, Keck BM, Hertz MI. Registry of the international society for heart and lung transplantation: Twenty-third official adult heart transplantation report--2006. *J Heart Lung Transplant*. 2006;25:869-879
6. Pahl E, Naftel DC, Kuhn MA, Shaddy RE, Morrow WR, Canter CE, Kirklin J. The impact and outcome of transplant coronary artery disease in a pediatric population: A 9-year multi-institutional study. *J Heart Lung Transplant*. 2005;24:645-651
7. Costanzo MR, Naftel DC, Pritzker MR, Heilman JK, 3rd, Boehmer JP, Brozena SC, Dec GW, Ventura HO, Kirklin JK, Bourge RC, Miller LW. Heart transplant coronary artery disease detected by coronary angiography: A multiinstitutional study of preoperative donor and recipient risk factors.

Cardiac transplant research database. *J Heart Lung Transplant*. 1998;17:744-753

8. Johnson DE, Alderman EL, Schroeder JS, Gao SZ, Hunt S, DeCampli WM, Stinson E, Billingham M. Transplant coronary artery disease: Histopathologic correlations with angiographic morphology. *J Am Coll Cardiol*. 1991;17:449-457
9. Spes CH, Klauss V, Rieber J, Schnaack SD, Tammen AR, Uberfuhr P, Reichart B, Theisen K, Angermann CE, Mudra H. Functional and morphological findings in heart transplant recipients with a normal coronary angiogram: An analysis by dobutamine stress echocardiography, intracoronary doppler and intravascular ultrasound. *J Heart Lung Transplant*. 1999;18:391-398
10. St Goar FG, Pinto FJ, Alderman EL, Valantine HA, Schroeder JS, Gao SZ, Stinson EB, Popp RL. Intracoronary ultrasound in cardiac transplant recipients. In vivo evidence of "angiographically silent" intimal thickening. *Circulation*. 1992;85:979-987
11. Tuzcu EM, Hobbs RE, Rincon G, Bott-Silverman C, De Franco AC, Robinson K, McCarthy PM, Stewart RW, Guyer S, Nissen SE. Occult and frequent transmission of atherosclerotic coronary disease with cardiac transplantation. Insights from intravascular ultrasound. *Circulation*. 1995;91:1706-1713
12. Gregory SA, Ferencik M, Achenbach S, Yeh RW, Hoffmann U, Inglessis I, Cury RC, Nieman K, McNulty IA, Laffan JA, Pomerantsev EV, Brady TJ, Semigran MJ, Jang IK. Comparison of sixty-four-slice multidetector computed tomographic coronary angiography to coronary angiography with

intravascular ultrasound for the detection of transplant vasculopathy. *Am J Cardiol*. 2006;98:877-884

13. Sharples LD, Jackson CH, Parameshwar J, Wallwork J, Large SR. Diagnostic accuracy of coronary angiography and risk factors for post-heart-transplant cardiac allograft vasculopathy. *Transplantation*. 2003;76:679-682

14. Kobashigawa J, Wener L, Johnson J, Currier JW, Yeatman L, Cassem J, Tobis J. Longitudinal study of vascular remodeling in coronary arteries after heart transplantation. *J Heart Lung Transplant*. 2000;19:546-550

15. Hirohata A, Nakamura M, Waseda K, Honda Y, Lee DP, Vagelos RH, Hunt SA, Valantine HA, Yock PG, Fitzgerald PJ, Yeung AC, Fearon WF. Changes in coronary anatomy and physiology after heart transplantation. *Am J Cardiol*. 2007;99:1603-1607

16. Wellnhofer E, Stypmann J, Bara CL, Stadlbauer T, Heidt MC, Kreider-Stempfle HU, Sohn HY, Zeh W, Comberg T, Eckert S, Dengler T, Ensminger SM, Hiemann NE. Angiographic assessment of cardiac allograft vasculopathy: Results of a consensus conference of the task force for thoracic organ transplantation of the german cardiac society. *Transpl Int*. 2010;23:1094-1104

17. Mehra MR, Crespo-Leiro MG, Dipchand A, Ensminger SM, Hiemann NE, Kobashigawa JA, Madsen J, Parameshwar J, Starling RC, Uber PA. International society for heart and lung transplantation working formulation of a standardized nomenclature for cardiac allograft vasculopathy-2010. *J Heart Lung Transplant*. 2010;29:717-727

18. Itagaki BK, Kobashigawa JA, Wu GW, Patel JK, Kawano MA, Kittleson MM, Fishbein MC. Widespread fibrosis of myocardial and adjacent tissues

causing restrictive cardiac physiology in patients needing re-do heart transplant. *J Heart Lung Transplant*. 2007;26:S138

19. Stork S, Behr TM, Birk M, Uberfuhr P, Klauss V, Spes CH, Angermann CE. Assessment of cardiac allograft vasculopathy late after heart transplantation: When is coronary angiography necessary? *J Heart Lung Transplant*. 2006;25:1103-1108

20. Dent CL, Canter CE, Hirsch R, Balzer DT. Transplant coronary artery disease in pediatric heart transplant recipients. *J Heart Lung Transplant*. 2000;19:240-248

21. Nicolas RT, Kort HW, Balzer DT, Trinkaus K, Dent CL, Hirsch R, Canter CE. Surveillance for transplant coronary artery disease in infant, child and adolescent heart transplant recipients: An intravascular ultrasound study. *J Heart Lung Transplant*. 2006;25:921-927

22. Mehra MR, Ventura HO, Stapleton DD, Smart FW, Collins TC, Ramee SR. Presence of severe intimal thickening by intravascular ultrasonography predicts cardiac events in cardiac allograft vasculopathy. *J Heart Lung Transplant*. 1995;14:632-639

23. Rickenbacher PR, Pinto FJ, Lewis NP, Hunt SA, Alderman EL, Schroeder JS, Stinson EB, Brown BW, Valantine HA. Prognostic importance of intimal thickness as measured by intracoronary ultrasound after cardiac transplantation. *Circulation*. 1995;92:3445-3452

24. Gao SZ, Hunt SA, Schroeder JS, Alderman EL, Hill IR, Stinson EB. Early development of accelerated graft coronary artery disease: Risk factors and course. *J Am Coll Cardiol*. 1996;28:673-679

25. Kobashigawa JA, Tobis JM, Starling RC, Tuzcu EM, Smith AL, Valantine HA, Yeung AC, Mehra MR, Anzai H, Oeser BT, Abeywickrama KH, Murphy J, Cretin N. Multicenter intravascular ultrasound validation study among heart transplant recipients: Outcomes after five years. *J Am Coll Cardiol*. 2005;45:1532-1537

26. Nissen SE, Tuzcu EM, Brewer HB, Sipahi I, Nicholls SJ, Ganz P, Schoenhagen P, Waters DD, Pepine CJ, Crowe TD, Davidson MH, Deanfield JE, Wisniewski LM, Hanyok JJ, Kassalow LM. Effect of acat inhibition on the progression of coronary atherosclerosis. *N Engl J Med*. 2006;354:1253-1263

27. Koning G, Dijkstra J, von Birgelen C, Tuinenburg JC, Brunette J, Tardif JC, Oemrawsingh PW, Sieling C, Melsa S, Reiber JH. Advanced contour detection for three-dimensional intracoronary ultrasound: A validation--in vitro and in vivo. *Int J Cardiovasc Imaging*. 2002;18:235-248

28. Kobashigawa JA. Cardiac allograft vasculopathy in heart transplant patients: Pathologic and clinical aspects for angioplasty/stenting. *J Am Coll Cardiol*. 2006;48:462-463

29. Hiemann NE, Wellnhofer E, Knosalla C, Lehmkuhl HB, Stein J, Hetzer R, Meyer R. Prognostic impact of microvasculopathy on survival after heart transplantation: Evidence from 9713 endomyocardial biopsies. *Circulation*. 2007;116:1274-1282

30. Fearon WF, Nakamura M, Lee DP, Rezaee M, Vagelos RH, Hunt SA, Fitzgerald PJ, Yock PG, Yeung AC. Simultaneous assessment of fractional and coronary flow reserves in cardiac transplant recipients: Physiologic investigation for transplant arteriopathy (pita study). *Circulation*. 2003;108:1605-1610

31. Suwaidi JA, Hamasaki S, Higano ST, Nishimura RA, Holmes DR, Jr., Lerman A. Long-term follow-up of patients with mild coronary artery disease and endothelial dysfunction. *Circulation*. 2000;101:948-954

32. Schachinger V, Britten MB, Zeiher AM. Prognostic impact of coronary vasodilator dysfunction on adverse long-term outcome of coronary heart disease. *Circulation*. 2000;101:1899-1906

33. Kubrich M, Petrakopoulou P, Kofler S, Nickel T, Kaczmarek I, Meiser BM, Reichart B, von Scheidt W, Weis M. Impact of coronary endothelial dysfunction on adverse long-term outcome after heart transplantation. *Transplantation*. 2008;85:1580-1587

34. Hollenberg SM, Klein LW, Parrillo JE, Scherer M, Burns D, Tamburro P, Oberoi M, Johnson MR, Costanzo MR. Coronary endothelial dysfunction after heart transplantation predicts allograft vasculopathy and cardiac death. *Circulation*. 2001;104:3091-3096

35. Giulia Gagliardi M, Crea F, Polletta B, Bassano C, La Vigna G, Ballerini L, Ragonese P. Coronary microvascular endothelial dysfunction in transplanted children. *Eur Heart J*. 2001;22:254-260

36. Schubert S, Abdul-Khaliq H, Wellnhofer E, Hiemann NE, Ewert P, Lehmkuhl HB, Meyer R, Miera O, Peters B, Hetzer R, Berger F. Coronary flow reserve measurement detects transplant coronary artery disease in pediatric heart transplant patients. *J Heart Lung Transplant*. 2008;27:514-521

37. Lee CM, Wu YW, Jui HY, Yen RF, Tzen KY, Chou NK, Wang SS. Intravascular ultrasound correlates with coronary flow reserve and predicts the survival in angiographically normal cardiac transplant recipients. *Cardiology*. 2008;109:93-98

38. Ng MK, Yeung AC, Fearon WF. Invasive assessment of the coronary microcirculation: Superior reproducibility and less hemodynamic dependence of index of microcirculatory resistance compared with coronary flow reserve. *Circulation*. 2006;113:2054-2061

39. Fearon WF, Balsam LB, Farouque HM, Caffarelli AD, Robbins RC, Fitzgerald PJ, Yock PG, Yeung AC. Novel index for invasively assessing the coronary microcirculation. *Circulation*. 2003;107:3129-3132

40. Hachamovitch R, Hayes SW, Friedman JD, Cohen I, Berman DS. Comparison of the short-term survival benefit associated with revascularization compared with medical therapy in patients with no prior coronary artery disease undergoing stress myocardial perfusion single photon emission computed tomography. *Circulation*. 2003;107:2900-2907

41. Shaw LJ, Berman DS, Maron DJ, Mancini GB, Hayes SW, Hartigan PM, Weintraub WS, O'Rourke RA, Dada M, Spertus JA, Chaitman BR, Friedman J, Slomka P, Heller GV, Germano G, Gosselin G, Berger P, Kostuk WJ, Schwartz RG, Knudtson M, Veledar E, Bates ER, McCallister B, Teo KK, Boden WE. Optimal medical therapy with or without percutaneous coronary intervention to reduce ischemic burden: Results from the clinical outcomes utilizing revascularization and aggressive drug evaluation (courage) trial nuclear substudy. *Circulation*. 2008;117:1283-1291

42. Ciliberto GR, Ruffini L, Mangiavacchi M, Parolini M, Sara R, Massa D, De Maria R, Gronda E, Vitali E, Parodi O. Resting echocardiography and quantitative dipyridamole technetium-99m sestamibi tomography in the identification of cardiac allograft vasculopathy and the prediction of long-term prognosis after heart transplantation. *Eur Heart J*. 2001;22:964-971

43. Wu YW, Yen RF, Lee CM, Ho YL, Chou NK, Wang SS, Huang PJ. Diagnostic and prognostic value of dobutamine thallium-201 single-photon emission computed tomography after heart transplantation. *J Heart Lung Transplant*. 2005;24:544-550

44. Ciliberto GR, Mangiavacchi M, Banfi F, Massa D, Danzi G, Cataldo G, Cipriani M, Piccalo G, Dabala A, Gronda E, et al. Coronary artery disease after heart transplantation: Non-invasive evaluation with exercise thallium scintigraphy. *Eur Heart J*. 1993;14:226-229

45. Mairesse GH, Marwick TH, Melin JA, Hanet C, Jacquet L, Dion R, Goenen M. Use of exercise electrocardiography, technetium-99m-mibi perfusion tomography, and two-dimensional echocardiography for coronary disease surveillance in a low-prevalence population of heart transplant recipients. *J Heart Lung Transplant*. 1995;14:222-229

46. Rodney RA, Johnson LL, Blood DK, Barr ML. Myocardial perfusion scintigraphy in heart transplant recipients with and without allograft atherosclerosis: A comparison of thallium-201 and technetium 99m sestamibi. *J Heart Lung Transplant*. 1994;13:173-180

47. Hacker M, Tausig A, Romuller B, Hoyer X, Klauss V, Stempfle U, Reichart B, Hahn K, Tiling R. Dobutamine myocardial scintigraphy for the prediction of cardiac events after heart transplantation. *Nucl Med Commun*. 2005;26:607-612

48. Manrique A, Bernard M, Hitzel A, Bubenheim M, Tron C, Agostini D, Cribier A, Vera P, Bessou JP, Redonnet M. Diagnostic and prognostic value of myocardial perfusion gated spect in orthotopic heart transplant recipients. *J Nucl Cardiol*. 2010;17:197-206

49. Lenihan DJ, Rosenbaum AF, Burwinkel P, Tseng CY, Bhat G, Wagoner L, Walsh RA, Gerson MC. Prediction of human transplantation arteriopathy and coronary events with lung/heart count ratios during intravenous dipyridamole thallium-201 imaging. *Am Heart J*. 1999;137:942-948

50. Verhoeven PP, Lee FA, Ramahi TM, Franco KL, Mendes de Leon C, Amatruda J, Gorham NA, Mattera JA, Wackers FJ. Prognostic value of noninvasive testing one year after orthotopic cardiac transplantation. *J Am Coll Cardiol*. 1996;28:183-189

51. Spes CH, Klauss V, Mudra H, Schnaack SD, Tammen AR, Rieber J, Siebert U, Henneke KH, Uberfuhr P, Reichart B, Theisen K, Angermann CE. Diagnostic and prognostic value of serial dobutamine stress echocardiography for noninvasive assessment of cardiac allograft vasculopathy: A comparison with coronary angiography and intravascular ultrasound. *Circulation*. 1999;100:509-515

52. Derumeaux G, Redonnet M, Mouton-Schleifer D, Bessou JP, Cribier A, Saoudi N, Koning R, Soyer R, Letac B. Dobutamine stress echocardiography in orthotopic heart transplant recipients. Vacomed research group. *J Am Coll Cardiol*. 1995;25:1665-1672

53. Derumeaux G, Redonnet M, Soyer R, Cribier A, Letac B. Assessment of the progression of cardiac allograft vasculopathy by dobutamine stress echocardiography. *J Heart Lung Transplant*. 1998;17:259-267

54. Bacal F, Moreira L, Souza G, Rodrigues AC, Fiorelli A, Stolf N, Bocchi E, Bellotti G, Ramires JA. Dobutamine stress echocardiography predicts cardiac events or death in asymptomatic patients long-term after heart

transplantation: 4-year prospective evaluation. *J Heart Lung Transplant*. 2004;23:1238-1244

55. Akosah KO, McDaniel S, Hanrahan JS, Mohanty PK. Dobutamine stress echocardiography early after heart transplantation predicts development of allograft coronary artery disease and outcome. *J Am Coll Cardiol*. 1998;31:1607-1614

56. Eroglu E, D'Hooge J, Sutherland GR, Marciniak A, Thijs D, Droogne W, Herbots L, Van Cleemput J, Claus P, Bijnens B, Vanhaecke J, Rademakers F. Quantitative dobutamine stress echocardiography for the early detection of cardiac allograft vasculopathy in heart transplant recipients. *Heart*. 2008;94:e3

57. Dipchand AI, Bharat W, Manlhiot C, Safi M, Lobach NE, McCrindle BW. A prospective study of dobutamine stress echocardiography for the assessment of cardiac allograft vasculopathy in pediatric heart transplant recipients. *Pediatr Transplant*. 2008;12:570-576

58. Larsen RL, Applegate PM, Dyar DA, Ribeiro PA, Fritzsche SD, Mulla NF, Shirali GS, Kuhn MA, Chinnock RE, Shah PM. Dobutamine stress echocardiography for assessing coronary artery disease after transplantation in children. *J Am Coll Cardiol*. 1998;32:515-520

59. Pahl E, Crawford SE, Swenson JM, Duffy CE, Fricker FJ, Backer CL, Mavroudis C, Chaudhry FA. Dobutamine stress echocardiography: Experience in pediatric heart transplant recipients. *J Heart Lung Transplant*. 1999;18:725-732

60. Di Filippo S, Semiond B, Roriz R, Sassolas F, Raboisson MJ, Bozio A. Non-invasive detection of coronary artery disease by dobutamine-stress

echocardiography in children after heart transplantation. *J Heart Lung Transplant*. 2003;22:876-882

61. Tona F, Osto E, Tarantini G, Gambino A, Cavallin F, Feltrin G, Montisci R, Caforio AL, Gerosa G, Iliceto S. Coronary flow reserve by transthoracic echocardiography predicts epicardial intimal thickening in cardiac allograft vasculopathy. *Am J Transplant*. 2010;10:1668-1676

62. Tona F, Caforio AL, Montisci R, Gambino A, Angelini A, Ruscazio M, Toscano G, Feltrin G, Ramondo A, Gerosa G, Iliceto S. Coronary flow velocity pattern and coronary flow reserve by contrast-enhanced transthoracic echocardiography predict long-term outcome in heart transplantation. *Circulation*. 2006;114:I49-55

63. Dandel M, Hummel M, Muller J, Wellnhofer E, Meyer R, Solowjowa N, Ewert R, Hetzer R. Reliability of tissue doppler wall motion monitoring after heart transplantation for replacement of invasive routine screenings by optimally timed cardiac biopsies and catheterizations. *Circulation*. 2001;104:I184-191

64. Lytrivi ID, Lai WW, Ko HH, Nielsen JC, Parness IA, Srivastava S. Color doppler tissue imaging for evaluation of right ventricular systolic function in patients with congenital heart disease. *J Am Soc Echocardiogr*. 2005;18:1099-1104

65. Savage A, Hlavacek A, Ringewald J, Shirali G. Evaluation of the myocardial performance index and tissue doppler imaging by comparison to near-simultaneous catheter measurements in pediatric cardiac transplant patients. *J Heart Lung Transplant*. 2010;29:853-858

66. Smart FW, Ballantyne CM, Cocanougher B, Farmer JA, Sekela ME, Noon GP, Young JB. Insensitivity of noninvasive tests to detect coronary artery

vasculopathy after heart transplant. *The American journal of cardiology*. 1991;67:243-247

67. Collings CA, Pinto FJ, Valantine HA, Popylisen S, Puryear JV, Schnittger I. Exercise echocardiography in heart transplant recipients: A comparison with angiography and intracoronary ultrasonography. *The Journal of heart and lung transplantation : the official publication of the International Society for Heart Transplantation*. 1994;13:604-613

68. Schartl M, Beckmann S, Bocksch W, Fateh-Moghadam S, Fleck E. Stress echocardiography in special groups: In women, in left bundle branch block, in hypertension and after heart transplantation. *European heart journal*. 1997;18 Suppl D:D63-67

69. Blacher J, Guerin AP, Pannier B, Marchais SJ, Safar ME, London GM. Impact of aortic stiffness on survival in end-stage renal disease. *Circulation*. 1999;99:2434-2439

70. Boutouyrie P, Tropeano AI, Asmar R, Gautier I, Benetos A, Lacolley P, Laurent S. Aortic stiffness is an independent predictor of primary coronary events in hypertensive patients: A longitudinal study. *Hypertension*. 2002;39:10-15

71. Cruickshank K, Riste L, Anderson SG, Wright JS, Dunn G, Gosling RG. Aortic pulse-wave velocity and its relationship to mortality in diabetes and glucose intolerance: An integrated index of vascular function? *Circulation*. 2002;106:2085-2090

72. Laurent S, Boutouyrie P, Asmar R, Gautier I, Laloux B, Guize L, Ducimetiere P, Benetos A. Aortic stiffness is an independent predictor of all-cause and

cardiovascular mortality in hypertensive patients. *Hypertension*. 2001;37:1236-1241

73. Laurent S, Katsahian S, Fassot C, Tropeano AI, Gautier I, Laloux B, Boutouyrie P. Aortic stiffness is an independent predictor of fatal stroke in essential hypertension. *Stroke*. 2003;34:1203-1206

74. Meaume S, Benetos A, Henry OF, Rudnichi A, Safar ME. Aortic pulse wave velocity predicts cardiovascular mortality in subjects >70 years of age. *Arterioscler Thromb Vasc Biol*. 2001;21:2046-2050

75. Benetos A, Waeber B, Izzo J, Mitchell G, Resnick L, Asmar R, Safar M. Influence of age, risk factors, and cardiovascular and renal disease on arterial stiffness: Clinical applications. *Am J Hypertens*. 2002;15:1101-1108

76. Fernandes VR, Polak JF, Cheng S, Rosen BD, Carvalho B, Nasir K, McClelland R, Hundley G, Pearson G, O'Leary DH, Bluemke DA, Lima JA. Arterial stiffness is associated with regional ventricular systolic and diastolic dysfunction: The multi-ethnic study of atherosclerosis. *Arterioscler Thromb Vasc Biol*. 2008;28:194-201

77. Mottram PM, Haluska BA, Leano R, Carlier S, Case C, Marwick TH. Relation of arterial stiffness to diastolic dysfunction in hypertensive heart disease. *Heart*. 2005;91:1551-1556

78. Najjar SS, Scuteri A, Shetty V, Wright JG, Muller DC, Fleg JL, Spurgeon HP, Ferrucci L, Lakatta EG. Pulse wave velocity is an independent predictor of the longitudinal increase in systolic blood pressure and of incident hypertension in the baltimore longitudinal study of aging. *J Am Coll Cardiol*. 2008;51:1377-1383

79. O'Sullivan JJ, Derrick G, Gray J. Blood pressure after cardiac transplantation in childhood. *J Heart Lung Transplant*. 2005;24:891-895

80. Mollet NR, Cademartiri F, van Mieghem CA, Runza G, McFadden EP, Baks T, Serruys PW, Krestin GP, de Feyter PJ. High-resolution spiral computed tomography coronary angiography in patients referred for diagnostic conventional coronary angiography. *Circulation*. 2005;112:2318-2323

81. Higashi M. Noninvasive assessment of coronary plaque using multidetector row computed tomography. *Circ J*. 2011

82. Leber AW, Knez A, von Ziegler F, Becker A, Nikolaou K, Paul S, Wintersperger B, Reiser M, Becker CR, Steinbeck G, Boekstegers P. Quantification of obstructive and nonobstructive coronary lesions by 64-slice computed tomography: A comparative study with quantitative coronary angiography and intravascular ultrasound. *J Am Coll Cardiol*. 2005;46:147-154

83. Sigurdsson G, Carrascosa P, Yamani MH, Greenberg NL, Perrone S, Lev G, Desai MY, Garcia MJ. Detection of transplant coronary artery disease using multidetector computed tomography with adaptative multisegment reconstruction. *J Am Coll Cardiol*. 2006;48:772-778

84. Romeo G, Houyel L, Angel CY, Brenot P, Riou JY, Paul JF. Coronary stenosis detection by 16-slice computed tomography in heart transplant patients: Comparison with conventional angiography and impact on clinical management. *J Am Coll Cardiol*. 2005;45:1826-1831

85. Iyengar S, Feldman DS, Cooke GE, Leier CV, Raman SV. Detection of coronary artery disease in orthotopic heart transplant recipients with 64-detector

row computed tomography angiography. *J Heart Lung Transplant*. 2006;25:1363-1366

86. Schepis T, Achenbach S, Weyand M, Raum P, Marwan M, Pflederer T, Daniel WG, Tandler R, Kondruweit M, Ropers D. Comparison of dual source computed tomography versus intravascular ultrasound for evaluation of coronary arteries at least one year after cardiac transplantation. *Am J Cardiol*. 2009;104:1351-1356

87. Bae KT, Hong C, Takahashi N, Gutierrez F, Sharkey AM, Hirsch R, Canter CE. Multi-detector row computed tomographic angiography in pediatric heart transplant recipients: Initial observations. *Transplantation*. 2004;77:599-602

88. Peng Y, Zeng J, Du Z, Sun G, Guo H. Usefulness of 64-slice mdct for follow-up of young children with coronary artery aneurysm due to kawasaki disease: Initial experience. *Eur J Radiol*. 2009;69:500-509

89. Kim WY, Danias PG, Stuber M, Flamm SD, Plein S, Nagel E, Langerak SE, Weber OM, Pedersen EM, Schmidt M, Botnar RM, Manning WJ. Coronary magnetic resonance angiography for the detection of coronary stenoses. *N Engl J Med*. 2001;345:1863-1869

90. Tangcharoen T, Bell A, Hegde S, Hussain T, Beerbaum P, Schaeffter T, Razavi R, Botnar RM, Greil GF. Detection of coronary artery anomalies in infants and young children with congenital heart disease by using mr imaging. *Radiology*. 2011;259:240-247

91. Greil GF, Stuber M, Botnar RM, Kissinger KV, Geva T, Newburger JW, Manning WJ, Powell AJ. Coronary magnetic resonance angiography in

adolescents and young adults with kawasaki disease. *Circulation*. 2002;105:908-911

92. Uribe S, Hussain T, Valverde I, Tejos C, Irarrazaval P, Fava M, Beerbaum P, Botnar RM, Razavi R, Schaeffter T, Greil GF. Congenital heart disease in children: Coronary mr angiography during systole and diastole with dual cardiac phase whole-heart imaging. *Radiology*. 2011;260:232-240
93. Nunoda S, Machida H, Sekikawa A, Shitakura K, Okajima K, Kubo Y, Ueno E, Otsuka K. Evaluation of cardiac allograft vasculopathy by multidetector computed tomography and whole-heart magnetic resonance coronary angiography. *Circ J*. 2010;74:946-953
94. Schwitter J, Wacker CM, van Rossum AC, Lombardi M, Al-Saadi N, Ahlstrom H, Dill T, Larsson HB, Flamm SD, Marquardt M, Johansson L. Mr-impact: Comparison of perfusion-cardiac magnetic resonance with single-photon emission computed tomography for the detection of coronary artery disease in a multicentre, multivendor, randomized trial. *Eur Heart J*. 2008;29:480-489
95. Nagel E, Lehmkuhl HB, Bocksch W, Klein C, Vogel U, Frantz E, Ellmer A, Dreysse S, Fleck E. Noninvasive diagnosis of ischemia-induced wall motion abnormalities with the use of high-dose dobutamine stress mri: Comparison with dobutamine stress echocardiography. *Circulation*. 1999;99:763-770
96. Muehling OM, Wilke NM, Panse P, Jerosch-Herold M, Wilson BV, Wilson RF, Miller LW. Reduced myocardial perfusion reserve and transmural perfusion gradient in heart transplant arteriopathy assessed by magnetic resonance imaging. *J Am Coll Cardiol*. 2003;42:1054-1060

97. Botnar RM, Kim WY, Bornert P, Stuber M, Spuentrup E, Manning WJ. 3d coronary vessel wall imaging utilizing a local inversion technique with spiral image acquisition. *Magn Reson Med*. 2001;46:848-854

98. Botnar RM, Stuber M, Kissinger KV, Kim WY, Spuentrup E, Manning WJ. Noninvasive coronary vessel wall and plaque imaging with magnetic resonance imaging. *Circulation*. 2000;102:2582-2587

99. Kim WY, Stuber M, Bornert P, Kissinger KV, Manning WJ, Botnar RM. Three-dimensional black-blood cardiac magnetic resonance coronary vessel wall imaging detects positive arterial remodeling in patients with nonsignificant coronary artery disease. *Circulation*. 2002;106:296-299

100. Steen H, Merten C, Refle S, Klingenberg R, Dengler T, Giannitsis E, Katus HA. Prevalence of different gadolinium enhancement patterns in patients after heart transplantation. *J Am Coll Cardiol*. 2008;52:1160-1167

101. Beerbaum P, Sarikouch S, Laser KT, Greil G, Burchert W, Korperich H. Coronary anomalies assessed by whole-heart isotropic 3d magnetic resonance imaging for cardiac morphology in congenital heart disease. *J.Magn Reson.Imaging*. 2009;29:320-327

102. Kim WY, Stuber M, Kissinger KV, Andersen NT, Manning WJ, Botnar RM. Impact of bulk cardiac motion on right coronary mr angiography and vessel wall imaging. *J Magn Reson Imaging*. 2001;14:383-390

103. Li D, Kaushikkar S, Haacke EM, Woodard PK, Dhawale PJ, Kroeker RM, Laub G, Kuginuki Y, Gutierrez FR. Coronary arteries: Three-dimensional mr imaging with retrospective respiratory gating. *Radiology*. 1996;201:857-863

104. Manning WJ, Li W, Boyle NG, Edelman RR. Fat-suppressed breath-hold magnetic resonance coronary angiography. *Circulation*. 1993;87:94-104

105. Botnar RM, Stuber M, Danias PG, Kissinger KV, Manning WJ. Improved coronary artery definition with t2-weighted, free-breathing, three-dimensional coronary mra. *Circulation*. 1999;99:3139-3148

106. Gharib AM, Herzka DA, Ustun AO, Desai MY, Locklin J, Pettigrew RI, Stuber M. Coronary mr angiography at 3t during diastole and systole. *J Magn Reson Imaging*. 2007;26:921-926

107. Zagrosek A, Noeske R, Abdel-Aty H, Friedrich MG, Dietz R, Schulz-Menger J. Mr coronary angiography using 3d-ssfp with and without contrast application. *J Cardiovasc Magn Reson*. 2005;7:809-814

108. Uribe S, Tangchaoren T, Parish V, Wolf I, Razavi R, Greil G, Schaeffter T. Volumetric cardiac quantification by using 3d dual-phase whole-heart mr imaging. *Radiology*. 2008;248:606-614

109. Potthast S, Mitsumori L, Stanescu LA, Richardson ML, Branch K, Dubinsky TJ, Maki JH. Measuring aortic diameter with different mr techniques: Comparison of three-dimensional (3d) navigated steady-state free-precession (ssfp), 3d contrast-enhanced magnetic resonance angiography (ce-mra), 2d t2 black blood, and 2d cine ssfp. *Journal of magnetic resonance imaging : JMRI*. 2010;31:177-184

110. Schievano S, Capelli C, Young C, Lurz P, Nordmeyer J, Owens C, Bonhoeffer P, Taylor AM. Four-dimensional computed tomography: A method of assessing right ventricular outflow tract and pulmonary artery deformations throughout the cardiac cycle. *European radiology*. 2011;21:36-45

111. McConnell MV, Khasgiwala VC, Savord BJ, Chen MH, Chuang ML, Edelman RR, Manning WJ. Comparison of respiratory suppression methods and navigator locations for mr coronary angiography. *AJR Am J Roentgenol*. 1997;168:1369-1375

112. Greil GF, Powell AJ, Gildein HP, Geva T. Gadolinium-enhanced three-dimensional magnetic resonance angiography of pulmonary and systemic venous anomalies. *Journal of the American College of Cardiology*. 2002;39:335-341

113. Makowski MR, Wiethoff AJ, Uribe S, Parish V, Botnar RM, Bell A, Kiesewetter C, Beerbaum P, Jansen CH, Razavi R, Schaeffter T, Greil GF. Congenital heart disease: Cardiovascular mr imaging by using an intravascular blood pool contrast agent. *Radiology*. 2011

114. Arai AE, Epstein FH, Bove KE, Wolff SD. Visualization of aortic valve leaflets using black blood mri. *Journal of magnetic resonance imaging : JMRI*. 1999;10:771-777

115. Valverde I, Parish V, Hussain T, Rosenthal E, Beerbaum P, Krasemann T. Planning of catheter interventions for pulmonary artery stenosis: Improved measurement agreement with magnetic resonance angiography using identical angulations. *Catheterization and cardiovascular interventions : official journal of the Society for Cardiac Angiography & Interventions*. 2011;77:400-408

116. Boubertakh R, Prieto C, Batchelor PG, Uribe S, Atkinson D, Eggers H, Sorensen TS, Hansen MS, Razavi RS, Schaeffter T. Whole-heart imaging using undersampled radial phase encoding (rpe) and iterative sensitivity encoding (sense) reconstruction. *Magnetic resonance in medicine : official*

journal of the Society of Magnetic Resonance in Medicine / Society of Magnetic Resonance in Medicine. 2009;62:1331-1337

117. Bornert P, Stuber M, Botnar RM, Kissinger KV, Koken P, Spuentrup E, Manning WJ. Direct comparison of 3d spiral vs. Cartesian gradient-echo coronary magnetic resonance angiography. *Magnetic resonance in medicine : official journal of the Society of Magnetic Resonance in Medicine / Society of Magnetic Resonance in Medicine*. 2001;46:789-794

118. Stehning C, Bornert P, Nehrke K, Eggers H, Stuber M. Free-breathing whole-heart coronary mra with 3d radial ssfp and self-navigated image reconstruction. *Magnetic resonance in medicine : official journal of the Society of Magnetic Resonance in Medicine / Society of Magnetic Resonance in Medicine*. 2005;54:476-480

119. Uribe S, Hussain T, Valverde I, Tejos C, Irarrazaval P, Fava M, Beerbaum P, Botnar RM, Razavi R, Schaeffter T, Greil GF. Congenital heart disease in children: Coronary mr angiography during systole and diastole with dual cardiac phase whole-heart imaging. *Radiology*. 2011

120. Geva T, Kreutzer J. Diagnostic pathways for evaluation of congenital heart disease. In: MH C, JP D, eds. *Cardiology*. London: Mosby International; 2001:7-41.

121. McCrindle BW, Li JS, Minich LL, Colan SD, Atz AM, Takahashi M, Vetter VL, Gersony WM, Mitchell PD, Newburger JW. Coronary artery involvement in children with kawasaki disease: Risk factors from analysis of serial normalized measurements. *Circulation*. 2007;116:174-179

122. Olivieri L, Arling B, Friberg M, Sable C. Coronary artery z score regression equations and calculators derived from a large heterogeneous population of

children undergoing echocardiography. *J Am Soc Echocardiogr*. 2009;22:159-164

123. Uribe S, Tangchaoren T, Parish V, Wolf I, Razavi R, Greil G, Schaeffter T. Volumetric cardiac quantification by using 3d dual-phase whole-heart mr imaging. *Radiology*. 2008

124. Ustun A, Desai M, Abd-Elmoniem KZ, Schar M, Stuber M. Automated identification of minimal myocardial motion for improved image quality on mr angiography at 3 t. *AJR Am J Roentgenol*. 2007;188:W283-290

125. Newburger JW, Takahashi M, Gerber MA, Gewitz MH, Tani LY, Burns JC, Shulman ST, Bolger AF, Ferrieri P, Baltimore RS, Wilson WR, Baddour LM, Levison ME, Pallasch TJ, Falace DA, Taubert KA. Diagnosis, treatment, and long-term management of kawasaki disease: A statement for health professionals from the committee on rheumatic fever, endocarditis and kawasaki disease, council on cardiovascular disease in the young, american heart association. *Circulation*. 2004;110:2747-2771

126. Lin K, Lloyd-Jones DM, Liu Y, Bi X, Li D, Carr JC. Noninvasive evaluation of coronary distensibility in older adults: A feasibility study with mr angiography. *Radiology*. 2011

127. Allender S, Scarborough P, O'Flaherty M, Capewell S. Patterns of coronary heart disease mortality over the 20th century in england and wales: Possible plateaus in the rate of decline. *BMC Public Health*. 2008;8:148

128. Lloyd-Jones D, Adams RJ, Brown TM, Carnethon M, Dai S, De Simone G, Ferguson TB, Ford E, Furie K, Gillespie C, Go A, Greenlund K, Haase N, Hailpern S, Ho PM, Howard V, Kissela B, Kittner S, Lackland D, Lisabeth L, Marelli A, McDermott MM, Meigs J, Mozaffarian D, Mussolino M, Nichol G,

Roger VL, Rosamond W, Sacco R, Sorlie P, Stafford R, Thom T, Wasserthiel-Smoller S, Wong ND, Wylie-Rosett J. Executive summary: Heart disease and stroke statistics--2010 update: A report from the american heart association. *Circulation*. 2010;121:948-954

129. Kim WY, Danias PG, Stuber M, Flamm SD, Plein S, Nagel E, Langerak SE, Weber OM, Pedersen EM, Schmidt M, Botnar RM, Manning WJ. Coronary magnetic resonance angiography for the detection of coronary stenoses. *The New England journal of medicine*. 2001;345:1863-1869

130. Morton G, Plein S, Nagel E. Noninvasive coronary angiography using computed tomography versus magnetic resonance imaging. *Ann Intern Med*. 2010;152:827-828; author reply 828-829

131. Boden WE, O'Rourke R A, Teo KK, Hartigan PM, Maron DJ, Kostuk W, Knudtson M, Dada M, Casperson P, Harris CL, Spertus JA, Shaw L, Chaitman BR, Mancini GB, Berman DS, Gau G, Weintraub WS. The evolving pattern of symptomatic coronary artery disease in the united states and canada: Baseline characteristics of the clinical outcomes utilizing revascularization and aggressive drug evaluation (courage) trial. *The American journal of cardiology*. 2007;99:208-212

132. Glagov S, Weisenberg E, Zarins CK, Stankunavicius R, Kolettis GJ. Compensatory enlargement of human atherosclerotic coronary arteries. *The New England journal of medicine*. 1987;316:1371-1375

133. Hatsukami TS, Yuan C. Mri in the early identification and classification of high-risk atherosclerotic carotid plaques. *Imaging Med*. 2010;2:63-75

134. Jansen CH, Perera D, Makowski MR, Wiethoff AJ, Phinikaridou A, Razavi RM, Marber MS, Greil GF, Nagel E, Maintz D, Redwood S, Botnar RM. Detection of

intracoronary thrombus by magnetic resonance imaging in patients with acute myocardial infarction. *Circulation*. 2011;124:416-424

135. Maintz D, Ozgun M, Hoffmeier A, Fischbach R, Kim WY, Stuber M, Manning WJ, Heindel W, Botnar RM. Selective coronary artery plaque visualization and differentiation by contrast-enhanced inversion prepared mri. *Eur Heart J*. 2006;27:1732-1736

136. Ibrahim T, Makowski MR, Jankauskas A, Maintz D, Karch M, Schachoff S, Manning WJ, Schomig A, Schwaiger M, Botnar RM. Serial contrast-enhanced cardiac magnetic resonance imaging demonstrates regression of hyperenhancement within the coronary artery wall in patients after acute myocardial infarction. *JACC. Cardiovascular imaging*. 2009;2:580-588

137. Kelle S, Schlendorf K, Hirsch GA, Gerstenblith G, Fleck E, Weiss RG, Stuber M. Gadolinium enhanced mr coronary vessel wall imaging at 3.0 tesla. *Cardiol Res Pract*. 2010;2010:856418

138. Stuber M, Botnar RM, Fischer SE, Lamerichs R, Smink J, Harvey P, Manning WJ. Preliminary report on in vivo coronary mra at 3 tesla in humans. *Magnetic resonance in medicine : official journal of the Society of Magnetic Resonance in Medicine / Society of Magnetic Resonance in Medicine*. 2002;48:425-429

139. Deshpande VS, Shea SM, Chung YC, McCarthy RM, Finn JP, Li D. Breath-hold three-dimensional true-fisp imaging of coronary arteries using asymmetric sampling. *Journal of magnetic resonance imaging : JMRI*. 2002;15:473-478

140. Bi X, Deshpande V, Simonetti O, Laub G, Li D. Three-dimensional breathhold ssfp coronary mra: A comparison between 1.5t and 3.0t. *Journal of magnetic resonance imaging : JMRI*. 2005;22:206-212

141. Zur Y, Stokar S, Bendel P. An analysis of fast imaging sequences with steady-state transverse magnetization refocusing. *Magnetic resonance in medicine : official journal of the Society of Magnetic Resonance in Medicine / Society of Magnetic Resonance in Medicine*. 1988;6:175-193

142. Katscher U, Bornert P. Parallel rf transmission in mri. *NMR Biomed*. 2006;19:393-400

143. Homann H, Graesslin I, Eggers H, Nehrke K, Vernickel P, Katscher U, Dossel O, Bornert P. Local sar management by rf shimming: A simulation study with multiple human body models. *MAGMA*. 2011

144. Hussain S, Chiribiri A, Ishida M, Morton G, Wiethoff A, Schuster A, Nagel E. A comparison of single-channel and multi-channel rf transmit coil for ssfp cine imaging at 3 tesla [abstract]. *Journal of Cardiovascular Magnetic Resonance*. 2011;13:s20

145. Stuber M, Botnar RM, Danias PG, Sodickson DK, Kissinger KV, Van Cauteren M, De Becker J, Manning WJ. Double-oblique free-breathing high resolution three-dimensional coronary magnetic resonance angiography. *Journal of the American College of Cardiology*. 1999;34:524-531

146. Spuentrup E, Buecker A, Stuber M, Botnar R, Nguyen TH, Bornert P, Kolker C, Gunther RW. Navigator-gated coronary magnetic resonance angiography using steady-state-free-precession: Comparison to standard t2-prepared gradient-echo and spiral imaging. *Investigative radiology*. 2003;38:263-268

147. Etienne A, Botnar RM, Van Muiswinkel AM, Boesiger P, Manning WJ, Stuber M. "Soap-bubble" visualization and quantitative analysis of 3d coronary magnetic resonance angiograms. *Magn Reson Med*. 2002;48:658-666

148. Deriche R. Fast algorithms for low-level vision. Ieee transactions on pattern analysis and machine intelligence. *PAMI*. 1990;12:78-87.

149. Austen WG, Edwards JE, Frye RL, Gensini GG, Gott VL, Griffith LS, McGoon DC, Murphy ML, Roe BB. A reporting system on patients evaluated for coronary artery disease. Report of the ad hoc committee for grading of coronary artery disease, council on cardiovascular surgery, american heart association. *Circulation*. 1975;51:5-40

150. Bi X, Li D. Coronary arteries at 3.0 t: Contrast-enhanced magnetization-prepared three-dimensional breathhold mr angiography. *Journal of magnetic resonance imaging : JMRI*. 2005;21:133-139

151. Nayak KS, Lee HL, Hargreaves BA, Hu BS. Wideband ssfp: Alternating repetition time balanced steady state free precession with increased band spacing. *Magnetic resonance in medicine : official journal of the Society of Magnetic Resonance in Medicine / Society of Magnetic Resonance in Medicine*. 2007;58:931-938

152. Henningsson M, Koken P, Stehning C, Razavi R, Prieto C, Botnar RM. Whole-heart coronary mr angiography with 2d self-navigated image reconstruction. *Magnetic resonance in medicine : official journal of the Society of Magnetic Resonance in Medicine / Society of Magnetic Resonance in Medicine*. 2011

153. Scott AD, Keegan J, Firmin DN. Beat-to-beat respiratory motion correction with near 100% efficiency: A quantitative assessment using high-resolution coronary artery imaging. *Magn Reson Imaging*. 2011;29:568-578

154. Jin H, Zeng MS, Ge MY, Ma JY, Chen CZ, Shen JZ, Li RC. Influence of applying nitroglycerin in whole-heart free-breathing 3d coronary mr angiography. *AJR. American journal of roentgenology*. 2010;194:927-932

155. Armstrong PW, Armstrong JA, Marks GS. Blood levels after sublingual nitroglycerin. *Circulation*. 1979;59:585-588

156. Andia M, Botnar R. Dynamic t2prep for flow-independent vessel wall imaging. *International Society of Magnetic Resonance Medicine 2011 Annual Meeting Proceedings*. 2011:1251

157. Ehman RL, Felmlee JP. Adaptive technique for high-definition mr imaging of moving structures. *Radiology*. 1989;173:255-263

158. Stuber M, Botnar RM, Danias PG, Kissinger KV, Manning WJ. Submillimeter three-dimensional coronary mr angiography with real-time navigator correction: Comparison of navigator locations. *Radiology*. 1999;212:579-587

159. Andia ME, Henningsson M, Hussain T, Phinikaridou A, Protti A, Greil G, Botnar RM. Flow-independent 3d whole-heart vessel wall imaging using an interleaved t2-preparation acquisition. *Magnetic resonance in medicine : official journal of the Society of Magnetic Resonance in Medicine / Society of Magnetic Resonance in Medicine*. 2013;69:150-157

160. Kim WY, Astrup AS, Stuber M, Tarnow L, Falk E, Botnar RM, Simonsen C, Pietraszek L, Hansen PR, Manning WJ, Andersen NT, Parving HH. Subclinical coronary and aortic atherosclerosis detected by magnetic resonance imaging in type 1 diabetes with and without diabetic nephropathy. *Circulation*. 2007;115:228-235

161. Terashima M, Nguyen PK, Rubin GD, Iribarren C, Courtney BK, Go AS, Fortmann SP, McConnell MV. Impaired coronary vasodilation by magnetic resonance angiography is associated with advanced coronary artery calcification. *JACC. Cardiovascular imaging*. 2008;1:167-173

162. Reichek N, Alexander D. Coronary artery function: Out of the cath lab and into the magnet. *JACC. Cardiovascular imaging*. 2008;1:174-176

163. Carr DH, Brown J, Bydder GM, Steiner RE, Weinmann HJ, Speck U, Hall AS, Young IR. Gadolinium-dtpa as a contrast agent in mri: Initial clinical experience in 20 patients. *AJR Am J Roentgenol*. 1984;143:215-224

164. Pujadas S, Bordes R, Bayes-Genis A. Ventricular non-compaction cardiomyopathy: Cmr and pathology findings. *Heart*. 2005;91:582

165. Kim RJ, Wu E, Rafael A, Chen EL, Parker MA, Simonetti O, Klocke FJ, Bonow RO, Judd RM. The use of contrast-enhanced magnetic resonance imaging to identify reversible myocardial dysfunction. *N Engl J Med*. 2000;343:1445-1453

166. Botnar RM, Buecker A, Wiethoff AJ, Parsons EC, Jr., Katoh M, Katsimaglis G, Weisskoff RM, Lauffer RB, Graham PB, Gunther RW, Manning WJ, Spuentrup E. In vivo magnetic resonance imaging of coronary thrombosis using a fibrin-binding molecular magnetic resonance contrast agent. *Circulation*. 2004;110:1463-1466

167. Moody AR, Murphy RE, Morgan PS, Martel AL, Delay GS, Allder S, MacSweeney ST, Tennant WG, Gladman J, Lowe J, Hunt BJ. Characterization of complicated carotid plaque with magnetic resonance direct thrombus imaging in patients with cerebral ischemia. *Circulation*. 2003;107:3047-3052

168. Look DC, Locker DR. Time saving in measurement of nmr and epr relaxation times. *Rev Sci Instrum*. 1970;41:250-251

169. Oakes RS, Badger TJ, Kholmovski EG, Akoum N, Burgon NS, Fish EN, Blauer JJ, Rao SN, DiBella EV, Segerson NM, Daccarett M, Windfelder J, McGann CJ, Parker D, MacLeod RS, Marrouche NF. Detection and quantification of left atrial structural remodeling with delayed-enhancement magnetic resonance imaging in patients with atrial fibrillation. *Circulation*. 2009;119:1758-1767

170. Desai MY, Stone JH, Foo TK, Hellmann DB, Lima JA, Bluemke DA. Delayed contrast-enhanced mri of the aortic wall in takayasu's arteritis: Initial experience. *AJR. American journal of roentgenology*. 2005;184:1427-1431

171. Dill T, Ekinci O, Hansel J, Kluge A, Breidenbach C, Hamm CW. Delayed contrast-enhanced magnetic resonance imaging for the detection of autoimmune myocarditis and long-term follow-up. *Journal of cardiovascular magnetic resonance : official journal of the Society for Cardiovascular Magnetic Resonance*. 2005;7:521-523

172. Bley TA, Wieben O, Leupold J, Uhl M. Images in cardiovascular medicine. Magnetic resonance imaging findings in temporal arteritis. *Circulation*. 2005;111:e260

173. Hussain T, Burch M, Fenton MJ, Whitmore PM, Rees P, Elliott M, Aurora P. Positive pretransplantation cytomegalovirus serology is a risk factor for cardiac allograft vasculopathy in children. *Circulation*. 2007;115:1798-1805

174. Kobashigawa JA. Cardiac allograft vasculopathy in heart transplant patients: Pathologic and clinical aspects for angioplasty/stenting. *Journal of the American College of Cardiology*. 2006;48:462-463

175. McGann CJ, Kholmovski EG, Oakes RS, Blauer JJ, Daccarett M, Segerson N, Airey KJ, Akoum N, Fish E, Badger TJ, DiBella EV, Parker D, MacLeod RS, Marrouche NF. New magnetic resonance imaging-based method for defining the extent of left atrial wall injury after the ablation of atrial fibrillation. *Journal of the American College of Cardiology*. 2008;52:1263-1271

176. Wasserman BA, Smith WI, Trout HH, 3rd, Cannon RO, 3rd, Balaban RS, Arai AE. Carotid artery atherosclerosis: In vivo morphologic characterization with gadolinium-enhanced double-oblique mr imaging initial results. *Radiology*. 2002;223:566-573

177. Makowski MR, Wiethoff AJ, Blume U, Cuello F, Warley A, Jansen CH, Nagel E, Razavi R, Onthank DC, Cesati RR, Marber MS, Schaeffter T, Smith A, Robinson SP, Botnar RM. Assessment of atherosclerotic plaque burden with an elastin-specific magnetic resonance contrast agent. *Nat Med*. 2011;17:383-388

178. Hussain T, Greil G, Taylor A, Muthurangu V, Fenton M, Botnar R, Burch M. Detection and grading of coronary allograft vasculopathy in children using late gadolinium enhancement mri. *The Journal of heart and lung transplantation : the official publication of the International Society for Heart Transplantation*. 2011;30:S133-S134

179. Radovancevic B, Poindexter S, Birovljev S, Velebit V, McAllister HA, Duncan JM, Vega D, Lonquist J, Burnett CM, Frazier OH. Risk factors for development of accelerated coronary artery disease in cardiac transplant recipients. *European journal of cardio-thoracic surgery : official journal of the European Association for Cardio-thoracic Surgery*. 1990;4:309-312; discussion 313

180. Greil GF, Seeger A, Miller S, Claussen CD, Hofbeck M, Botnar RM, Sieverding L. Coronary magnetic resonance angiography and vessel wall imaging in children with kawasaki disease. *Pediatr Radiol*. 2007;37:666-673

181. Matteucci MC, Giordano U, Calzolari A, Rizzoni G. Total peripheral vascular resistance in pediatric renal transplant patients. *Kidney Int*. 2002;62:1870-1874

182. Ou P, Celermajer DS, Jolivet O, Buyens F, Herment A, Sidi D, Bonnet D, Mousseaux E. Increased central aortic stiffness and left ventricular mass in normotensive young subjects after successful coarctation repair. *American heart journal*. 2008;155:187-193

183. Report of the second task force on blood pressure control in children--1987. Task force on blood pressure control in children. National heart, lung, and blood institute, bethesda, maryland. *Pediatrics*. 1987;79:1-25

184. Update on the 1987 task force report on high blood pressure in children and adolescents: A working group report from the national high blood pressure education program. National high blood pressure education program working group on hypertension control in children and adolescents. *Pediatrics*. 1996;98:649-658

185. U.S. DEPARTMENT OF HEALTH AND HUMAN SERVICES National Institutes of Health National Heart L, and Blood Institute. The fourth report on the diagnosis, evaluation, and treatment of high blood pressure in children and adolescents. *NIH Publication No. 05-5267*. 2005

186. Grotenhuis HB, Westenberg JJ, Steendijk P, van der Geest RJ, Ottenkamp J, Bax JJ, Jukema JW, de Roos A. Validation and reproducibility of aortic pulse

wave velocity as assessed with velocity-encoded mri. *Journal of magnetic resonance imaging : JMRI*. 2009;30:521-526

187. Klinge A, Allen J, Murray A, O'Sullivan J. Increased pulse wave velocity and blood pressure in children who have undergone cardiac transplantation. *The Journal of heart and lung transplantation : the official publication of the International Society for Heart Transplantation*. 2009;28:21-25

188. Greene ES, Gerson JI. Arterial pulse wave velocity: A limited index of systemic vascular resistance during normotensive anesthesia in dogs. *J Clin Monit*. 1985;1:219-226

189. Yambe T, Meng X, Hou X, Wang Q, Sekine K, Shiraishi Y, Watanabe M, Yamaguchi T, Shibata M, Kuwayama T, Maruyama M, Konno S, Nitta S. Cardio-ankle vascular index (cavi) for the monitoring of the atherosclerosis after heart transplantation. *Biomed Pharmacother*. 2005;59 Suppl 1:S177-179

190. Schroeder JS, Gao SZ, Alderman EL, Hunt SA, Johnstone I, Boothroyd DB, Wiederhold V, Stinson EB. A preliminary study of diltiazem in the prevention of coronary artery disease in heart-transplant recipients. *The New England journal of medicine*. 1993;328:164-170

191. Petrakopoulou P, Kubrich M, Pehlivanli S, Meiser B, Reichart B, von Scheidt W, Weis M. Cytomegalovirus infection in heart transplant recipients is associated with impaired endothelial function. *Circulation*. 2004;110:II207-212

192. Simmonds J, Fenton M, Dewar C, Ellins E, Storry C, Cubitt D, Deanfield J, Klein N, Halcox J, Burch M. Endothelial dysfunction and cytomegalovirus

replication in pediatric heart transplantation. *Circulation*. 2008;117:2657-2661

193. Nagano M, Nakamura M, Sato K, Tanaka F, Segawa T, Hiramori K. Association between serum c-reactive protein levels and pulse wave velocity: A population-based cross-sectional study in a general population. *Atherosclerosis*. 2005;180:189-195

194. Franklin SS. Arterial stiffness and hypertension: A two-way street? *Hypertension*. 2005;45:349-351

195. O'Rourke MF, Staessen JA, Vlachopoulos C, Duprez D, Plante GE. Clinical applications of arterial stiffness; definitions and reference values. *American journal of hypertension*. 2002;15:426-444

196. Takase H, Dohi Y, Toriyama T, Okado T, Tanaka S, Sonoda H, Sato K, Kimura G. Brachial-ankle pulse wave velocity predicts increase in blood pressure and onset of hypertension. *American journal of hypertension*. 2011;24:667-673

197. Laurent S, Cockcroft J, Van Bortel L, Boutouyrie P, Giannattasio C, Hayoz D, Pannier B, Vlachopoulos C, Wilkinson I, Struijker-Boudier H. Expert consensus document on arterial stiffness: Methodological issues and clinical applications. *European heart journal*. 2006;27:2588-2605

198. Berger JS, Jordan CO, Lloyd-Jones D, Blumenthal RS. Screening for cardiovascular risk in asymptomatic patients. *J Am Coll Cardiol*. 2010;55:1169-1177

199. Solberg LA, Strong JP. Risk factors and atherosclerotic lesions. A review of autopsy studies. *Arteriosclerosis*. 1983;3:187-198

200. Fazio GP, Redberg RF, Winslow T, Schiller NB. Transesophageal echocardiographically detected atherosclerotic aortic plaque is a marker for coronary artery disease. *J Am Coll Cardiol*. 1993;21:144-150

201. Khoury Z, Gottlieb S, Stern S, Keren A. Frequency and distribution of atherosclerotic plaques in the thoracic aorta as determined by transesophageal echocardiography in patients with coronary artery disease. *Am J Cardiol*. 1997;79:23-27

202. Fayad ZA, Nahar T, Fallon JT, Goldman M, Aguinaldo JG, Badimon JJ, Shinnar M, Chesebro JH, Fuster V. In vivo magnetic resonance evaluation of atherosclerotic plaques in the human thoracic aorta: A comparison with transesophageal echocardiography. *Circulation*. 2000;101:2503-2509

203. Jaffer FA, O'Donnell CJ, Larson MG, Chan SK, Kissinger KV, Kupka MJ, Salton C, Botnar RM, Levy D, Manning WJ. Age and sex distribution of subclinical aortic atherosclerosis: A magnetic resonance imaging examination of the framingham heart study. *Arterioscler Thromb Vasc Biol*. 2002;22:849-854

204. Oyama N, Gona P, Salton CJ, Chuang ML, Jhaveri RR, Blease SJ, Manning AR, Lahiri M, Botnar RM, Levy D, Larson MG, O'Donnell CJ, Manning WJ. Differential impact of age, sex, and hypertension on aortic atherosclerosis: The framingham heart study. *Arterioscler Thromb Vasc Biol*. 2008;28:155-159

205. Buecker A, Adam G, Neuerburg JM, Glowinski A, van Vaals JJ, Guenther RW. Mr-guided biopsy using a t2-weighted single-shot zoom imaging sequence (local look technique). *J Magn Reson Imaging*. 1998;8:955-959

206. Dietrich O, Raya JG, Reeder SB, Reiser MF, Schoenberg SO. Measurement of signal-to-noise ratios in mr images: Influence of multichannel coils, parallel imaging, and reconstruction filters. *J Magn Reson Imaging*. 2007;26:375-385

207. Feinberg DA, Hoenninger JC, Crooks LE, Kaufman L, Watts JC, Arakawa M. Inner volume mr imaging: Technical concepts and their application. *Radiology*. 1985;156:743-747

208. Schneider JT, Kalayciyan R, Haas M, Herrmann SR, Ruhm W, Hennig J, Ullmann P. Inner-volume imaging in vivo using three-dimensional parallel spatially selective excitation. *Magnetic resonance in medicine : official journal of the Society of Magnetic Resonance in Medicine / Society of Magnetic Resonance in Medicine*. 2012

209. Feinberg DA, Turner R, Jakab PD, von Kienlin M. Echo-planar imaging with asymmetric gradient modulation and inner-volume excitation. *Magnetic resonance in medicine : official journal of the Society of Magnetic Resonance in Medicine / Society of Magnetic Resonance in Medicine*. 1990;13:162-169

210. Mitsouras D, Mulkern RV, Rybicki FJ. Strategies for inner volume 3d fast spin echo magnetic resonance imaging using nonselective refocusing radio frequency pulses. *Med Phys*. 2006;33:173-186

211. Alley MT, Pauly JM, Sommer FG, Pelc NJ. Angiographic imaging with 2d rf pulses. *Magnetic resonance in medicine : official journal of the Society of Magnetic Resonance in Medicine / Society of Magnetic Resonance in Medicine*. 1997;37:260-267

212. Yang GZ, Gatehouse PD, Keegan J, Mohiaddin RH, Firmin DN. Three-dimensional coronary mr angiography using zonal echo planar imaging. *Magnetic resonance in medicine : official journal of the Society of Magnetic*

Resonance in Medicine / Society of Magnetic Resonance in Medicine. 1998;39:833-842

213. Luk-Pat GT, Gold GE, Olcott EW, Hu BS, Nishimura DG. High-resolution three-dimensional in vivo imaging of atherosclerotic plaque. *Magnetic resonance in medicine : official journal of the Society of Magnetic Resonance in Medicine / Society of Magnetic Resonance in Medicine*. 1999;42:762-771

214. Taniguchi H, Momiyama Y, Fayad ZA, Ohmori R, Ashida K, Kihara T, Hara A, Arakawa K, Kameyama A, Noya K, Nagata M, Nakamura H, Ohsuzu F. In vivo magnetic resonance evaluation of associations between aortic atherosclerosis and both risk factors and coronary artery disease in patients referred for coronary angiography. *Am Heart J*. 2004;148:137-143

215. Botnar RM, Bucker A, Kim WY, Viohl I, Gunther RW, Spuentrup E. Initial experiences with in vivo intravascular coronary vessel wall imaging. *J Magn Reson Imaging*. 2003;17:615-619

216. Yorgun H, Hazirolan T, Kaya EB, Canpolat U, Sunman H, Ertugrul O, Ates AH, Aksoy H, Aytemir K, Tokgozoglu L, Kabakci G, Oto A. Aortic atherosclerosis predicts the extent and severity of coronary atherosclerosis detected by multidetector computed tomography coronary angiography. *Angiology*. 2010

217. Agatston AS, Janowitz WR, Hildner FJ, Zusmer NR, Viamonte M, Jr., Detrano R. Quantification of coronary artery calcium using ultrafast computed tomography. *J Am Coll Cardiol*. 1990;15:827-832

218. Khoury Z, Schwartz R, Gottlieb S, Chenzbraun A, Stern S, Keren A. Relation of coronary artery disease to atherosclerotic disease in the aorta, carotid,

and femoral arteries evaluated by ultrasound. *Am J Cardiol*. 1997;80:1429-1433

219. Cohn JN. Arterial stiffness, vascular disease, and risk of cardiovascular events. *Circulation*. 2006;113:601-603

220. Cecelja M, Chowienczyk P. Dissociation of aortic pulse wave velocity with risk factors for cardiovascular disease other than hypertension: A systematic review. *Hypertension*. 2009;54:1328-1336